Electronic Thesis and Dissertation Repository

10-20-2022 8:30 AM

The Arg76 Residue of Cx50, Cx43 and Cx45 is Important for the Formation of Functional Gap Junction Channels

Tianhe Li, *The University of Western Ontario*

Supervisor: Bai, Donglin, *The University of Western Ontario*
A thesis submitted in partial fulfillment of the requirements for the Master of Science degree in Physiology and Pharmacology
© Tianhe Li 2022

Recommended Citation

Abstract

Arginine76 (R76) or the equivalent residue is highly conserved in most connexins, mutations on this residue in six connexins have been linked to five different inherited diseases, indicating its functional importance. Here we examined the functional status and properties of gap junctions (GJs) containing R76 mutations in Cx50 (R76H and R76C), Cx45 (R75H) and Cx43 (R76H/S/C) with an emphasis on GJ function by pairing the mutants with corresponding wildtype or another docking compatible connexin. Cx50 R76H, R76C and Cx45 R75H failed to form functional homomeric homotypic or heterotypic GJs. Cx43 R76H and R76S formed functional GJs by themselves or paired with wildtype Cx43, but with altered properties. However, Cx43 R76C failed to form functional GJs by itself or with Cx43. Interestingly all three Cx43 mutants formed functional GJs when paired with Cx45. Our findings and homology structure models provide molecular insights into the possible pathogenic mechanism of R76 mutants in these connexins.

Keywords

Summary for Lay Audience

Most tissue cells communicate directly with each other to maintain synchronized activities via protein channels known as gap junctions (GJs). Each GJ is made up of two hemichannels and each hemichannel is formed by the oligomerization of six connexin proteins. Tissue cells typically express more than one connexin type and different tissues often express different types of connexins. Thus, different types of GJs can be formed to synchronize cells in the same tissue or to propagate signals between different tissues to meet physiological demands. The arginine residue at the 76th position (R76) is at a critical structural junction in the GJ structure and this residue never changes during the evolutionary process of different species and among different connexins. Mutations at the R76 or equivalent residue in six different connexins have been associated with five inherited diseases, although the molecular mechanisms have not been fully studied, especially on GJs formed by mutant expressing cells paired with wildtype connexins. Here, we studied the functional status and properties of R76 mutations in connexin 50 (Cx50), Cx45, and Cx43 with an emphasis on mutant expressing cells paired with cells expressing wildtype connexin or another connexin normally capable of forming functional GJs. We found that Cx50 R76H, R76C and Cx45 R75H were unable to form functional GJs in any of our tested pairings. Cx43 R76H and R76S formed functional GJs as well as forming functional GJs when paired with wildtype Cx43, but with altered channel properties. Cx43 mutants (R76H, R76S, and R76C) all formed functional GJs when paired with Cx45. Our study indicated that most of the R76 mutations in these studied connexins are loss-of-function mutations for GJ function, even when paired with wildtype or different compatible connexins. We also developed molecular structure models to see possible changes associated with each mutant on this residue. We revealed that mutations on R76 or equivalent residue led to various degrees of loss in local molecular interactions within the same connexin or between neighbouring connexins in a hemichannel, which could lead to impaired GJ function and disease state for patients who carry mutations on this residue.

Co-Authorship Statement

Chapter 2 will be submitted as a manuscript with additional localization data with the following authors:

Tianhe Li, Honghong Chen, Xiaole Li, Peter Stathopulos, and Donglin Bai

Tianhe Li designed and performed 90% patch clamp experiments, data analysis, figure construction, and wrote an early draft of the manuscript. Honghong Chen designed and generated all expression vectors for all connexin mutants. Xiaole Li performed some patch clamp experiments, data analysis, and contributed to some figure constructions. Peter Stathopulos developed homology structure models. Donglin Bai designed the project, obtained funding for this project, supervised data analysis and figure construction, and critically revised the manuscript.

Acknowledgments

Table of Contents

List of Tables

List of Figures

List of Abbreviations

A   represents steepness of V_j-gating sensitivity in Boltzmann equation

CL   Cytoplasmic loop of a connexin

CMT1X   X-linked Charcot Marie Tooth disease

Cryo-EM   Cryogenic Electron Microscopy

CT   Carboxyl-terminus of a connexin

Cx26   Connexin26

Cx32   Connexin32

Cx43   Connexin43

Cx46   Connexin46

Cx50   Connexin50

DMEM   Dulbecco's Modified Eagle's medium

DsRed   Red fluorescent protein

EGTA   Ethylene glycol-bis(β-aminoethyl ether)-N,N,N',N'-tetraacetic acid

E1   The first extracellular loop domain of a connexin

E2   The second extracellular loop domain of a connexin

ECS   Extracellular solution

FBS   Fetal Bovine Serum

GFP   Green Fluorescent protein

Gmax   Maximum normalized conductance in Boltzmann equation

G_{min}	Minimum normalized conductance in Boltzmann equation
GJ	Gap junction
G_j	Transjunctional coupling conductance
$G_{j,ss}$	Normalized steady state transjunctional coupling conductance
HEPES	4-(2-hydroxyethyl)-1-piperazineethanesulfonic acid
ICS	Intracellular solution
I_j	Macroscopic junctional current
i_j	Unitary junctional current
IQR	Interquartile range
kDa	Kilo Dalton
M1 – M4	Transmembrane domain 1 – 4 of a connexin
mV	Millivolts
N2A	Mouse neuroblastoma cells
nS	Nanosiemens
NT	Amino terminus
ODDD	Oculodentodigital dysplasia
pIRES	Plasmid containing internal ribosome entry site
pS	Picosiemens
SEM	Standard error of the mean

V_0	Voltage at which the conductance is half between the maximum and minimum
V_j	Transjunctional voltage
γ_j	Gap junction unitary channel conductance

Chapter 1

Introductions

Gap Junctions and Connexins

Gap junctions (GJs) provide direct passage of ions, nutrients, metabolic wastes, and small signalling molecules less than one kiloDalton (kDa) between two adjacent cells (Kumar & Gilula, 1996; Goldberg *et al.*, 1999; Goodenough & Paul, 2009). GJs are formed from two head-to-head docked hemichannels (or connexons), and each hemichannel is oligomerized by six connexin subunits (Saez *et al.*, 2003; Bai, 2016). There are 21 connexin genes in the human genome, encoding connexins that share similar topological structures consisting of four transmembrane domains (M1–M4), two extracellular loops (E1 and E2), one cytoplasmic loop (CL), and amino terminus (NT) and carboxyl terminus (CT) in the cytosol (Fig. 1-1A; Kumar & Gilula, 1996). As most tissue cells express more than one type of connexin isoform, this leads to the formation of a homomeric hemichannel that comprises six identical connexins or a heteromeric hemichannel that is formed by more than one type of connexin isoforms. At the gap junctional level, two identical homomeric hemichannels form homotypic GJs, and two homomeric hemichannels each with different connexins could form functional heterotypic GJ if they are docking compatible (Fig. 1-1; White *et al.*, 1994; Saez *et al.*, 2003; Koval *et al.*, 2014). Gap junctions formed by different connexins give rise to different channel properties, including different unitary channel conductance (γ_j), channel open probability and stability, and transjunctional voltage-dependent gating (known as V_j-gating), which could fine-tune the physiological processes (Goodenough & Paul, 2009).
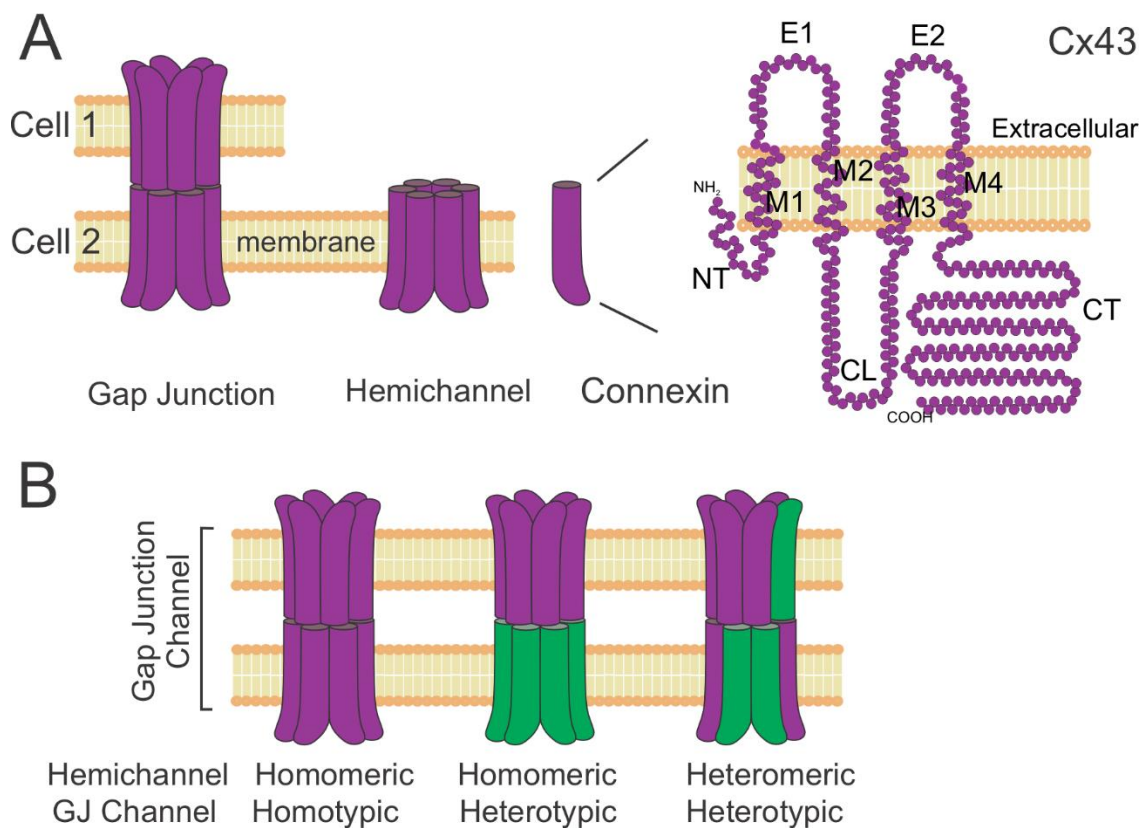
Fig. 1-1. Gap junction structure models and nomenclature.

(A) A GJ channel consists of two docked hemichannels. Each hemichannel is formed by six connexins. The topological structure of Cx43 showed a cytosolic amino terminus (NT), four transmembrane domains (M1 – M4), two extracellular loops (E1 and E2), a cytoplasmic loop (CL), and a carboxyl terminus (CT). (B) GJ channel nomenclature is based on the composition of connexins and hemichannels. Modified from (Bai *et al.*, 2018).

Different connexin isoforms are specifically expressed in different tissue cells of the body. Therefore, heterotypic GJs could be formed at the boundary of two cell types to facilitate intercellular communication. For example, Cx45 is primarily expressed in the sinoatrial (SA) node of the heart, whereas the neighbouring atrial cardiomyocytes express Cx40 and Cx43 (Gourdie *et al.*, 1993; Kanter *et al.*, 1993; Vozzi *et al.*, 1999; van der Velden & Jongsma, 2002). Thus, homomeric or heteromeric heterotypic GJs Cx43 / Cx45 or Cx40 / Cx45 are likely to be found between the SA node and myocytes to maintain the rapid action potential propagation (Severs *et al.*, 2008; Davis *et al.*, 1995; Gros & Jongsma, 1996;

Desplantez *et al.*, 2007). Similarly, homomeric heterotypic GJ could be found between astrocytes and oligodendrocytes in the mammalian central nervous system that exclusively express Cx43, Cx30 and Cx26, and Cx47, Cx32, and Cx29, respectively (Orthmann-Murphy *et al.*, 2007; Magnotti *et al.*, 2011; Kim *et al.*, 2013). Given the high anticipation of heterotypic GJ-mediated intercellular communication throughout the body, connexin gene mutations are likely to disrupt heterotypic GJs and further lead to pathological states.

Each connexin domain is commonly associated with one or more specific GJ functions. The NT domain of several connexins has been shown to play a critical role in GJ channel biophysical properties, including unitary channel conductance (γ_j) and transjunctional voltage-dependent gating (V_j-gating; Verselis *et al.*, 1994; Oh *et al.*, 2004). The charges in the beginning part of the NT domain of Cx26 or Cx32 form a voltage-sensor for V_j-gating (Verselis *et al.*, 1994; Purnick *et al.*, 2000; Oh *et al.*, 2004). A near-atomic resolution structure of human Cx26 supports the model that the NT domain could act as a gating sensor and gating particle to 'plug' the channel pore preventing ion permeation during V_j-gating (Maeda *et al.*, 2009). Meanwhile, E1 and E2 domains are essential for the docking process of hemichannels in Cx32, Cx40, Cx43, Cx46, and Cx50 (White *et al.*, 1994; Haubrich *et al.*, 1996; Pfahnl *et al.*, 1997; Foote *et al.*, 1998). Studies involving the chimera approach, by swapping the extracellular domains of one connexin with the corresponding domains of another connexin, revealed a critical functional role of the E2 domain, but not E1, in determining the heterotypic docking compatibility among lens connexins (White *et al.*, 1994, 1995). The structure model of human Cx26 GJ showed that both E1 and E2 participate in docking (Maeda *et al.*, 2009). The docking of E1-E1 was found to be staggered, with each E1 interacting with 2 E1s on the opposing hemichannel, likely playing a role of the E1 domain in forming a seal to prevent leakage from the inner channel to the extracellular space. In addition, there are 60 hydrogen bonds (HBs) at the docking interface of a Cx26 GJ; 24 of them at the E1-E1 docking interface and 36 at the E2-E2 interface between two hemichannels (Maeda *et al.*, 2009; Bai & Wang, 2014). The formation of these non-covalent interactions between two hemichannels is likely a force to hold two hemichannels together (Bai & Wang, 2014). Transmembrane domains, M1–M4, are four α-helices membrane-spanning regions critical in intra- as well as inter-subunit interactions and contribute to determining the transjunctional voltage-dependent gating and

the unitary channel conductance depending on their position relative to the permeation passage (Jara *et al.*, 2012). Lastly, the less conserved CL and CT domains differ in length in each connexin isoform. The CT domain is important in trafficking and contains many post-translational modulation sites (such as phosphorylation sites), which could also modulate GJ channel clustering and interactions with other proteins (Lampe & Lau, 2004; Leithe *et al.*, 2018).

Transjunctional voltage-dependent gating

Gap junctions (GJ) function can be regulated by a variety of electrical and chemical factors, including transjunctional voltage (V_j), membrane potential (V_m), pH, and intracellular divalent cation concentrations, such as Ca^{2+} and Mg^{2+} (Spray *et al.*, 1981). V_j is the difference in electrical potential between two GJ-coupled cells, which can promote a GJ channel from a fully open state to a much lower conducting state, known as V_j-dependent gating or V_j-gating and it exists in all GJ channels investigated so far (Barrio *et al.*, 1991; Verselis *et al.*, 1994; Revilla *et al.*, 2000). Several connexin domains, including the NT, E1, CL, and CT, have been suggested to be involved in V_j-gating (Nielsen *et al.*, 2012). A substitution in the M1/E1 border domain changed the V_j-gating and unitary channel conductance of the Cx50 GJs (Tong *et al.*, 2014). Negative charge substitutions in the NT domain reversed the Cx32 V_j-gating polarity (Purnick *et al.*, 2000). Moreover, variants at S2 and R8 residues on the NT domain could result in significantly altered V-gating properties with a longer deactivation process in Cx45 GJs (Santos-Miranda *et al.*, 2020). Truncations of the CT domain eliminated the V_j-gating of Cx32, Cx43, and Cx40 and it has been proposed that the CT domain acts as a gating particle in these connexins to close the channel pore when it binds to the CL domain to affect the V_j-gating (Revilla *et al.*, 1999; Anumonwo *et al.*, 2001).

V_j-gating of a GJ can be studied using the dual whole cell patch clamp technique on GJ-deficient cell lines (i.e., mouse neuroblastoma cells, N2A, or human cervical carcinoma cells, HeLa) that are transfected with connexins of interest (Bai & Cameron, 2017). The transjunctional currents (I_js) are recorded in response to the V_j pulses. The relationship of

the normalized steady-state junctional conductance, $G_{j,ss}$ ($G_{j,ss}$ is the normalized steady-state-to-peak-state conductance ratio), and V_j could be fitted with a two-state Boltzmann equation at each V_j polarity (Spray et al. 1981). The fitting parameters quantitatively describe the GJ V_j-gating properties, including the normalized minimal residue conductance (G_{min}, reflecting the extent of V_j-gating), the normalized maximal conductance (G_{max}), half deactivation voltage (V_0, $G_{j,ss} = (G_{max} - G_{min})/2$), and the slope of the Boltzmann fitting curve (*A*, reflecting the V_j sensitivity) (Spray *et al.*, 1981; Harris *et al.*, 1981). Cx50 GJ exhibits prominent V_j-gating with a V_0 of ~40 mV, a low G_{min} (~0.2) and an *A* value of ~0.1 (White *et al.*, 1994; Srinivas *et al.*, 1999). Whereas the V_j-gating of Cx43 GJs is characterized by a big half deactivation voltage (V_0 of 65–70 mV) and a relatively bigger G_{min} (0.35–0.4) and *A* value (~0.15). The I_js of Cx43 GJs could show slight asymmetry because of their dependence on the V_m (White *et al.*, 1994). Unlike Cx50 and Cx43, Cx45 GJ has much lower G_{min} (0.07–0.09) and V_0 (18–23 mV) values and an *A* of ~0.07, making it one of the most V_j-sensitive GJs with a fast deactivation at high levels of V_j and a slow recovery (Desplantez *et al.*, 2004; Rackauskas *et al.*, 2007; Ye *et al.*, 2017; Santos-Miranda *et al.*, 2020).

Connexins in the Lens

Connexin expression in the human lens and cataracts

In the mammalian eyes, the lens is a transparent avascular organ responsible for transmitting light and focusing it on the retina (Goodenough, 1992). There are two cell types in the lens: epithelial cells and lens fiber cells (Fig. 1-2). Epithelial cells form a single layer at the anterior surface. Lens fiber cells are differentiated from epithelial cells through cell elongation and nuclei and organelles degradation (Goodenough, 1992; Beyer *et al.*, 2013). GJ channels mediate the intercellular transfer of ions, nutrients, and metabolic wastes between cells in this avascular organ. Cx43, Cx46 and Cx50 are the three connexins expressed in the lens. Cx43 and Cx50 are expressed in the outer epithelial cells, while Cx46 and Cx50 are found in the mature lens fiber cells that make up the bulk of the lens (Beyer *et al.*, 1989; Paul *et al.*, 1991; White *et al.*, 1992). Because the mature fiber cells contain minimal metabolism, the GJ-mediated circulation from the neighbouring compartments is highly critical to the lens homeostasis (Mathias *et al.*, 2010; Beyer *et al.*, 2013).
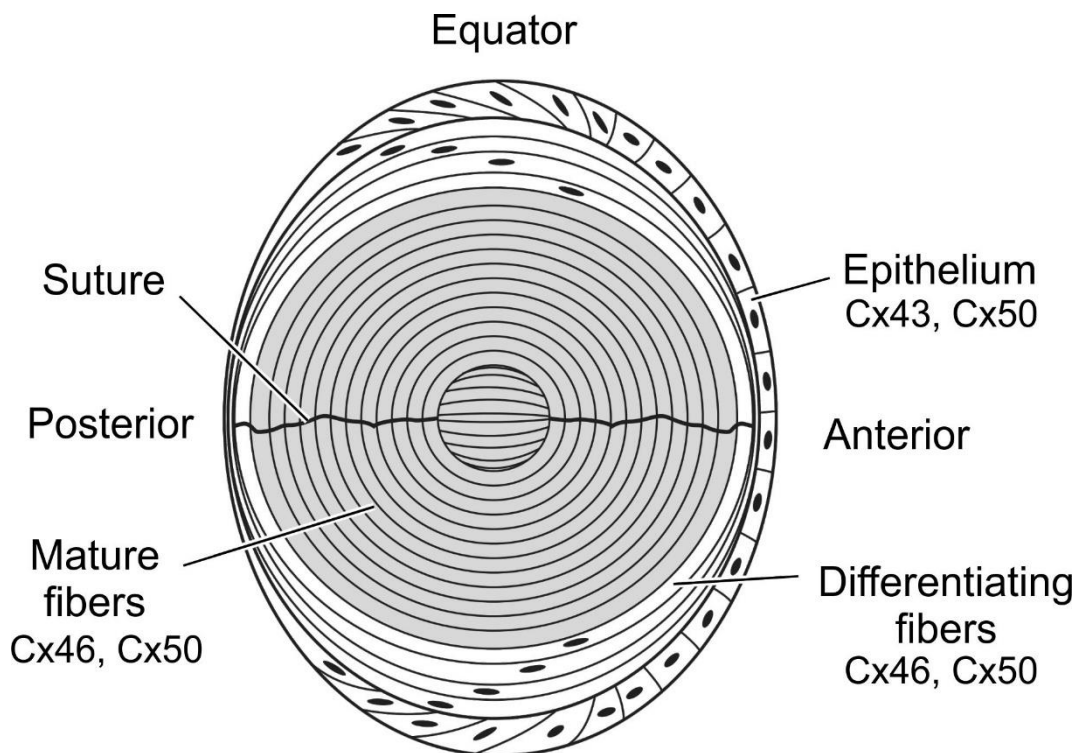
Fig. 1-2. Structure of lens and distribution of lens connexins, Cx43, Cx46, and Cx50.

Cx43, Cx46 and Cx50 are expressed within the human lens. Cx43 and Cx50 are mainly expressed in the epithelial cells. Cx46 and Cx50 are co-expressed within the fiber cells. Modified figure from (Mathias *et al.*, 2010).

A cataract is an opacity or cloudiness in the lens. Patients with cataracts suffer from poor vision, and it is a leading cause of blindness worldwide (Resnikoff *et al.*, 2004). Approximately 50% of cataract cases have a genetic root, and more than 30 genes were involved in non-syndromic forms of congenital cataract (Khan *et al.*, 2018). Mutations in Cx46 and Cx50 genes account for about 20% of non-syndromic inherited cataract cases with 116 reported variants, mainly in autosomal dominant inheritance mode (Bai *et al.*, 2021; Qiu *et al.*, 2022). Mutations in Cx43 genes are primarily associated with oculodentodigital dysplasia, which is rarely accompanied by cataracts and will be described below (Paznekas *et al.*, 2003*a*).

Cx46 and Cx50 knockout mouse models and functional studies of human cataract-linked Cx46 and Cx50 mutations

Genetic studies in mice have demonstrated the importance of GJs and GJ-mediated intercellular communication for normal lens growth and the maintenance of lens transparency. Homozygous knockout (KO) mice of either Cx46 or Cx50 result in cataracts with disrupted proteolysis and crystallite solubility (Gong *et al.*, 1997; Xia *et al.*, 2006). The Cx46 KO mice developed nuclear cataracts with normal lens fiber cell differentiation and early lens development. Whereas the Cx50 KO mice exhibited microphthalmia accompanied with disrupted fiber cell formation, indicating that both Cx46 and Cx50 are critical for lens transparency, but they have different roles pertaining to lens development and physiology (Gong *et al.*, 1997; Rong *et al.*, 2002). Cx43 KO mouse embryos showed normal eyes and lens development and transparency (White *et al.*, 2001); however, Gao and Spray (1998) have observed a more loose connection of epithelial cells and an apparent dilation of extracellular spaces and intracellular vacuoles between fiber cells in those Cx43 KO newborn mice, which indicates an early stage of cataract (Gao & Spray, 1998). Overall, genetic mice studies demonstrated the functional importance of each lens connexin isoform for maintaining lens development and transparency.

Mutations in human Cx46 and Cx50 genes have been associated with human cataracts of various phenotypes. These mutations potentially affect different biochemical and physiological processes of GJ-mediated communication in the human lens. To reveal the molecular and cellular mechanisms of Cx46 and Cx50 mutants leading to cataracts, studies used various model cells to investigate the defects associated with the mutants. For example, Cx50 D47N was identified in a family with autosomal dominant nuclear pulverulent cataracts (Arora *et al.*, 2008). The anti-Cx50 immunoreactivity was restricted to the endoplasmic reticulum (ER) of HeLa cells transfected with Cx50 D47N indicating that Cx50 was unable to form GJ plaques at the cell-cell junctions. Cx50 D47N did not form functional GJ channels when expressed in *Xenopus* oocyte pairs. In addition, the mutant did not act in a dominant-negative manner to inhibit the function of co-expressed wildtype Cx50 (Arora *et al.*, 2008). Another Cx50 mutation, Cx50 P88S, could not form functional GJ channels when paired oocytes homotypically but functioned in a dominant-

negative manner to impair wildtype Cx50 in co-expressed wildtype Cx50 (Pal *et al.*, 1999). These two loss-of-function mutations in Cx50 reduced intercellular communication and thus would be anticipated to reduce the circulation of ions and molecules between lens cells (Beyer *et al.*, 2013).

Functional studies using model cells have increasingly emerged to reveal the molecular and cellular mechanisms of cataracts-linked mutants in Cx46 and Cx50 mostly in homotypic GJ channel function (Pal *et al.*, 1999; Arora *et al.*, 2008; Minogue *et al.*, 2009). Because of the expression of Cx50 in both epithelial cells and fiber cells and the specific expressions of Cx43 and Cx46 in epithelial cells and fiber cells, respectively. It is likely to have homomeric heterotypic GJs formed from two different connexins, including Cx43 / Cx46 GJs between lens fibre cells and epithelial cells and Cx46 / Cx50 GJs between lens fibre cells (Fig. 1-2.). Interestingly, functional studies using oocyte expression of these lens connexins showed that both Cx46 / Cx43 and Cx46 / Cx50 heterotypic GJs, but not Cx50 / Cx43 GJs, are functional (White *et al.*, 1994). However, how cataract-linked connexin mutants affect homomeric heterotypic GJ channel function and channel properties have not been fully studied, leaving a knowledge gap in GJ-mediated cataract pathophysiology.

Cx43 expression and its mutations in oculodentodigital dysplasia (ODDD)

Cx43 is the most widely expressed connexin in various organs of the human body, including the brain, heart, stomach, intestine and bone (Laird, 2006). Mutations in the Cx43 gene linked to oculodentodigital dysplasia (ODDD) and ~89 ODDD-linked mutations were identified in Cx43 (Paznekas *et al.*, 2003*b*, 2009; Bai *et al.*, 2021). The majority of the identified mutations are autosomal dominant missense mutations that occur in the first half of the protein, including the highly conserved domains (NT, M1–4, E1 and E2) (Bai *et al.*, 2021). Because of the wide expression of Cx43 throughout the body, ODDD patients show disease symptoms including teeth and eyes abnormalities, craniofacial deformities, and digital malformations involving multiple digits (Boyadjiev *et al.*, 1999). ODDD patients can also show symptoms such as neuropathies, skin disease, bladder incontinence and other conditions (Loddenkemper *et al.*, 2002; De Bock *et al.*, 2013). There are only a few mutations in Cx43 that have been identified with ocular complications of ODDD, most

commonly glaucoma, possibly due to the expression of Cx43 in the eyes, including the lens, ciliary body, and retina (Musa *et al.*, 2009). Surprisingly, it is rare for ODDD patients with Cx43 mutations to bear a severe heart defect, although Cx43 is highly expressed in the heart (Izumi *et al.*, 2013; Laird, 2014).

Functional studies of ODDD-linked Cx43 mutations

Several ODDD-linked Cx43 mutations have been functionally studied for localization and electrical coupling using a combination of different techniques and various model cells. The initial functional studies of ODDD-associated mutations were conducted on three mutations of the CL domain, I130T, K134E, and G138R. All three mutants impaired the GJ function differently, including reduced GJ plaques formation, low or no electrical coupling and reduced unitary conductance as compared to the wildtype Cx43 (Seki *et al.*, 2004). Another study examined the functional properties of two additional ODDD-associated mutations, Cx43 G21R and G138R. Both mutants were able to transport to the plasma membrane and form GJ plaques (Roscoe *et al.*, 2005). However, neither one of the mutants formed functional GJ channels and exhibited a dominant-negative effect on wildtype Cx43 (Roscoe *et al.*, 2005). In a separate study, eight mutations were examined for localization and GJ electrical coupling analysis. Three of those mutations have been investigated in the two prior studies. Among the rest of them, a codon duplication of the E1 domain, Cx43 F52dup and a missense mutation in the E2 domain, R202H produced full-length connexins but failed to form GJ plaques. Y17S, A40V, and L90V mutants formed GJ plaques but had little or no electrical coupling compared to the wildtype Cx43 (Shibayama *et al.*, 2005). Overall, these functional studies demonstrated the variable functional consequences of homotypic GJ channels formed by connexins with ODDD-linked mutations and the dominant-negative effect of these mutations on co-expressed heteromeric Cx43 GJs, which could be the reason for the pleiotropic nature of ODDD clinical symptoms. In the physiological context, the impairments of heterotypic GJ channels formed by Cx43 mutants and other docking compatible wildtype connexins could also contribute to the complexity of ODDD symptoms. It is imperative that further functional studies are conducted in order to gain a better understanding of the pathophysiological mechanisms of ODDD.

Connexins in the heart

Connexins expression in the human heart

There are three major connexin isoforms in the human heart: Cx40, Cx43 and Cx45. Cx45 is predominantly expressed in the conduction system, including the sinoatrial (SA) or atrioventricular node (AV) and the His-Purkinje system, but in low quantities in ventricles and atria (Fig. 1-3. Bao *et al.*, 2011). Cx43 is the most abundant cardiac connexin that is primarily expressed in the atrial and ventricular cardiomyocytes and is less expressed in the conduction system (Fig. 1-3. Desplantez, 2017). Cx40 is specifically expressed in the atrium and the ventricular conduction system (Fig. 1-3. van der Velden & Jongsma, 2002).
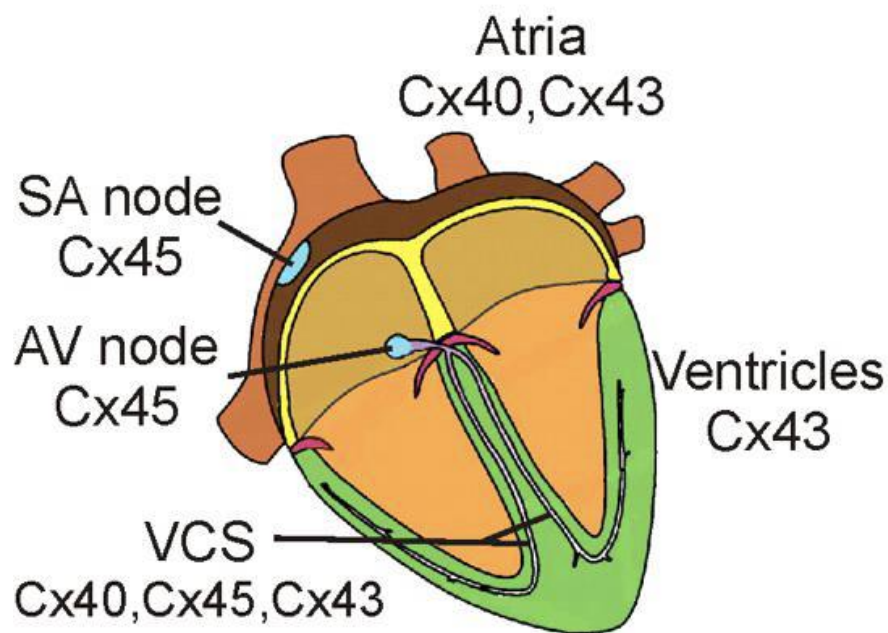
Fig. 1-3. Cardiac connexins distribution in the heart.

There are three connexin isoforms abundantly expressed within the human heart. Cx45 is mainly expressed within the sinoatrial (SA) and the atrioventricular (AV) nodes. Cx40 and Cx43 are expressed within the atria, and all three connexins are expressed in the ventricular conducting system (VCS). Cx43 is also abundantly expressed in the ventricles. Modified from (Severs *et al.*, 2008).

Genetic knockout (KO) or mutations in genes encoding Cx40, Cx43, and Cx45 indicate that these connexins play an important role in normal heart physiology. In the mouse model, cardiomyocyte-specific Cx43 gene KO mice exhibited slow action potential propagation and ventricular arrhythmia, implying the importance of Cx43 in ventricular conduction (Gutstein *et al.*, 2001). Germline or myocardium-specific Cx45 gene KO mice had AV nodal conduction block and embryonic death around embryonic day 10 (Kruger *et al.*, 2000; Nishii *et al.*, 2003). Mutations in the cardiac connexin genes were identified in various heart diseases. Mutations in Cx40 were associated with the early onset of atrial fibrillation (AF), a common cardiac arrhythmia (Goldberg *et al.*, 1999; Bai, 2014). Two missense mutations in Cx45 have also been linked to progressive atrial conduction defect and atrial fibrillation (Seki *et al.*, 2017; Li *et al.*, 2021). Mutations in Cx43 are commonly associated with a pleiotropic disease, ODDD, in which cardiac abnormalities could be rarely seen in ODDD patients (Paznekas *et al.*, 2003*b*). More recently, several Cx43 single-nucleotide polymorphisms (SNPs) were identified and could be potentially related to the risk of AF (Sinner *et al.*, 2014; Ladenvall *et al.*, 2015; Chen *et al.*, 2020; Okamura *et al.*, 2021).

Mutations in Cx45

Cx45 is essential for embryonic survival and abundant at the early stage of cardiac development but decreases drastically in the adult heart (Kumai *et al.*, 2000; Kruger *et al.*, 2000; Nishii *et al.*, 2003). Despite the low expression, a mutation in Cx45 was identified by Seki et al. (2017) in two unrelated families who presented with progressive AV block, which resulted in the atrial standstill without ventricular conduction abnormalities. This mutation, Cx45 R75H, was able to form GJ plaques; however, dye transferring and electrophysiology studies showed that homotypic Cx45 R75H GJs and GJ formed from co-expressed R75H with wildtype Cx45 were severely affected compared to the wildtype Cx45, indicating this mutant acts in a dominant-negative manner (Seki *et al.*, 2017). The homomeric heterotypic GJs Cx45 / Cx43 are likely to be found between the cardiac conduction system to the cardiomyocytes, but the formation of homomeric heterotypic GJs Cx43 / Cx40 and Cx45 / Cx40 showed contradicting results in different studies (Bruzzone

et al., 1993; White *et al.*, 1994; Valiunas *et al.*, 2000; Cottrell & Burt, 2001; Jassim *et al.*, 2016; Ye *et al.*, 2017).

Python-based statistical coupling (pySCA) of the connexins from different species

For years, biologists have tried to decode what information amino acid sequences carry and the relation between the primary sequence of a protein and its function and tertiary structure. Alignment of the primary sequences of a protein family tells us the level of sequence conservation at each amino acid position, and high conservation at a given position indicates the presence of selective pressure and is most likely to be functionally significant (Schneider *et al.*, 1986; Zvelebil *et al.*, 1987). When a larger set of protein sequences from many species becomes available, higher-order statistics such as the correlation between the amino acids found at two sequence positions can be calculated. Highly correlated pairs of amino acid positions are likely to evolve together. This means that a mutation at one position of a protein has to be coupled to another mutation at a different position to survive during evolution selection pressure. Pairwise correlation reveals information about the structure and function of a protein (Russ *et al.*, 2005; Socolich *et al.*, 2005; Weigt *et al.*, 2009). Statistical coupling analysis (SCA) allows the identification of groups of coevolving residues that are functionally important, with different groups controlling different biochemical properties of the protein (Teşileanu *et al.*, 2015; Rivoire *et al.*, 2016).

The connexin protein family is a group of highly conserved transmembrane proteins essential for intercellular communication throughout the human body. Their channel properties were studied through various functional studies and homology modelling of the resolved connexin isoform structure. To better understand the connexin structure and function, our lab previously performed SCA on the connexin protein family (a total of 9201 sequences) using a python-based SCA package (Halabi *et al.*, 2009; Rivoire *et al.*, 2016). A co-variation matrix combing the conservation and correlation information for each residue was generated from a multiple sequence alignment of connexin sequences. Eventually, two sectors that were grouped from eight independent components, including

96 positions, were identified through the spectral analysis (Bai *et al.*, 2021). Interestingly, one sector has residues that map at the interface of intra- and inter-subunits, therefore likely serving a role in the connexin folding and inter-subunit interaction (Bai *et al.*, 2021). The other sector contains residues clustered at the E1 and E2 domains in the primary structure, including the three cysteine residues that form strong disulfate bonds between E1 and E2 domains (Fig. 1-4. C54, C61, and C65 in Cx50) and two HB forming residues in the E1 domain (N55 and Q58 in Cx50). Thus, residues in this sector are likely to be critical for the docking process between two hemichannels and the formation of functional GJs (Bai *et al.*, 2021). Several residues (i.e., P71, S73, H74, R76 and W78 shown in Fig. 1-4) belonging to this sector do not directly lie on the docking interface but could potentially form a strong network with the docking-relevant residues in the 3D structure. SCA uncovered hidden information about amino acid residues in the connexin sequence. Mutagenesis experiments can be conducted to further characterize the functional importance of these residues.
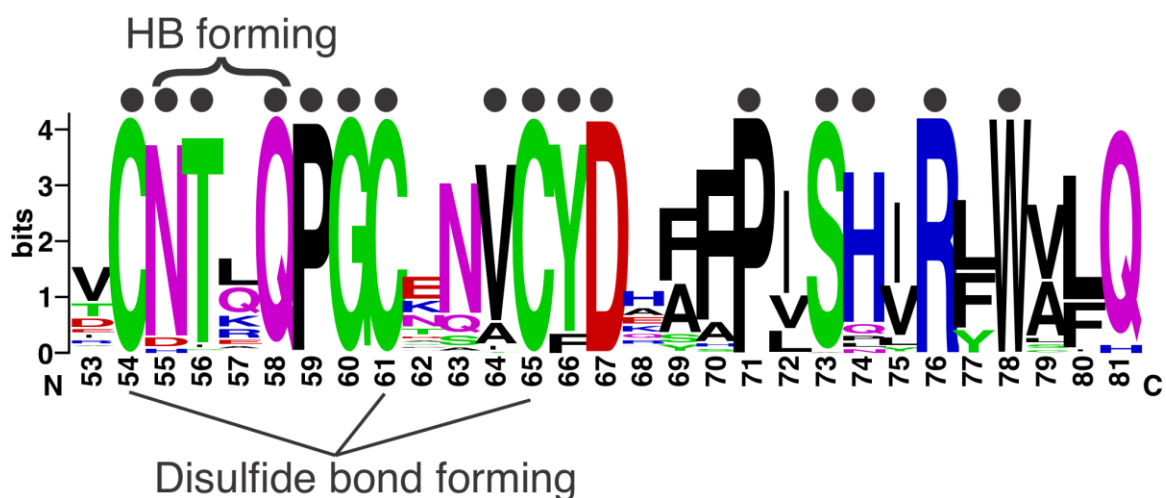
Fig. 1-4. Sequence logo analysis of E1 domain containing triple cystines and the HB-forming residues.

Part of the E1 domain containing triple cystines, HB-forming residues, and residues identified from pySCA analysis from 19 connexins of all available species are aligned with the ClustalO algorithm in the Jalview program (version 2.11.2), and the sequence logo was generated with WebLogo. The triple cystines and docking HB-forming residues are indicated in the figure. They are the C54, C61, C65, N55, and Q58. The closed circles are the indication of residues identified by the pySCA in this part of the E1 domain.

Rationale and hypothesis

It has been found that missense mutations of different amino acid substitutions at Arg 76 (R76 or the equivalent residue) are associated with at least five diseases in six different connexins, indicating that this residue plays an important role in connexin function (Fig. 1-5). Functional studies carried out on *Xenopus* oocytes or model cells expressing these R76 mutants of different connexins showed different degrees of cellular transport and GJ coupling impairments in homotypic mutant GJs (Chen *et al.*, 2005; Huang *et al.*, 2013; Abrams *et al.*, 2013, 2018; Seki *et al.*, 2017); however, the detailed pathophysiological mechanisms of R76 mutations remain unclear in two unstudied connexins, including the congenital cataract-linked mutations, R76H and R76C in Cx50 and the ODDD-linked mutations R76S and R76C in Cx43. Furthermore, it is unclear whether homomeric heterotypic GJs, which are formed when a mutant hemichannel docks with a wildtype hemichannel, are involved in the etiology of various diseases, such as congenital cataracts, ODDD, and progressive atrial conduction defects. Our pySCA analysis of the connexins from many species revealed a cluster of amino acid residues that are covaried with those residues on the docking interface between two hemichannels. Some of the residues in this cluster, including R76, are physically quite distant from the docking interface from the high-resolution structure models (Fig. 1-4), which implies a potential functional role of R76 in the formation of functional homotypic or heterotypic GJ channels (Bai *et al.*, 2021).
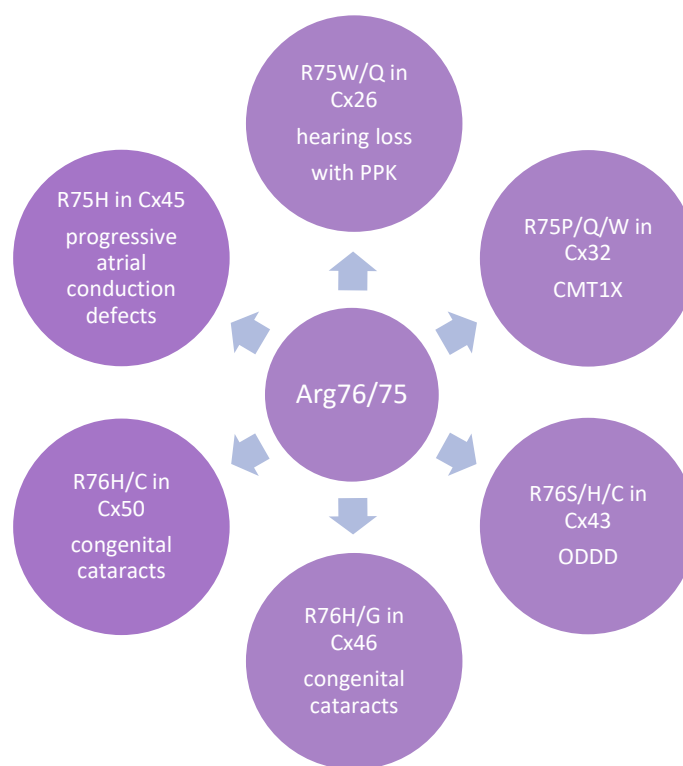
Fig. 1-5. R76 mutations and their associated diseases in different connexins.

Thirteen mutations at R76 or the equivalent residue in six different connexins that associate with five diseases, including hearing loss with palmoplantar keratoderma (PPK), type 1 X-linked Charcot-Marie-Tooth disease (CMT1X), ODDD, congenital cataracts, and progressive atrial conduction defects.

Abram et al. (2018) have shown that the variants at R76 residue (including two cataract-linked mutations and two un-naturally occurring variants) in Cx46 formed GJs with reduced electrical coupling but normal hemichannel functions. Their homology modelling and in silico mutagenesis further demonstrated that R76 residue is in strong dynamic motion with other residues at the docking interface to stabilize the extracellular domain confirmation in Cx46, inferring the reduced electrical coupling observed in mutant GJs was due to the failure of hemichannel docking or formation of functional GJs (Abrams *et al.*, 2018). Together with our pySCA results, R76 is likely a critical residue in the formation of functional GJs in most connexins. To further test this idea and gain insights into cellular

and molecular mechanisms of pathogenic mutations at this well-conserved residue in three connexins, we used dual whole cell patch clamp to examine the functional status of N2A cells transfected with GFP-untagged constructs of cataract-linked mutations, Cx50 R76H and R76C, the ODDD-linked mutations, Cx43 R76H, R76S, and R76C, and the progressive atrial conduction defect-associated mutations, Cx45 R75H.

Objectives

a. To study the GJ functional status of the congenital cataract-linked Cx50 mutations R76H and R76C in homotypic GJs, as well as the mutant hemichannel docked with wildtype Cx50 or Cx46 hemichannels.

b. To study the GJ functional status and Vj-gating properties of the ODDD-associated Cx43 mutations R76H/S/C in homotypic GJs, as well as the mutant hemichannel docked with wildtype Cx43 or Cx45 hemichannels.

c. To study the GJ functional status of the progressive atrial conduction defect-linked Cx45 mutation R75H in homotypic GJ, as well as the mutant hemichannel docked with wildtype Cx45 or Cx43.

d. To investigate whether a lower intracellular or extracellular solution pH (to 6.8) has any effects on GJ coupling status and coupling conductance of Cx45 R75H and Cx50 R76H.

e. To construct homology structure models of these connexin mutants to explore possible structural defects in these mutant GJs.

References

Abrams CK, Islam M, Mahmoud R, Kwon T, Bargiello TA & Freidin MM (2013). Functional Requirement for a Highly Conserved Charged Residue at Position 75 in the Gap Junction Protein Connexin 32*. *J Biol Chem* **288,** 3609–3619.

Abrams CK, Peinado A, Mahmoud R, Bocarsly M, Zhang H, Chang P, Botello-Smith WM, Freidin MM & Luo Y (2018). Alterations at Arg76 of human connexin 46, a residue associated with cataract formation, cause loss of gap junction formation but preserve hemichannel function. *Am J Physiol Cell Physiol* **315,** C623–C635.

Anumonwo JM, Taffet SM, Gu H, Chanson M, Moreno AP & Delmar M (2001). The carboxyl terminal domain regulates the unitary conductance and voltage dependence of connexin40 gap junction channels. *Circ Res* **88,** 666–673.

Arora A, Minogue PJ, Liu X, Addison PK, Russel-Eggitt I, Webster AR, Hunt DM, Ebihara L, Beyer EC, Berthoud VM & Moore AT (2008). A novel connexin50 mutation associated with congenital nuclear pulverulent cataracts. *J Med Genet* **45,** 155–160.

Bai D (2014). Atrial fibrillation-linked GJA5/connexin40 mutants impaired gap junctions via different mechanisms. *FEBS Lett* **588,** 1238–1243.

Bai D (2016). Structural analysis of key gap junction domains—Lessons from genome data and disease-linked mutants. *Semin Cell Dev Biol* **50,** 74–82.

Bai D & Cameron JA (2017). Patch Clamp Analysis of Gap Junction Channel Properties. In *Gap Junction Channels and Hemichannels*, 1st edn., pp. 93–114. CRC Press.

Bai D & Wang AH (2014). Extracellular domains play different roles in gap junction formation and docking compatibility. *Biochem J* **458,** 1–10.

Bai D, Wang J, Li T, Chan R, Atalla M, Chen RC, Khazaneh MT, An RJ & Stathopulos PB (2021). Differential Domain Distribution of gnomAD- and Disease-Linked Connexin Missense Variants. *Int J Mol Sci*; DOI: 10.3390/ijms22157832.

Bai D, Yue B & Aoyama H (2018). Crucial motifs and residues in the extracellular loops influence the formation and specificity of connexin docking. *Biochim Biophys Acta BBA - Biomembr* **1860,** 9–21.

Bao M, Kanter EM, Huang RY, Maxeiner S, Frank M, Zhang Y, Schuessler RB, Smith TW, Townsend RR, Rohrs HW, Berthoud VM, Willecke K, Laing JG & Yamada KA (2011). Residual Cx45 and its relationship to Cx43 in Murine ventricular myocardium. *Channels* **5,** 489–499.

Barrio LC, Suchyna T, Bargiello T, Xu LX, Roginski RS, Bennett MV & Nicholson BJ (1991). Gap junctions formed by connexins 26 and 32 alone and in combination

are differently affected by applied voltage. *Proc Natl Acad Sci U S A* **88,** 8410–8414.

Beyer EC, Ebihara L & Berthoud VM (2013). Connexin mutants and cataracts. *Front Pharmacol* **4,** 43.

Beyer EC, Kistler J, Paul DL & Goodenough DA (1989). Antisera directed against connexin43 peptides react with a 43-kD protein localized to gap junctions in myocardium and other tissues. *J Cell Biol* **108,** 595–605.

Boyadjiev SA, Jabs EW, LaBuda M, Jamal JE, Torbergsen T, Ptáček LJ, Rogers RC, Nyberg-Hansen R, Opjordsmoen S, Zeller CB, Stine OC, Stalker HJ, Zori RT & Shapiro RE (1999). Linkage Analysis Narrows the Critical Region for Oculodentodigital Dysplasia to Chromosome 6q22–q23. *Genomics* **58,** 34–40.

Bruzzone R, Haefliger JA, Gimlich RL & Paul DL (1993). Connexin40, a component of gap junctions in vascular endothelium, is restricted in its ability to interact with other connexins. *Mol Biol Cell* **4,** 7–20.

Chen X, Li G, Zhang J, Huang X, Ye Z & Zhao Y (2020). Association Between GJA1 rs13216675 T>C Polymorphism and Risk of Atrial Fibrillation: A Systematic Review and Meta-Analysis. *Front Cardiovasc Med* **7,** 585268.

Chen Y, Deng Y, Bao X, Reuss L & Altenberg GA (2005). Mechanism of the defect in gap-junctional communication by expression of a connexin 26 mutant associated with dominant deafness. *FASEB J* **19,** 1516–1518.

Cottrell GT & Burt JM (2001). Heterotypic gap junction channel formation between heteromeric and homomeric Cx40 and Cx43 connexons. *Am J Physiol-Cell Physiol* **281,** C1559–C1567.

Davis LM, Rodefeld ME, Green K, Beyer EC & Saffitz JE (1995). Gap Junction Protein Phenotypes of the Human Heart and Conduction System. *J Cardiovasc Electrophysiol* **6,** 813–822.

De Bock M, Kerrebrouck M, Wang N & Leybaert L (2013). Neurological manifestations of oculodentodigital dysplasia: a Cx43 channelopathy of the central nervous system? *Front Pharmacol*; DOI: 10.3389/fphar.2013.00120.

Desplantez T (2017). Cardiac Cx43, Cx40 and Cx45 co-assembling: involvement of connexins epitopes in formation of hemichannels and Gap junction channels. *BMC Cell Biol* **18,** 3.

Desplantez T, Dupont E, Severs NJ & Weingart R (2007). Gap Junction Channels and Cardiac Impulse Propagation. *J Membr Biol* **218,** 13–28.

Desplantez T, Halliday D, Dupont E & Weingart R (2004). Cardiac connexins Cx43 and Cx45: formation of diverse gap junction channels with diverse electrical properties. *Pflüg Arch* **448,** 363–375.

Foote CI, Zhou L, Zhu X & Nicholson BJ (1998). The Pattern of Disulfide Linkages in the Extracellular Loop Regions of Connexin 32 Suggests a Model for the Docking Interface of Gap Junctions. *J Cell Biol* **140,** 1187–1197.

Gao Y & Spray DC (1998). Structural changes in lenses of mice lacking the gap junction protein connexin43. *Invest Ophthalmol Vis Sci* **39,** 1198–1209.

Goldberg GS, Lampe PD & Nicholson BJ (1999). Selective transfer of endogenous metabolites through gap junctions composed of different connexins. *Nat Cell Biol* **1,** 457–459.

Gong X, Li E, Klier G, Huang Q, Wu Y, Lei H, Kumar NM, Horwitz J & Gilula NB (1997). Disruption of α3 Connexin Gene Leads to Proteolysis and Cataractogenesis in Mice. *Cell* **91,** 833–843.

Goodenough DA (1992). The crystalline lens. A system networked by gap junctional intercellular communication. *Semin Cell Biol* **3,** 49–58.

Goodenough DA & Paul DL (2009). Gap Junctions. *Cold Spring Harb Perspect Biol* **1,** a002576.

Gourdie RG, Severs NJ, Green CR, Rothery S, Germroth P & Thompson RP (1993). The spatial distribution and relative abundance of gap-junctional connexin40 and connexin43 correlate to functional properties of components of the cardiac atrioventricular conduction system. *J Cell Sci* **105 (Pt 4),** 985–991.

Gros DB & Jongsma HJ (1996). Connexins in mammalian heart function. *BioEssays* **18,** 719–730.

Gutstein DE, Morley GE, Tamaddon H, Vaidya D, Schneider MD, Chen J, Chien KR, Stuhlmann H & Fishman GI (2001). Conduction Slowing and Sudden Arrhythmic Death in Mice With Cardiac-Restricted Inactivation of Connexin43. *Circ Res* **88,** 333–339.

Halabi N, Rivoire O, Leibler S & Ranganathan R (2009). Protein Sectors: Evolutionary Units of Three-Dimensional Structure. *Cell* **138,** 774–786.

Harris AL, Spray DC & Bennett MV (1981). Kinetic properties of a voltage-dependent junctional conductance. *J Gen Physiol* **77,** 95–117.

Haubrich S, Schwarz HJ, Bukauskas F, Lichtenberg-Fraté H, Traub O, Weingart R & Willecke K (1996). Incompatibility of connexin 40 and 43 Hemichannels in gap junctions between mammalian cells is determined by intracellular domains. *Mol Biol Cell* **7,** 1995–2006.

Huang T, Shao Q, MacDonald A, Xin L, Lorentz R, Bai D & Laird DW (2013). Autosomal recessive GJA1 (Cx43) gene mutations cause oculodentodigital dysplasia by distinct mechanisms. *J Cell Sci* **126,** 2857–2866.

Izumi K, Lippa AM, Wilkens A, Feret HA, McDonald-McGinn DM & Zackai EH (2013). Congenital heart defects in oculodentodigital dysplasia: Report of two cases. *Am J Med Genet A* **161,** 3150–3154.

Jara O, Acuña R, García IE, Maripillán J, Figueroa V, Sáez JC, Araya-Secchi R, Lagos CF, Pérez-Acle T, Berthoud VM, Beyer EC & Martínez AD (2012). Critical role of the first transmembrane domain of Cx26 in regulating oligomerization and function. *Mol Biol Cell* **23,** 3299–3311.

Jassim A, Aoyama H, Ye WG, Chen H & Bai D (2016). Engineered Cx40 variants increased docking and function of heterotypic Cx40/Cx43 gap junction channels. *J Mol Cell Cardiol* **90,** 11–20.

Kanter HL, Laing JG, Beyer EC, Green KG & Saffitz JE (1993). Multiple connexins colocalize in canine ventricular myocyte gap junctions. *Circ Res* **73,** 344–350.

Khan L, Shaheen N, Hanif Q, Fahad S & Usman M (2018). Genetics of congenital cataract, its diagnosis and therapeutics. *Egypt J Basic Appl Sci* **5,** 252–257.

Kim MS, Gloor GB & Bai D (2013). The distribution and functional properties of Pelizaeus–Merzbacher-like disease-linked Cx47 mutations on Cx47/Cx47 homotypic and Cx47/Cx43 heterotypic gap junctions. *Biochem J* **452,** 249–258.

Koval M, Molina SA & Burt JM (2014). Mix and match: Investigating heteromeric and heterotypic gap junction channels in model systems and native tissues. *FEBS Lett* **588,** 1193–1204.

Kruger O, Plum A, Kim JS, Winterhager E, Maxeiner S, Hallas G, Kirchhoff S, Traub O, Lamers WH & Willecke K (2000). Defective vascular development in connexin 45-deficient mice. *Development* **127,** 4179–4193.

Kumai M, Nishii K, Nakamura K, Takeda N, Suzuki M & Shibata Y (2000). Loss of connexin45 causes a cushion defect in early cardiogenesis. *Dev Camb Engl* **127,** 3501–3512.

Kumar NM & Gilula NB (1996). The Gap Junction Communication Channel. *Cell* **84,** 381–388.

Ladenvall P, Andersson B, Dellborg M, Hansson P-O, Eriksson H, Thelle D & Eriksson P (2015). Genetic variation at the human connexin 43 locus but not at the connexin 40 locus is associated with left bundle branch block. *Open Heart* **2,** e000187.

Laird DW (2006). Life cycle of connexins in health and disease. *Biochem J* **394,** 527–543.

Laird DW (2014). Syndromic and non-syndromic disease-linked Cx43 mutations. *FEBS Lett* **588,** 1339–1348.

Lampe PD & Lau AF (2004). The effects of connexin phosphorylation on gap junctional communication. *Int J Biochem Cell Biol* **36,** 1171–1186.

Leithe E, Mesnil M & Aasen T (2018). The connexin 43 C-terminus: A tail of many tales. *Biochim Biophys Acta BBA - Biomembr* **1860,** 48–64.

Li R-G, Xu Y-J, Ye WG, Li Y-J, Chen H, Qiu X-B, Yang Y-Q & Bai D (2021). Connexin45 (GJC1) loss-of-function mutation contributes to familial atrial fibrillation and conduction disease. *Heart Rhythm* **18,** 684–693.

Loddenkemper T, Grote K, Evers S, Oelerich M & Stögbauer F (2002). Neurological manifestations of the oculodentodigital dysplasia syndrome. *J Neurol* **249,** 584–595.

Maeda S, Nakagawa S, Suga M, Yamashita E, Oshima A, Fujiyoshi Y & Tsukihara T (2009). Structure of the connexin 26 gap junction channel at 3.5 Å resolution. *Nature* **458,** 597–602.

Magnotti LM, Goodenough DA & Paul DL (2011). Functional heterotypic interactions between astrocyte and oligodendrocyte connexins. *Glia* **59,** 26–34.

Mathias RT, White TW & Gong X (2010). Lens Gap Junctions in Growth, Differentiation, and Homeostasis. *Physiol Rev* **90,** 179–206.

Minogue PJ, Tong J-J, Arora A, Russell-Eggitt I, Hunt DM, Moore AT, Ebihara L, Beyer EC & Berthoud VM (2009). A Mutant Connexin50 with Enhanced Hemichannel Function Leads to Cell Death. *Invest Ophthalmol Vis Sci* **50,** 5837–5845.

Musa FU, Ratajczak P, Sahu J, Pentlicky S, Fryer A, Richard G & Willoughby CE (2009). Ocular manifestations in oculodentodigital dysplasia resulting from a heterozygous missense mutation (L113P) in GJA1 (connexin 43). *Eye* **23,** 549–555.

Nielsen MS, Axelsen LN, Sorgen PL, Verma V, Delmar M & Holstein-Rathlou N-H (2012). Gap junctions. *Compr Physiol* **2,** 1981–2035.

Nishii K, Kumai M, Egashira K, Miwa T, Hashizume K, Miyano Y & Shibata Y (2003). Mice lacking connexin45 conditionally in cardiac myocytes display embryonic lethality similar to that of germline knockout mice without endocardial cushion defect. *Cell Commun Adhes* **10,** 365–369.

Oh S, Rivkin S, Tang Q, Verselis VK & Bargiello TA (2004). Determinants of Gating Polarity of a Connexin 32 Hemichannel. *Biophys J* **87,** 912–928.

Okamura S, Onohara Y, Ochi H, Tokuyama T, Hironobe N, Okubo Y, Ikeuchi Y, Miyauchi S, Chayama K, Kihara Y & Nakano Y (2021). Minor allele of GJA1 gene polymorphism is associated with higher heart rate during atrial fibrillation. *Sci Rep* **11,** 2549.

Orthmann-Murphy JL, Freidin M, Fischer E, Scherer SS & Abrams CK (2007). Two distinct heterotypic channels mediate gap junction coupling between astrocyte and oligodendrocyte connexins. *J Neurosci Off J Soc Neurosci* **27,** 13949–13957.

Pal JD, Berthoud VM, Beyer EC, Mackay D, Shiels A & Ebihara L (1999). Molecular mechanism underlying a Cx50-linked congenital cataract. *Am J Physiol-Cell Physiol* **276,** C1443–C1446.

Paul DL, Ebihara L, Takemoto LJ, Swenson KI & Goodenough DA (1991). Connexin46, a novel lens gap junction protein, induces voltage-gated currents in nonjunctional plasma membrane of Xenopus oocytes. *J Cell Biol* **115,** 1077–1089.

Paznekas WA, Boyadjiev SA, Shapiro RE, Daniels O, Wollnik B, Keegan CE, Innis JW, Dinulos MB, Christian C, Hannibal MC & Jabs EW (2003*a*). Connexin 43 (GJA1) Mutations Cause the Pleiotropic Phenotype of Oculodentodigital Dysplasia. *Am J Hum Genet* **72,** 408–418.

Paznekas WA, Boyadjiev SA, Shapiro RE, Daniels O, Wollnik B, Keegan CE, Innis JW, Dinulos MB, Christian C, Hannibal MC & Jabs EW (2003*b*). Connexin 43 (GJA1) Mutations Cause the Pleiotropic Phenotype of Oculodentodigital Dysplasia. *Am J Hum Genet* **72,** 408–418.

Paznekas WA, Karczeski B, Vermeer S, Lowry RB, Delatycki M, Laurence F, Koivisto PA, Van Maldergem L, Boyadjiev SA, Bodurtha JN & Wang Jabs E (2009). GJA1 mutations, variants, and connexin 43 dysfunction as it relates to the oculodentodigital dysplasia phenotype. *Hum Mutat* **30,** 724–733.

Pfahnl A, Zhou X-W, Werner R & Dahl G (1997). A chimeric connexin forming gap junction hemichannels. *Pflüg Arch* **433,** 773.

Purnick PE, Oh S, Abrams CK, Verselis VK & Bargiello TA (2000). Reversal of the gating polarity of gap junctions by negative charge substitutions in the N-terminus of connexin 32. *Biophys J* **79,** 2403–2415.

Qiu Y, Zheng J, Chen S & Sun Y (2022). Connexin Mutations and Hereditary Diseases. *Int J Mol Sci* **23,** 4255.

Rackauskas M, Kreuzberg MM, Pranevicius M, Willecke K, Verselis VK & Bukauskas FF (2007). Gating Properties of Heterotypic Gap Junction Channels Formed of Connexins 40, 43, and 45. *Biophys J* **92,** 1952–1965.

Resnikoff S, Pascolini D, Etya'ale D, Kocur I, Pararajasegaram R, Pokharel GP & Mariotti SP (2004). Global data on visual impairment in the year 2002. *Bull World Health Organ* **82,** 844–851.

Revilla A, Bennett MVL & Barrio LC (2000). Molecular determinants of membrane potential dependence in vertebrate gap junction channels. *Proc Natl Acad Sci U S A* **97,** 14760–14765.

Revilla A, Castro C & Barrio LC (1999). Molecular dissection of transjunctional voltage dependence in the connexin-32 and connexin-43 junctions. *Biophys J* **77,** 1374–1383.

Rivoire O, Reynolds KA & Ranganathan R (2016). Evolution-Based Functional Decomposition of Proteins. *PLoS Comput Biol*; DOI: 10.1371/journal.pcbi.1004817.

Rong P, Wang X, Niesman I, Wu Y, Benedetti LE, Dunia I, Levy E & Gong X (2002). Disruption of Gja8 (α8 connexin) in mice leads to microphthalmia associated with retardation of lens growth and lens fiber maturation. *Development* **129,** 167–174.

Roscoe W, Veitch GIL, Gong X-Q, Pellegrino E, Bai D, McLachlan E, Shao Q, Kidder GM & Laird DW (2005). Oculodentodigital Dysplasia-causing Connexin43 Mutants Are Non-functional and Exhibit Dominant Effects on Wild-type Connexin43*. *J Biol Chem* **280,** 11458–11466.

Russ WP, Lowery DM, Mishra P, Yaffe MB & Ranganathan R (2005). Natural-like function in artificial WW domains. *Nature* **437,** 579–583.

Saez JC, Berthoud VM, Branes MC, Martinez AD & Beyer EC (2003). Plasma membrane channels formed by connexins: their regulation and functions. *Physiol Rev* **83,** 1359–1401.

Santos-Miranda A, Chen H, Chen RC, Odoko-Ishimoto M, Aoyama H & Bai D (2020). The amino terminal domain plays an important role in transjunctional voltage-dependent gating kinetics of Cx45 gap junctions. *J Mol Cell Cardiol* **143,** 71–84.

Schneider TD, Stormo GD, Gold L & Ehrenfeucht A (1986). Information content of binding sites on nucleotide sequences. *J Mol Biol* **188,** 415–431.

Seki A et al. (2017). Progressive Atrial Conduction Defects Associated With Bone Malformation Caused by a Connexin-45 Mutation. *J Am Coll Cardiol* **70,** 358–370.

Seki A, Coombs W, Taffet SM & Delmar M (2004). Loss of electrical communication, but not plaque formation, after mutations in the cytoplasmic loop of connexin43. *Heart Rhythm* **1,** 227–233.

Severs NJ, Bruce AF, Dupont E & Rothery S (2008). Remodelling of gap junctions and connexin expression in diseased myocardium. *Cardiovasc Res* **80,** 9–19.

Shibayama J, Paznekas W, Seki A, Taffet S, Jabs EW, Delmar M & Musa H (2005). Functional Characterization of Connexin43 Mutations Found in Patients With Oculodentodigital Dysplasia. *Circ Res* **96,** e83–e91.

Sinner MF et al. (2014). Integrating Genetic, Transcriptional, and Functional Analyses to Identify 5 Novel Genes for Atrial Fibrillation. *Circulation* **130,** 1225–1235.

Socolich M, Lockless SW, Russ WP, Lee H, Gardner KH & Ranganathan R (2005). Evolutionary information for specifying a protein fold. *Nature* **437,** 512–519.

Spray DC, Harris AL & Bennett MV (1981). Equilibrium properties of a voltage-dependent junctional conductance. *J Gen Physiol* **77,** 77–93.

Srinivas M, Costa M, Gao Y, Fort A, Fishman GI & Spray DC (1999). Voltage dependence of macroscopic and unitary currents of gap junction channels formed by mouse connexin50 expressed in rat neuroblastoma cells. *J Physiol* **517,** 673–689.

Teşileanu T, Colwell LJ & Leibler S (2015). Protein Sectors: Statistical Coupling Analysis versus Conservation ed. Wilke CO. *PLOS Comput Biol* **11,** e1004091.

Tong X, Aoyama H, Tsukihara T & Bai D (2014). Charge at the 46th residue of connexin 50 is crucial for the gap-junctional unitary conductance and transjunctional voltage-dependent gating. *J Physiol* **592,** 5187–5202.

Valiunas V, Weingart R & Brink PR (2000). Formation of heterotypic gap junction channels by connexins 40 and 43. *Circ Res* **86,** E42-49.

van der Velden HMW & Jongsma HJ (2002). Cardiac gap junctions and connexins: their role in atrial fibrillation and potential as therapeutic targets. *Cardiovasc Res* **54,** 270–279.

Verselis VK, Ginter CS & Bargiello TA (1994). Opposite voltage gating polarities of two closely related connexins. *Nature* **368,** 348–351.

Vozzi C, Dupont E, Coppen SR, Yeh HI & Severs NJ (1999). Chamber-related differences in connexin expression in the human heart. *J Mol Cell Cardiol* **31,** 991–1003.

Weigt M, White RA, Szurmant H, Hoch JA, Hwa T & Fersht A (2009). Identification of Direct Residue Contacts in Protein-Protein Interaction by Message Passing. *Proc Natl Acad Sci U S A* **106,** 67–72.

White TW, Bruzzone R, Goodenough DA & Paul DL (1992). Mouse Cx50, a functional member of the connexin family of gap junction proteins, is the lens fiber protein MP70. *Mol Biol Cell* **3,** 711–720.

White TW, Bruzzone R, Wolfram S, Paul DL & Goodenough DA (1994). Selective interactions among the multiple connexin proteins expressed in the vertebrate lens: the second extracellular domain is a determinant of compatibility between connexins. *J Cell Biol* **125,** 879–892.

White TW, Paul DL, Goodenough DA & Bruzzone R (1995). Functional analysis of selective interactions among rodent connexins. *Mol Biol Cell* **6,** 459–470.

White TW, Sellitto C, Paul DL & Goodenough DA (2001). Prenatal Lens Development in Connexin43 and Connexin50 Double Knockout Mice. *Invest Ophthalmol Vis Sci* **42,** 2916–2923.

Xia C, Cheng C, Huang Q, Cheung D, Li L, Dunia I, Benedetti LE, Horwitz J & Gong X (2006). Absence of α3 (Cx46) and α8 (Cx50) connexins leads to cataracts by affecting lens inner fiber cells. *Exp Eye Res* **83,** 688–696.

Ye WG, Yue B, Aoyama H, Kim NK, Cameron JA, Chen H & Bai D (2017). Junctional delay, frequency, and direction-dependent uncoupling of human heterotypic Cx45/Cx43 gap junction channels. *J Mol Cell Cardiol* **111,** 17–26.

Zvelebil MJ, Barton GJ, Taylor WR & Sternberg MJE (1987). Prediction of protein secondary structure and active sites using the alignment of homologous sequences. *J Mol Biol* **195,** 957–961.

Chapter 2

Manuscript

Abstract

Connexins are a group of integral membrane proteins that form gap junctions (GJs) through the docking of two hemichannels between opposed cells, mediating direct intercellular communication and maintaining homeostasis within tissues and organs. Mutations in genes encoding connexins are frequently associated with inherited diseases, however the underlying molecular and structural mechanisms have not been fully studied. The arginine residue at the 76th (R76) position in connexin50 (Cx50) and the equivalent position in other connexins is fully conserved across the entire connexin family, and is a hot spot for at least five connexin-linked inherited diseases. To better understand the molecular and structural mechanism of mutations on this conserved residue in different connexins, we examined the functional status and properties of GJs containing R76 mutations in Cx50 (R76H and R76C), Cx45 (R75H) and Cx43 (R76H/S/C) with an emphasis on homomeric heterotypic GJs formed by pairing mutant expressing cells with docking compatible connexins. Our data indicated that all tested mutants showed a significantly decreased percentage of coupled cell pairs and a lowered coupling conductance (G_j), except for Cx43 R76H and R76S, but had altered channel gating properties. Most of our tested mutants also showed reduced % of coupled cell pair and G_j when paired with corresponding wildtype or a docking-compatible connexin. Our homology structure models indicated that mutants on R76 or the equivalent residue in these connexins led to a loss of intra- or inter-connexin non-covalent interactions (salt bridges) at the sidechain of this residue, which could contribute to the observed GJ impairments and/or functional changes of the mutants leading to diseases.

Introduction

Gap junctions (GJs) are clusters of intercellular channels that provide direct passage of ions, nutrients, metabolic wastes, and small signaling molecules between two adjacent cells (Kumar & Gilula, 1996; Goldberg *et al.*, 1999; Goodenough & Paul, 2009). Each GJ is formed from two head-to-head docked hemichannels (or connexons), of which each hemichannel is comprised of six connexins (Goodenough & Paul, 2009). A total of 21 connexin genes are found in the human genome, encoding for connexins that share similar topological structures consisting of four transmembrane domains (M1–M4), two extracellular loops (E1 and E2), one cytoplasmic loop (CL), and amino terminus (NT) and carboxyl terminus (CT) in the cytosol (Kumar & Gilula, 1996). Connexin expression is tissue- and cell-specific and each tissue cell expresses one or more connexin isoforms, leading to the formation of homotypic, heterotypic, and/or heteromeric GJs (Saez *et al.*, 2003; Goodenough & Paul, 2009). GJs of different connexins display different channel properties, including distinct sensitivity to pH changes, different rates of ion permeation (also known as single channel conductance) as well as channel open stability, various permeability, and transjunctional voltage-dependent gating (also known as V_j-gating) (Goodenough & Paul, 2009; Bargiello *et al.*, 2018).

Connexin 43 (Cx43), Cx46 and Cx50 are expressed in the lens of the mammalian eyes within the lens epithelial cells and the lens fiber cells, to facilitate ion and nutrient circulation as well as maintain lens homeostasis and transparency (Goodenough, 1992). Cx43 and Cx50 are expressed in the epithelial cells that form a single layer at the anterior surface of the lens, while Cx46 and Cx50 are found in the mature lens fiber cells that make up the bulk of the lens (Beyer *et al.*, 1989; Paul *et al.*, 1991; White *et al.*, 1992). In the human heart, Cx40, Cx43 and Cx45 are predominantly expressed. Cx40 is mainly expressed in the atria and the ventricular conduction system. Cx43 is found in the atrial and ventricular cardiomyocytes, and the Cx45 is expressed in the sinoatrial (SA) node, atrioventricular (AV) node, and the ventricular conduction system (van der Velden & Jongsma, 2002; Bao *et al.*, 2011; Desplantez, 2017). The intercellular communication mediated by cardiac GJs is critical to the rapid propagation of action potentials and for maintaining a synchronized myocardial contraction (Guo & Yang, 2022). Given the

specific expression patterns in the lens and the heart as well as many other organs in the human body, both homomeric homotypic and heterotypic GJs could be formed from different connexins; these GJs are expected to participate in various biological processes, such as development, differentiation, and the synchronized electrical activities, such as the GJs within the heart (Goodenough & Paul, 2009).

The importance of the extracellular loop domains (E1 and E2) in hemichannel docking and formation of functional GJs are predicted as they are the only extracellular domains for all connexins. Both connexin E1 and E2 domains showed many conserved residues among different connexins, including regularly spaced triple cysteine residues in both E1 and E2 which form intra-connexin disulfide bonds between E1 and E2, which are likely important for the connexin to fold into a proper structure capable of oligomerization into hemichannels (Dahl *et al.*, 1991; Foote *et al.*, 1998; Bao *et al.*, 2004; Tong *et al.*, 2007). High-resolution GJ structures provide excellent experimental evidence for the critical role of several key residues in E1 and E2 for docking interactions, specifically 60 hydrogen bonds (HB) could be formed between two docked hemichannels at the E1-E1 and E2-E2 docking interface (Maeda *et al.*, 2009; Bai & Wang, 2014). Mutations on some of these HB-forming residues impaired formation of morphological and functional GJs in Cx26, Cx32, and Cx46 (Nakagawa *et al.*, 2011; Gong *et al.*, 2013; Schadzek *et al.*, 2016*b*, 2016*a*; Karademir *et al.*, 2016). For example, a variant of Cx32, N175D on the E2 domain is predicted to lose most of the HBs at the E2-docking interface, which failed to form GJ-plaques and functional GJs. However, designed complementary Cx26 variants could restore a sufficient number of the HBs and the GJ channel functions, indicating that this HB forming residue of Cx32 is critical in the docking process to form functional homotypic Cx32 and heterotypic Cx32 / Cx26 GJ channels (Gong *et al.*, 2013). Some of these HB-forming residues in the E1 and E2 have also been shown to be important for heterotypic docking compatibility in cardiac and vascular connexins (Jassim *et al.*, 2016; Ye *et al.*, 2017; Kim *et al.*, 2019). More importantly these docking HB-forming residues are hot spots for inherited human disease-linked connexin mutants (Bai *et al.*, 2018), arguing their importance for normal GJ function. In addition to these residues' direct contribution to docking at the docking interface, several other residues in E1 are also well conserved among different connexins and are hotspots for inherited human diseases linked to

connexin mutants. One such residue is arginine76 (R76) which is located at the end of the E1 domain (near the M2 domain) quite distant from the hemichannel docking interface. Thirteen mutations at the R76 or equivalent residues in six connexins have been found in five different inherited diseases (Richard *et al.*, 1998; Uyguner *et al.*, 2002; Yum *et al.*, 2002; Paznekas *et al.*, 2003; Pizzuti *et al.*, 2004; Burdon *et al.*, 2004; Devi *et al.*, 2005; Reis *et al.*, 2013; Izumi *et al.*, 2013; Yu *et al.*, 2016). However, the molecular and structural mechanisms of the mutations at R76 or equivalent residues have not been fully studied, while some of the recently identified connexin mutants on this residue have not been characterized at all.

Two independent approaches have shown some evidence that R76 or equivalent residue in different connexins may correlate with those HB-forming residues at the docking interface. First, Abram et al. (2018) demonstrated the importance of the R76 residue in forming functional homotypic Cx46 GJs. The two cataract-linked R76 mutations, R76H and R76G in Cx46 formed GJ with reduced GJ coupling conductance as well as the GJ plaques. Their Cx46 GJ homology models based on a crystal structure of Cx26 GJ revealed that R76 residue could form intra- and inter-subunit salt bridges to stabilize the extracellular domain conformation and dynamics affecting hemichannel docking. Thus, the R76 mutants in Cx46 greatly affected the Cx46 hemichannel docking to form a GJ channels (Abrams *et al.*, 2018). Next, we had previously performed a python-based statistical coupling analysis (pySCA) on over 9000 connexin protein sequences and identified a group of residues, including R76, that are co-evolving during evolution. Most importantly, R76 or equivalent residue co-varies (or co-evolves) with those HB forming residues and several other residues near the hemichannel docking interface (Bai *et al.*, 2021). These pySCA results provided further evidence that R76 may be important in hemichannel docking and GJ formation. In the present study, we tested this idea in a total of six disease-linked mutations in three connexins, including the cataract-linked mutations, Cx50 R76H and R76C (Reis *et al.*, 2013; Yu *et al.*, 2016; Wang *et al.*, 2020), ODDD-linked mutations, Cx43 R76H, R76S, and R76C (Paznekas *et al.*, 2003; Pizzuti *et al.*, 2004; Izumi *et al.*, 2013), and a progressive atrial conduction defect-linked mutation, Cx45 R75H (Seki *et al.*, 2017). We examined the functional status and properties of cell pairs both expressing the R76 mutants or cell pairs with one expressing the mutants and the other expressing the wildtype docking

compatible connexins, as most of these R76 mutants are linked to autosomal dominantly inherited diseases. Our results showed that out of all the connexin mutant expressing cell pairs, only the Cx43 R76H and R76S formed functional homotypic GJs as well as functional homomeric heterotypic GJs with wildtype Cx45. Our results suggest that inherited disease-linked mutants Cx45 R75H, and Cx50 R76H, R76C showed impaired GJ function in mutant GJs and GJs between cell pairs with one expressing mutant and the other expressing corresponding wildtype or docking compatible connexins. The functional status of Cx43 R76S and R76H appeared to be similar to wildtype Cx43, but the V_j-gating properties were partially altered. In addition, our preliminary data indicates that the unitary channel conductance (γ_j) of GJs formed by R76S mutants was decreased. Such impairments in these mutants on homomeric homotypic or heterotypic GJs may play a role in the pathogenesis of mutant-associated diseases.

Method

Plasmid construction

We used expression constructs (pIRES2) with an untagged fluorescent reporter gene, encoding either GFP or DsRed. Sheep Cx50-IRES-GFP (also known as Cx49 or sCx50) and Cx50-IRES-DsRed, Cx46-IRES-GFP (sCx46, also known as Cx44) and Cx46-IRES-DsRed, human Cx45-IRES-GFP, Cx45-IRES-DsRed, and human Cx43-IRES-GFP and Cx43-IRES-DsRed were generated as previously described (Ye *et al.*, 2017; Yue *et al.*, 2021). Briefly the cDNAs of Cx50 or Cx46 were synthesized and each of them was inserted into the expression vector at the restriction enzyme sites, XhoI and EcoRI (NorClone Biotech Laboratories, London, Ontario). The cDNAs of Cx43 and Cx45 were inserted at the restriction enzyme sites, EcoRI and BamHI (Cx43) and SacI and EcoRI (Cx45). These vectors were used as templates to generate point mutations at R76 (or R75 in Cx45) position. The following primers were used:

Cx50 R76H: forward 5'C ATC TCC CAC ATC CAT CTC TGG GTC CTG3' and reverse 5'C ATC TCC CAC ATC CAT CTC TGG GTC CTG3'

Cx50 R76C: forward 5'C ATC TCC CAC ATC TGT CTC TGG GTC CTG3' and reverse 5'CAG GAC CCA GAG ACA GAT GTG GGA GAT G3'

Cx45 R75H: forward 5' CTC TCC CAT GTA CAC TTC TGG GTG TTC 3' and reverse 5' GAA CAC CCA GAA GTG TAC ATG GGA GAG 3'

Cx43 R76H: 5'CCA ATC TCT CAT GTG CAC TTC TGG GTC CTG3' and reverse 5'CAG GAC CCA GAA GTG CAC ATG AGA GAT TGG3'

Cx43 R76S: forward 5'CCA ATC TCT CAT GTG AGC TTC TGG GTC CTG3' and reverse 5'CAG GAC CCA GAA GCT CAC ATG AGA GAT TGG3'

Cx43 R76C: forward 5'CCA ATC TCT CAT GTG TGC TTC TGG GTC CTG3' and reverse 5'CAG GAC CCA GAA GCA CAC ATG AGA GAT TGG3'

Cell culture and transient transfection

Gap junction deficient neuroblastoma (N2A) cells (American Type Culture Collection, Manassas, VA) were cultured and grown in Dulbecco's modified Eagle's medium (DMEM) containing 4.5 g/L D-(+)-glucose, 584 mg/L L-glutamine (4 mM), 110 mg/L sodium pyruvate, 10% fetal bovine serum (FBS), 1% penicillin (100 units/mL), and 1% streptomycin (100 μg/mL or 172 μM), in an incubator with 5% CO_2 at 37°C (Sun *et al.*, 2013). N2A cells at ~60% confluence were transfected with 1.0 μg of a cDNA construct and 2 μL of X-tremeGENE HP DNA transfection reagent (Roche Diagnostics GmbH, Indianapolis, IN, USA) in Opti-MEM + GlutaMAX medium for 5 hours following the manufacture's guidelines. The medium was changed back to FBS-containing DMEM after transfection and cells were incubated overnight. For cells expressing connexin mutants for homotypic GJ studies, the transfected cells were replated onto glass coverslips for 5 hours for Cx50 mutants, 2 hours for Cx45 mutant, and 40 minutes for Cx43 mutants, before being transferred to the recording chamber. For studies involving cell pairs with one expressing GFP and the other expressing DsRed, independent transfections were performed and then the cells with different transfections were mixed during the replating step after 5 hours for Cx50 mutants, 2 hours for Cx45 mutants (in some cases 12 hours was required to allow for sufficient GJ formation), and 40 min for Cx43 mutants.

Electrophysiological recording

Glass coverslips with transfected cells were placed into a recording chamber on an upright microscope (BX51WI, Olympus). The chamber was filled with extracellular solution (ECS) at room temperature (21 - 24 ºC). The ECS contained (in mM): 135 NaCl, 2 CsCl, 2 CaCl$_2$, 1 MgCl$_2$, 1 BaCl$_2$, 10 HEPES, 5 KCl, 5 D-(+)-glucose, 2 Sodium pyruvate, pH 7.4 or 6.8 with 1M NaOH, and had an osmolarity of 310-320 mOsm. Patch pipettes were pulled using a micropipette puller (PC-100, Narishige International USA Inc., Amityville, NY, USA) and filled with intracellular solution (ICS) containing (in mM): 130 CsCl, 10 EGTA, 0.5 CaCl$_2$, 5 Na$_2$ATP, 10 HEPES, adjusted to pH 7.2 (or 6.8 in some experiments) with 1 M CsOH, and an osmolarity of 290-300 mOsm. Cell pairs both expressing reporter gene (GFP) for studying homotypic GJ function green fluorescent or one with GFP (green) and the other with DsRed (red) for studying mutant / wildtype GJs under a fluorescent microscope were selected for dual whole cell patch clamp recordings. For cell pairs both expressing GFP, cells with different intensities of fluorescence were selected to improve the success rate of obtaining meaningful data. For Cx43 and its mutants, cell pairs expressed low levels of fluorescence were in favour to avoid high G$_j$ as Cx43 forms GJ in less than 40 mins. During whole cell patch clamp, both cells were initially voltage clamped at 0 mV, then a series of voltage pulses ($\pm$20 to $\pm$100 mV with 20 mV increment) were administrated to one of the cells to establish transjunctional voltage (V$_j$). The other cell was held at 0 mV to record transjunctional current (I$_j$) with a MultiClamp 700A amplifier (Molecular Devices, Sunnyvale, CA, USA). The I$_j$ was low-pass filtered (cut-off frequency at 1 kHz) and digitized via an AD/DA converter at a sampling rate of 10 kHz (Digidata 1550, Molecular Devices, Sunnyvale, CA, USA).

Transjunctional voltage-dependent gating

For each selected cell pair, a series of voltage pulses was applied to one cell ($\pm$20 to $\pm$100 mV. In experiments with Cx45 mutants, V$_j$ pulses of $\pm$5 mV were also used because Cx45 is the most sensitive connexins which exhibit V$_j$-gating at $\pm$20 mV.), while transjunctional current (I$_j$) was obtained from the other cell. In most cases, I$_j$ peaked at the beginning of a

7-second V_j pulse, then declines to a steady state at the end (more pronounced with high V_j, ± 40 to ± 100 mV). The gap junctional coupling conductance (G_j) was calculated by $G_j = I_j / V_j$ and a steadier current point towards the last 3 S of a protocol was selected usually the first trace (i.e., ± 20 mV for Cx50 and Cx43, and ± 5 mV for Cx45). Only cell pairs that have G_j lower than 50 nS were selected for the percentage of coupled cell pairs and the coupling conductance calculations to avoid cytoplasmic bridges. Recordings with bad seals were eliminated by examining the current response to a 10 mV pulse before the protocol (current responses over 50 pA were eliminated). Only cell pairs that have G_j lower than 9 nS were selected for the transjunctional voltage-dependent gating (V_j-gating) study to avoid voltage clamp errors. The steady-state G_j was normalized to the peak G_j to obtain a normalized steady-state junctional current ($G_{j,ss}$) for each V_j. A $G_{j,ss}$ to V_j plot was then generated and fitted with a two-state Boltzmann equation for both V_j polarity to obtain gating parameters. The Boltzmann equation is:

$$G_{j,ss} = \frac{G_{max} - G_{min}}{1 + \exp\left[A(V_j - V_0)\right]} + G_{min}$$

V_0 is the voltage at which the conductance, $G_{j,ss}$ is reduced by half [(G_{max} - G_{min})/2]. G_{max} is the normalized maximum conductance, while G_{min} is the normalized minimum conductance. "A" is the slope of the fitted curve that represents the V_j-gating sensitivity (Spray *et al.*, 1981).

Unitary channel analysis

We recorded unitary channel currents (i_js) in cell pairs that showed 1-2 functional GJ channels. The recorded currents were filtered using a lowpass Gaussian filter (200 Hz) in Clampfit10.3 (Molecular Devices, Sunnyvale, CA, USA). All-point histograms were generated for a portion of i_js in response to V_js and used to determine the amplitude of the open state and the subconductance (also known as substate or residue state) state after fitting these histograms with two or more Gaussian functions. The i_js at each V_j (regardless of V_j polarity) of different cell pairs were plotted against V_j to generate the i_j–V_j plot. Unitary channel conductance (γ_j) was determined by the slope of linear regression of i_j-V_j plot using GraphPad Prism (version 9.3.1, San Diego, California, USA).

Homology structure modelling

Homology structure models of human Cx43 and Cx45 were generated based on the sheep Cx50 GJ cryogenic electron microscopy (Cryo-EM)-derived structure (7JJP) (Flores *et al.*, 2020) using Modeller (version 9.17, Andrej Sali Lab, San Francisco, CA, USA). The Cx50 R76H/C, Cx43 R76H/S/C or Cx45 R75H mutants' structures were generated using the mutagenesis tool in pyMOL (version 2.4.1). We chose the side chain orientations that had low level clash with the neighbouring residues and also tried to keep similar orientation to the wildtype arginine orientation.

Statistical analysis

All bar graphs of the percentage of cell pairs coupled (% cell pairs coupled) and coupling conductance (G_j) are expressed as median (interquartile range, IQR). Kruskal Wallis followed by an uncorrected Dunn's post-hoc test was used to compare % cell pairs coupled and G_j for Cx50, Cx43, and their mutant cell pairs. For analyses of % cell pairs coupled and G_j of Cx45 and its mutant, a Mann-Whitney test was used. For analyses of V_j-gatings of the Boltzmann fitting parameters for mutants to compare with the wildtype, an unpaired t-test was used and the mean ±SEM. Statistical significance is indicated with the asterisks on the graphs only for biologically meaningful group comparisons (*$P < 0.05$; **$P < 0.01$; or ***$P < 0.001$).

Results

Cx50 mutants, R76H and R76C showed decreased percentages of cell pairs coupled and coupling conductance (G_j) than those of the wildtype Cx50

To study the functional status of two cataract-linked mutants, Cx50R76H and R76C, isolated N2A cell pairs expressing Cx50-IRES-GFP, Cx50-R76H-IRES-GFP, or Cx50-R76C-IRES-GFP were selected for dual whole cell patch clamp. The transjunctional currents (I_js) of cell pairs expressing one of the mutants or wildtype Cx50 were recorded in response to a 20 mV V_j pulse. Representative I_js are shown in Fig. 2-1A (left panel). On

average more than half of the tested cell pairs expressing wildtype Cx50 showed I_js in 9 different transfections (50 (50-87.5)% cell pairs coupled, N = 9), while cell pairs expressing either R76H or R76C showed no coupling in 7 out of 8 transfections for each of these mutants (Fig. 2-1B left panel). In one transfection, I_j was only observed in one of 5 recorded cell pairs for each of these mutants. The average percentages of cell pairs coupled for these mutants were significantly reduced from that of wildtype Cx50 (0 (0)% for R76H, 0 (0)% for R76C, ***P < 0.001 for both mutants). In addition, coupling conductance (G_j) was measured for each cell pair expressing R76H or R76C (Fig. 2-1C left panel). The average G_js were 0 (0) nS for R76H (n = 30) and 0 (0) nS for R76C (n = 36), which were significantly lower than the G_j of wildtype Cx50 (0.85 (0-4.02) nS, n = 32, ***P < 0.001 for both mutants).

Cx50 mutants, R76H and R76C pairing with wildtype Cx50 and Cx46

Similar experiments were conducted on cell pairs with one expressing R76H (or R76C) and the other expressing either wildtype Cx50 or Cx46 each with an untagged red fluorescent reporter (i.e., Cx50-IRES-DsRed or Cx46-IRES-DsRed). Representative I_js are shown in Fig. 2-1A middle and right panels. As shown in Fig. 2-1B middle and right panels, these cell pairs showed a significantly reduced percentage of cell pairs coupled (12.5 (0-35)%, N = 10, *P = 0.027 for R76H / Cx50; 20 (0-25)% for R76C / Cx50, N = 9, *P = 0.02; 20 (0-25)% for R76H / Cx46, N = 7, *P = 0.015; 8.35 (0-25)% for R76C / Cx46, N = 14, ***P < 0.001) comparing with those of wildtype Cx50 or Cx50 / Cx46 (60 (25-71)%, N = 9 for Cx50, and 45 (25-52)%, N = 14 for Cx50 / Cx46). Moreover, G_j was measured for these cell pairs (Fig. 2-1C middle and right panels). The average G_js for cell pairs with one R76H (or R76C) and the other one with either wildtype Cx50 or Cx46, were significantly reduced (0 (0) nS for R76H / Cx50, n = 40, *P = 0.012; 0 (0) nS for R76C / Cx50, n = 31, **P = 0.002; 0 (0) nS for R76H / Cx46, n = 34, *P = 0.02; 0 (0) nS for R76C / Cx46, n = 50, **P = 0.001) when compared with those of wildtype Cx50 and Cx50 / Cx46 (0.1 (0-0.58) nS, N = 32 for Cx50 and 0 (0-0.9) nS, N = 47 for Cx50 / Cx46). These results indicate that both Cx50 R76H and R76C when paired with wildtype Cx50 or Cx46 showed reduced functional coupling (G_j) and decreases in % of cell pair coupled for R76C / Cx50 and R76C / Cx46.

Fig. 2-1. Representative junctional current (I_js) and bar graphs to show percentages (%) of cell pairs coupled and coupling conductance (G_j) of homotypic Cx50 mutant GJs, and mutant expressing cells paired with cells expressing wildtype Cx50 or Cx46.

(A) Dual whole cell patch clamp technique was used to measure junctional current (I_j) in response to indicated V_j in N2A cell pairs expressing homotypic wildtype and mutant GJs (left panel), mutant expressing cell paired with wildtype Cx50 (middle panel) or Cx46 (right panel) expressing cell. Representative I_js are shown, and the text colour indicates the untagged reporter fluorescent proteins, green (GFP) and red (DsRed). (B) Bar graphs summarize the average percentage of coupled cell pairs (% cell pairs coupled) expressing homotypic wildtype and mutant GJs (left panel), mutant expressing cell paired with wildtype Cx50 (middle panel) or Cx46 (right panel) expressing cell. Data points represent the number of transfections, and the error bars are ± standard deviation (SD). (C) Bar

graphs illustrate the average coupling conductance ($G_j \pm SD$) of cell pairs examined expressing homotypic wildtype or mutant GJs (left panel), mutant expressing cell paired with wildtype Cx50 (middle panel) or Cx46 (right panel) expressing cell as indicated. Kruskal-Wallis test followed by uncorrected Dunn's post hoc test was used to compare each mutant with their respective controls for all bar graphs. The statistical significance was indicated (* $P < 0.05$, ** $P < 0.01$, and *** $P < 0.001$).

V_j-gating properties of homotypic Cx50 and heterotypic Cx50 / Cx46 GJ channels

Cell pairs expressing wildtype Cx50 or cell pairs expressing Cx50 in one and Cx46 in the other were selected for dual whole patch clamp study on homotypic Cx50 GJs or heterotypic Cx50 / Cx46 GJs, respectively. I_js were recorded in response to a series of V_j pluses from ±20 to ±100 mV (20 mV increment as shown in Fig. 2-2A). The I_js of both homotypic Cx50 and heterotypic Cx50 / Cx46 GJs showed near symmetrical V_j-dependent deactivation (Fig. 2-2A). I_js showed strong deactivation to V_j values in the range from ±40 to ±100 mV and no deactivation when V_j absolute values were ≤ 20 mV (Fig. 2-2A). The normalized steady state conductance ($G_{j,ss}$) was plotted as a function of V_j, which could be fitted by a Boltzmann equation for each V_j polarity (Fig. 2-2B). The Boltzmann fitting parameters of homotypic Cx50 GJs or heterotypic Cx50 / Cx46 GJs are listed in Table 2-1. V_j-gating analysis for cell pairs expressing mutants GJs, or mutants paired with wildtype Cx50 or Cx46 are not shown, as the majority of them did not demonstrate functional coupling (Fig. 2-1B).

Fig. 2-2. V_j-gating of homotypic Cx50 and heterotypic Cx50 / Cx46 GJs.

(A) Superimposed junctional currents (I_js) recorded from cell pairs expressing wildtype Cx50 or cell pairs expressing Cx50 in one and Cx46 in the other in response to a series of V_j pulses (shown on the top, 7 seconds Vj pulse from ±20 to ±100 mV with 20 mV increment). (B) Normalized steady state junctional conductance, $G_{j,ss}$ of homotypic Cx50 GJs or heterotypic Cx50 / Cx46 GJs were plotted as a function of V_js. A Boltzmann equation was used to fit $G_{j,ss} - V_j$ plot for each V_j polarity (smooth lines). Error bars on the plots represent SD and the number of cell pairs is indicated.

Cx43 mutants R76C, but not R76H or R76S showed decreased percentages of coupled cell pairs and coupling conductance (G_j) than those of the wildtype Cx43

To investigate the functional status of ODDD-linked Cx43 mutations, R76H, R76S, and R76C, we used the dual whole cell patch clamp technique to study cell pairs expressing Cx43-IRES-GFP, Cx43-R76H-IRES-GFP, Cx43-R76S-IRES-GFP or Cx43-R76C-IRES-GFP. The I_js of cell pairs expressing one of the mutants or wildtype Cx43 were recorded in response to a 20 mV V_j pulse. Representative I_js are shown in Fig. 2-3A left panel. The percentage of cell pairs coupled for R76C was significantly reduced (0 (0)%, N = 7, **P =

0.002) compared to wildtype Cx43 (58.4 (47.5-100)%, N = 6), but not for R76H (60 (42.5-70.9)%, N = 5, P = 0.837) and R76S (60 (42.5-83.4)%, N = 5, P = 0.915). The G_j was measured for each cell pair expressing one of these mutants (Fig 2-3C left panel). The average G_j was 0 (0) nS for R76C (n = 23), which was significantly lower than wildtype Cx43 (4 (0-25.1) nS, n = 24, ***P < 0.001). Neither R76H nor R76S showed any change in G_j from Cx43 G_j (6.3 (0-24.3) nS, n = 19, P = 0.804 for R76H and 0.7 (0-6.7) nS, n = 22, P = 0.229 for R76S).

Cx43 mutants, R76H, R76S and R76C pairing with wildtype Cx43 or Cx45

We conducted similar experiments on cell pairs with one expressing R76H (or R76S, R76C) and the other expressing either wildtype Cx43 or Cx45 with an untagged DsRed (i.e., Cx43-IRES-DsRed or Cx45-IRES-DsRed). Representative I_js are shown in Fig. 2-3A middle and right panels. The percentage of cell pairs coupled were calculated and summarized in Fig. 2-3B middle and right panels. Cell pairs with one expressing R76C and the other expressing wildtype Cx43 showed a lower percentage of cell pairs coupled (0 (0-19)% for R76C / Cx43, N = 8, **P = 0.003) compared to its control (67 (50-90)%, N = 5, Fig. 2-3B middle panel). However, when R76C expressing cells paired with Cx45 expressing cells, the % of cell pairs coupled (40 (29.2-80)%, N = 5, P = 0.252, Fig. 2-3B right panels) was not different from Cx43 / Cx45 cell pairs (58.4 (48.2-100)%, N = 6). In addition, no changes in % cell pairs coupled were observed for R76H or R76S when paired with wildtype Cx43 or Cx45 (Fig. 2-3B middle and right panels). The G_j of cell pairs with one expressing R76C and the other expressing wildtype Cx43 (0 (0) nS, n = 31, ***P < 0.001) were significantly lower than those of its control (3.5 (0-21.1) nS for Cx43, n = 18) but the G_j of R76C / Cx45 (0.05 (0-1.80) nS, n = 24, P = 0.084) was not significantly different from the wildtype Cx43 / Cx45 (7.5 ± 12 nS, n = 20) (Fig. 2-3C middle and right panels). Lastly, the G_js of R76H (or R76S) / Cx43 and R76H (or R76S) / Cx45 were not statistically different from the respective wildtype controls (0.4 (0-10.9) nS, n = 18, P = 0.338 for R76H / Cx43; 4.8 (0-28.1) nS, n = 20, P = 0.819 for R76S / Cx43; 0 (0-4.8) nS, n = 24, P = 0.233 for R76H / Cx45; 0.35 (0-8.98) nS, n = 22, P = 0.745 for R76S / Cx45).
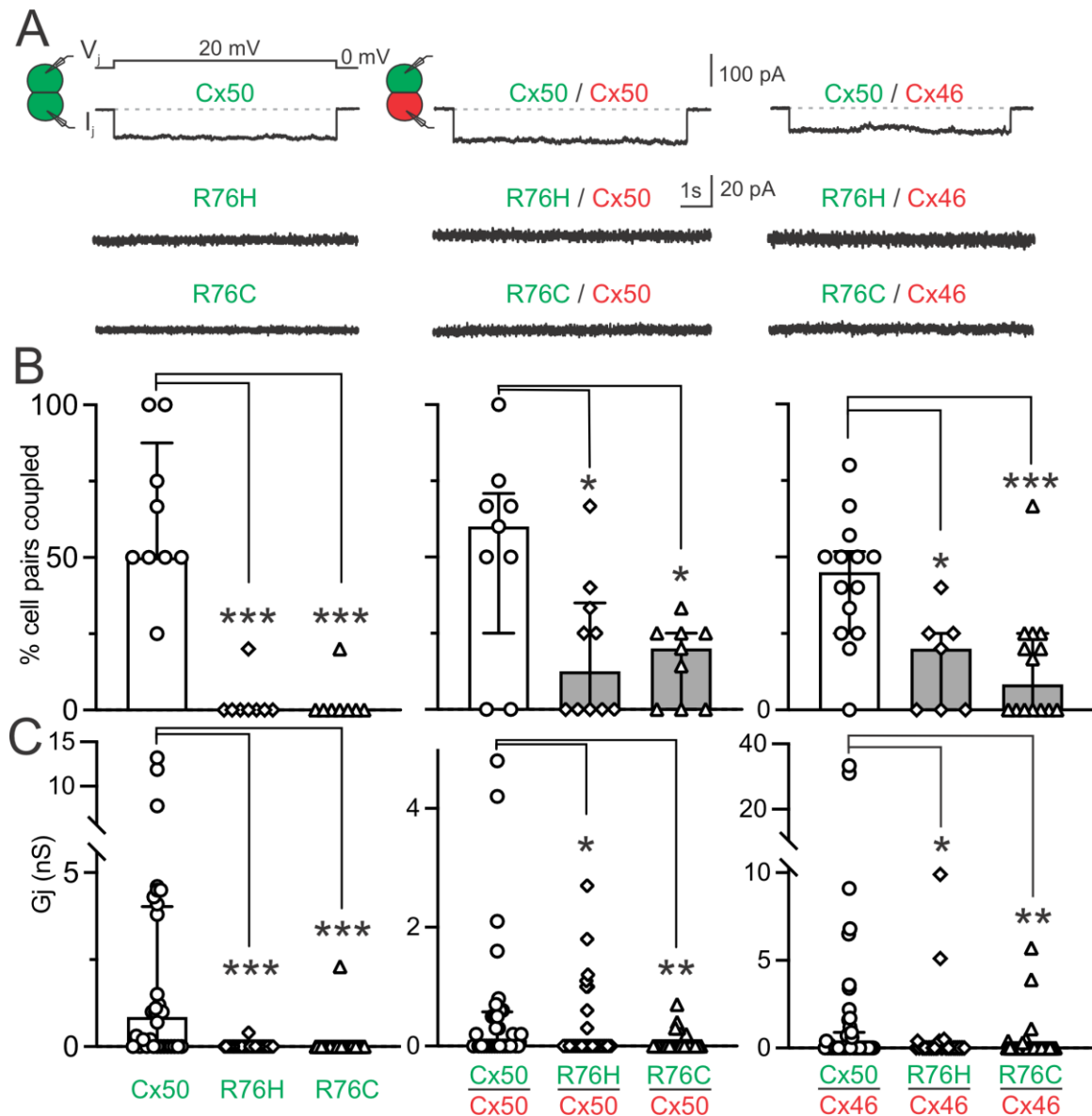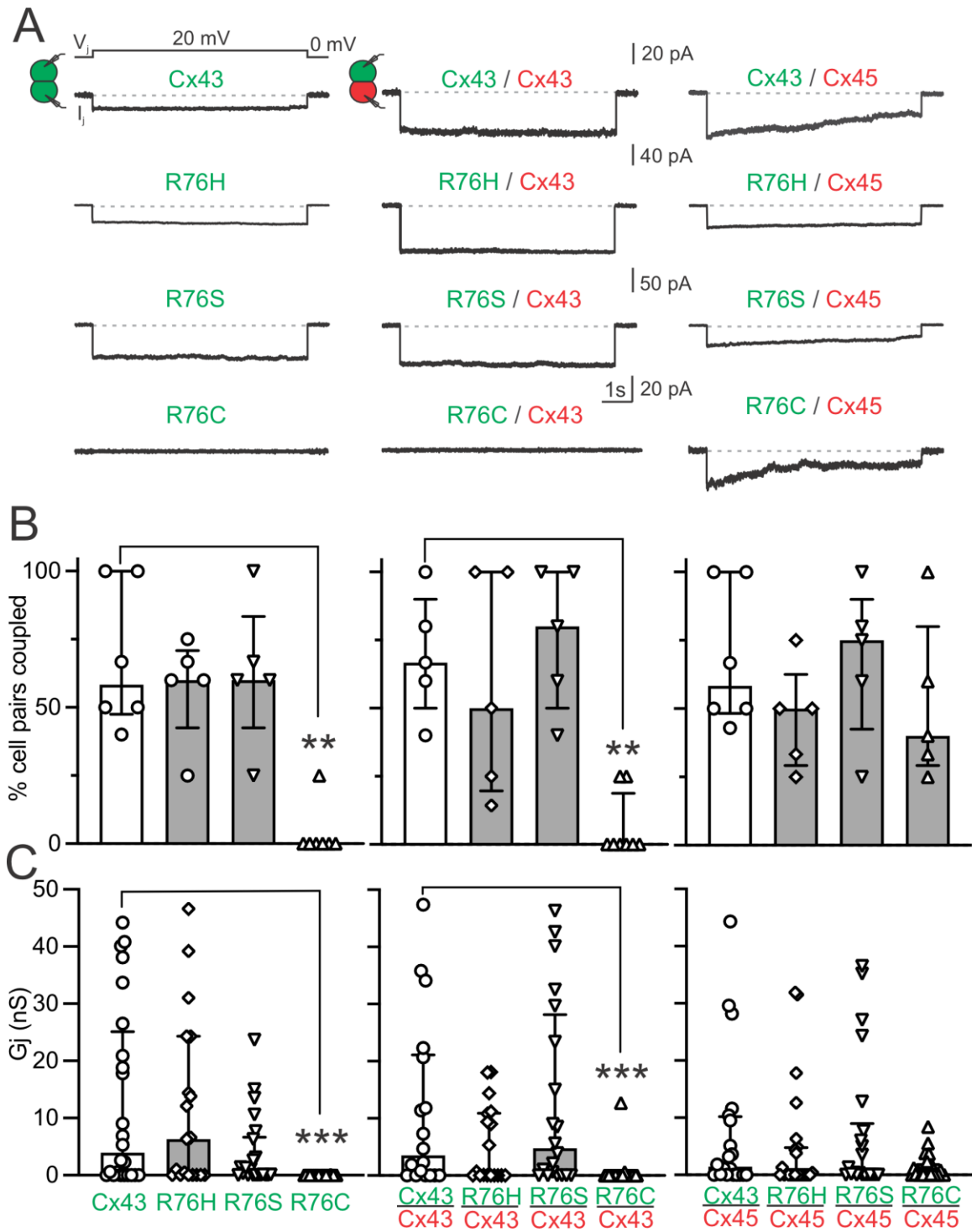
Fig. 2-3. Representative junctional current (I_js) and bar graphs to show percentages (%) of cell pairs coupled and coupling conductance (G_j) of homotypic Cx43 mutant GJs, mutant expressing cells paired with cells expressing either wildtype Cx43 or Cx45.

(A) Dual whole cell patch clamp technique was used to measure junctional current (I_j) in response to indicated V_j in N2A cell pairs expressing homotypic wildtype or mutant GJs (left panel), mutant expressing cell paired with either wildtype Cx43 (middle panel) or wildtype Cx45 (right panel) expressing cell. Representative I_js are shown, and the text colour indicates the untagged fluorescent proteins, green (GFP) and red (DsRed). (B) Bar graphs summarize % cell pairs coupled expressing homotypic wildtype or mutant GJs (left panel), mutant expressing cell paired with either wildtype Cx43 (middle panel) or Cx45 (right panel) expressing cell. Data points represent the number of transfections, and the error bars are ± SD. (C) Bar graphs illustrate the average coupling conductance (G_j ± SD) of cell pairs examined expressing homotypic wildtype or mutant GJs (left panel), mutant expressing cell paired with wildtype Cx43 (middle panel) or Cx45 (right panel) expressing cell as indicated. Kruskal-Wallis test followed by uncorrected Dunn's post hoc test was used to compare each mutant with their respective controls for all bar graphs. The statistical significance was indicated (* $P < 0.05$, ** $P < 0.01$, and *** $P < 0.001$).

V_j-gating properties of homotypic Cx43 and heterotypic Cx43 / Cx45 GJ channels

Cell pairs with one expressing wildtype Cx43 (with untagged GFP) and the other one expressing either Cx43 (with untagged DsRed) or Cx45 (with untagged DsRed) were selected for dual whole cell patch clamp study on homotypic Cx43 GJs or heterotypic Cx43 / Cx45 GJs, respectively. I_js were recorded in response to a series of V_j pulses from ±5 to ±100 mV as shown Fig. 2-4A. The I_js of homotypic Cx43 GJs showed apparent symmetrical V_j-dependent deactivation, and substantial deactivation could be observed from ±80 to ±100 mV (Fig. 2-4A). The I_js of heterotypic Cx43 / Cx45 GJs showed asymmetrical V_j-gating, with strong V_j-dependent inactivation of I_js when the Cx43-expressing cell with +V_js (or the Cx45-expressing cell with -V_js), while no V_j-dependent inactivation of I_js or in this case apparent V_j-dependent activation of I_js at V_js of -60 to -100 mV was observed at opposite V_j polarity (Fig. 2-4A). The normalized steady state conductance ($G_{j,ss}$) was plotted as a function of V_j for homotypic Cx43 and heterotypic Cx43 / Cx45 GJs (Fig. 2-4B). The $G_{j,ss}$ – V_j plot for homotypic Cx43 were well fitted by a Boltzmann equation for each V_j polarity, but the $G_{j,ss}$ – V_j plot for heterotypic Cx43 / Cx45 GJs could only be well fitted when Cx43 cells with +V_js (Fig. 2-4B). Boltzmann fitting parameters of homotypic Cx43 GJs or heterotypic Cx43 / Cx45 GJs are listed in Table 2-2.
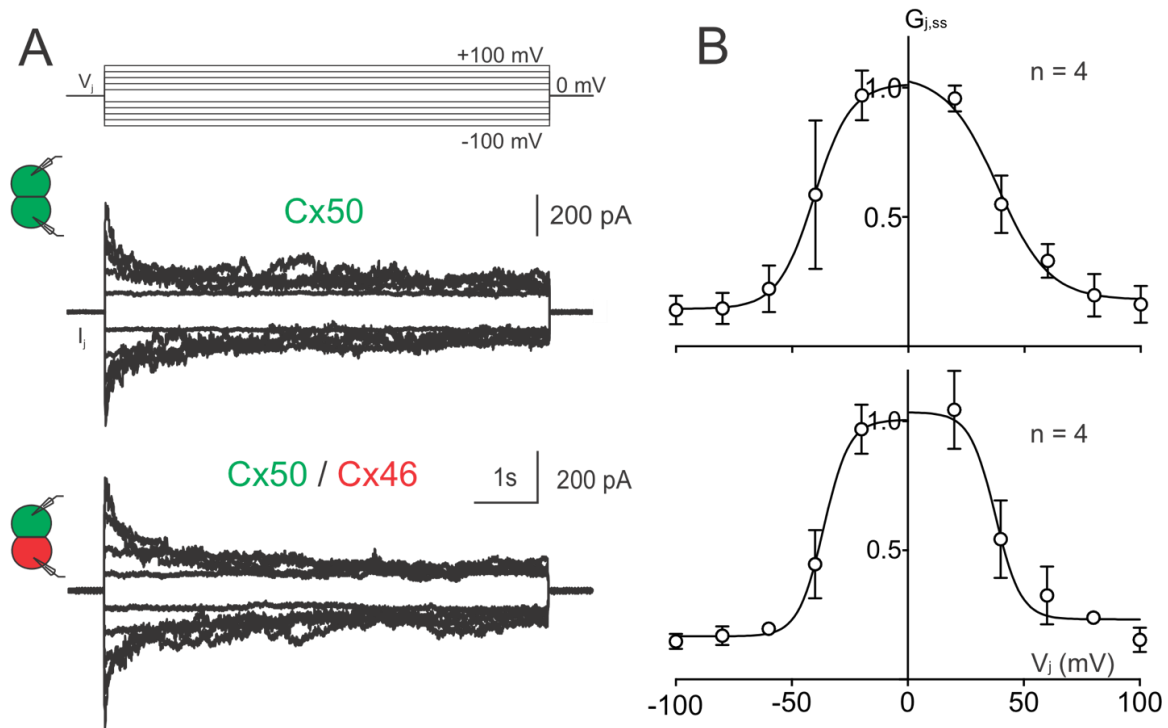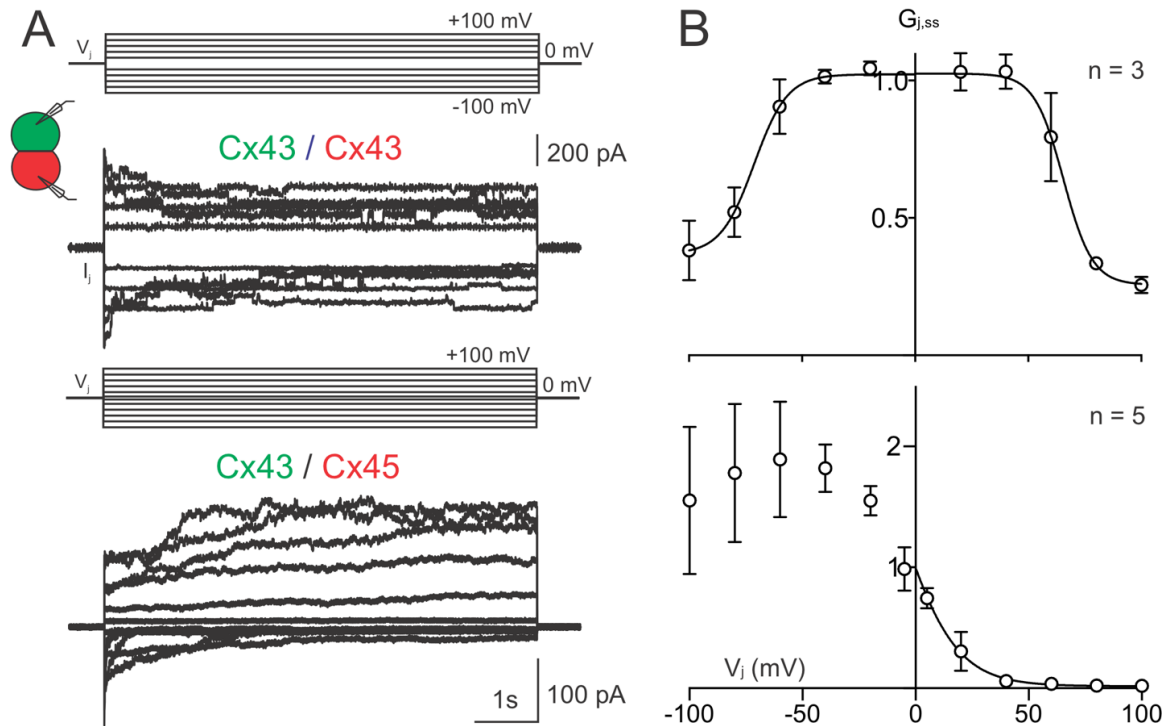
Fig. 2-4. V_j-gating of homotypic Cx43 and heterotypic Cx43 / Cx45 GJs.

(A) Superimposed junctional currents (I_js) recorded from cell pairs with one expressing wildtype Cx43 (with untagged GFP) and the other expressing either Cx43 (with untagged DsRed) or Cx45 (with untagged DsRed) in response to a series of V_j pulses (shown on the top of Fig 2-4A, ±20 to ±100 mV for Cx43 / Cx45 GJs ±5 mV to ±100 mV was used). (B) Normalized steady state junctional conductance, $G_{j,ss}$ of homotypic Cx43 GJs or heterotypic Cx43 / Cx45 GJs were plotted as a function of V_js. A Boltzmann equation was used to fit $G_{j,ss} - V_j$ plot for each V_j polarity. Error bars represent SD, and the number of cell pairs is indicated.

V_j-gating properties of Cx43 R76H and R76S GJs

To investigate whether cell pairs expressing R76H or R76S GJs had alternated V_j-gating properties, their I_js were recorded in response to a series of V_j pulses from ±20 to ±100 mV (Fig. 2-5A). The I_js of R76H and R76S showed near symmetrical V_j-dependent I_j deactivation, and strong deactivation could be observed from ±80 to ±100 mV (Fig. 2-5A). The normalized steady state conductance ($G_{j,ss}$) was plotted as a function of V_j for R76H and R76S GJs (Fig. 2-5B). The $G_{j,ss} - V_j$ plot for R76H were well fitted by a Boltzmann equation for $-V_j$ (Fig. 2-5B top panel). The $G_{j,ss} - V_j$ plot for R76S were well fitted by a

Boltzmann equation for both V_j polarities (Fig. 2-5B bottom panel). Boltzmann fitting parameters of R76H and R76S GJs are listed in Table 2-2. There were no significant differences observed for all Boltzmann parameters between mutants and wildtype Cx43 GJs, except for the G_{min} and V_0 values for the negative polarity of R76S GJs (Table 2-2). V_j-gating properties for Cx43 R76C GJs were not studied because most cell pairs expressing R76C did not exhibit GJ coupling (see Fig. 2-3A).
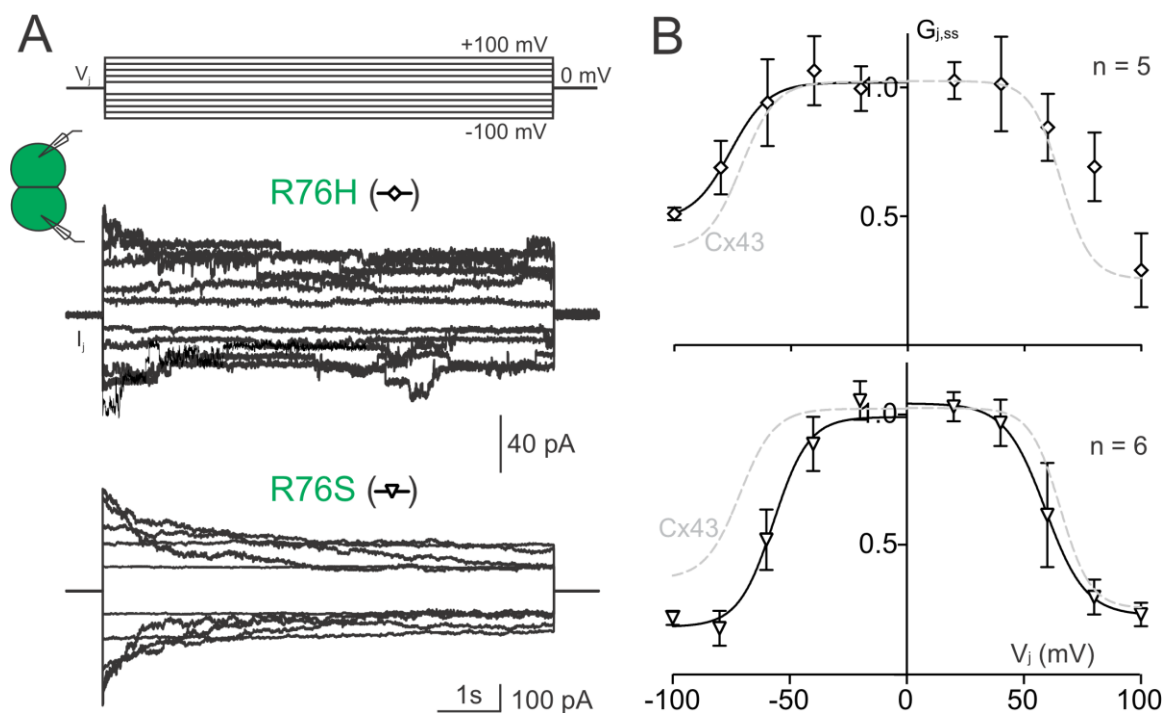
Fig. 2-5. V_j-gating of homotypic Cx43 R76H and R76S GJs.

(A) Superimposed junctional currents (I_js) recorded from cell pairs expressing Cx43 R76H or R76S in response to a series of V_j pulses (shown on the top, ±20 to ±100 mV with 20 mV increment). (B) Normalized steady state junctional conductance, $G_{j,ss}$ of Cx43 R76H or R76C GJs were plotted as a function of V_js. Boltzmann equations were used to fit $G_{j,ss}$ – V_j plots. Error bars represent SD and the number of cell pairs is indicated.

V_j-gating properties of R76H / Cx43 and R76S / Cx43 GJs

I_js were also recorded in cell pairs expressing R76H (or R76S) in one and wildtype Cx43 in the other in response to a series of V_j pulses from ±20 to ±100 mV (Fig. 2-6A). The I_js of both R76H / Cx43 and R76S / Cx43 GJs were asymmetrical with strong V_j-gating observed only when the mutant cell (R76H or R76S) with $+V_j$s (or the wildtype Cx43 cell with $-V_j$s) from $+60$ to $+100$ mV (Fig. 2-6A). The normalized steady-state conductance ($G_{j,ss}$) was plotted as a function of V_j and the $G_{j,ss} - V_j$ plots for R76H / Cx43 and R76S / Cx43 were fitted well by a Boltzmann equation for the $+V_j$ polarity (Fig. 2-6B). Boltzmann fitting parameters of R76H / Cx43 and R76S / Cx43 GJs are listed in Table 2-2. For each Boltzmann fitting parameter, no significant differences were observed when compared to those of wildtype Cx43, except for the V_0 values for the $+V_j$ polarity of R76S / Cx43 GJs (Table 2-2). V_j-gating properties for R76C/Cx43 GJs were not studied because most cell pairs expressing R76C in one and wildtype Cx43 in the other did not exhibit GJ coupling (see Fig. 2-3A).
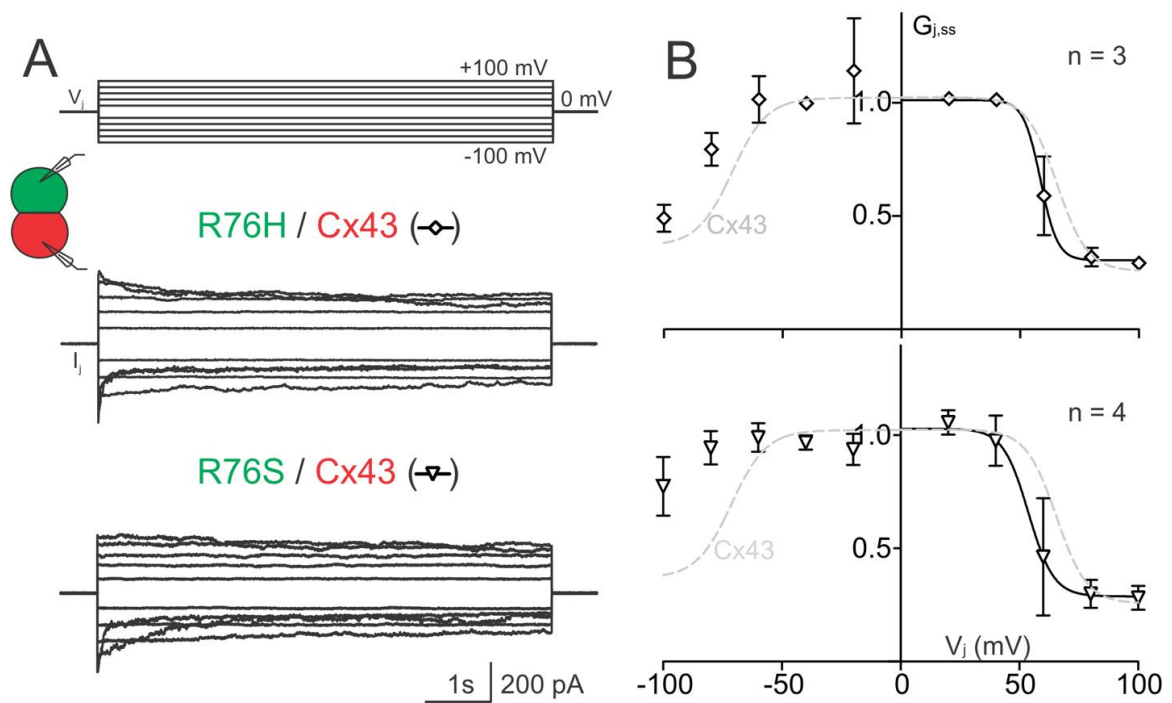
Fig. 2-6. V_j-gating of R76H / Cx43 and R76S / Cx43 GJs.

(A) Superimposed junctional currents (I_js) recorded from cell pairs expressing R76H / Cx43 or R76S / Cx43 in response to a series of V_j pulses (shown on the top of Fig 2-6A, ±20 to ±100 mV with 20 mV increment). (B) Normalized steady state junctional conductance, $G_{j,ss}$ of R76H / Cx43 or R76C / Cx43 GJs were plotted as a function of V_js. A Boltzmann equation was used to fit $G_{j,ss} - V_j$ plot on the +V_js. Error bars on the plots represent SD and the number of cell pairs is indicated.

V_j-gating properties of R76H / Cx45, R76S / Cx45 and R76C / Cx45 GJs

Cell pairs with one expressing R76H (or R76S or R76C each with untagged GFP) and the other expressing wildtype Cx45 (with untagged DsRed) were selected to study R76H / Cx45, R76S / Cx45 or R76C / Cx45 GJs. I_js were recorded in response to a series of V_j pluses from ±5 to ±100 mV, showing asymmetrical V_j-dependent deactivation (Fig. 2-7A). Strong V_j-gating was observed when the mutant-expressing cell was with +V_js (or when the Cx45-expressing cell was in -V_js, Fig. 2-7A). The normalized steady state conductance ($G_{j,ss}$) was plotted as a function of V_j for R76H / Cx45, R76S / Cx45 or R76C / Cx45 GJs (Fig. 2-7B). The $G_{j,ss} - V_j$ plots were fitted well by a Boltzmann equation for the +V_j polarity (Fig. 2-7B). Boltzmann fitting parameters of R76H / Cx45, R76S / Cx45 or R76C / Cx45 GJs are listed in Table 2-2. No significant differences compared to the heterotypic Cx43 / Cx45 GJs were observed for every corresponding parameter (Table 2-2).
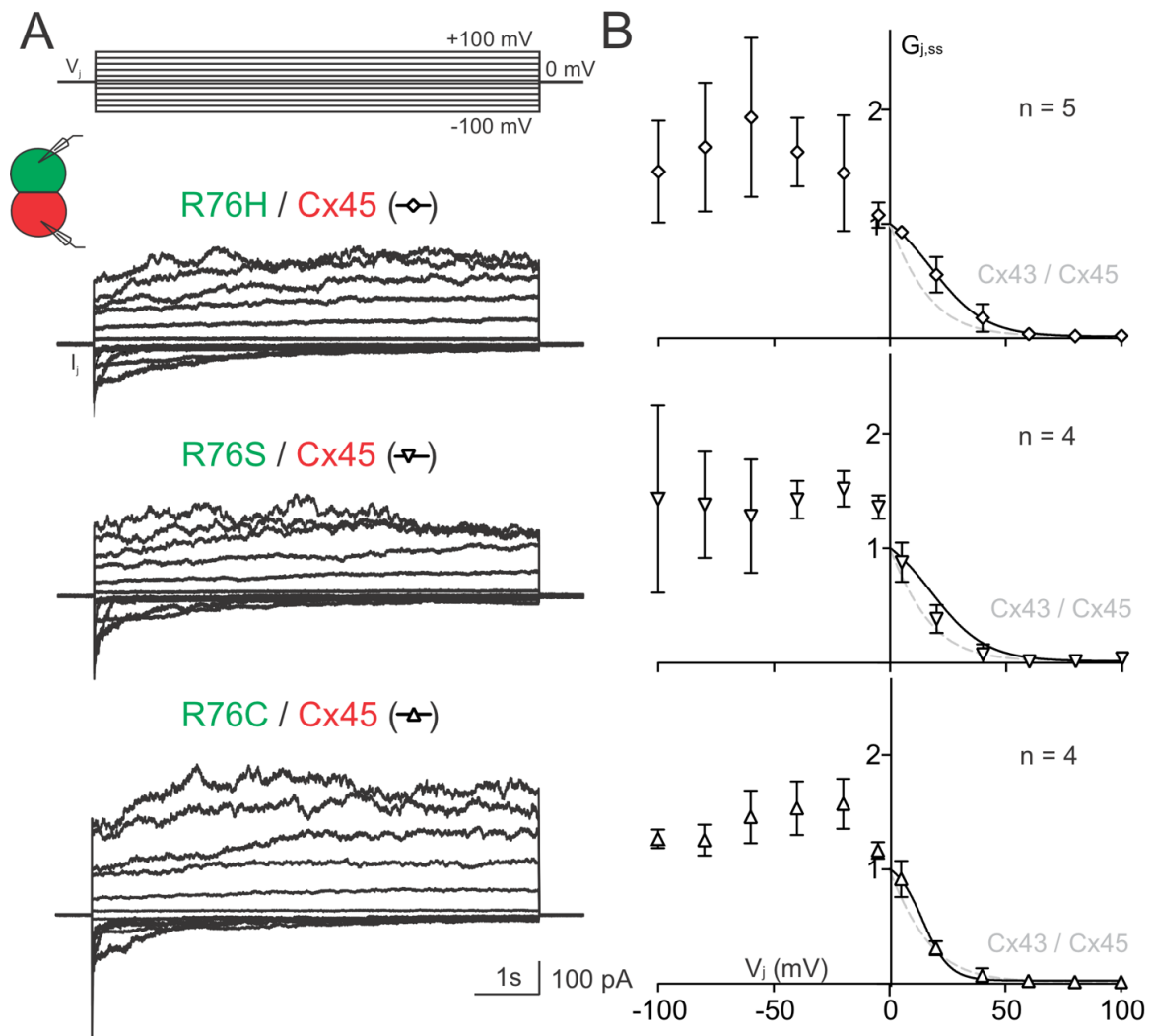
Fig. 2-7. V_j-gating of heterotypic R76H / Cx45, R76S / Cx45 and R76C / Cx45 GJs.

(A) Superimposed junctional currents (I_js) were recorded from cell pairs expressing R76H / Cx45, R76S / Cx45 or R76C / Cx45 GJs in response to a series of V_j pulses (shown on the top). (B) Normalized steady state junctional conductance, $G_{j,ss}$ of R76H / Cx45, R76S / Cx45 or R76C / Cx45 were plotted as a function of V_js. A Boltzmann equation was used to fit $G_{j,ss} - V_j$ plots. The $G_{j,ss} - V_j$ curve of wildtype heterotypic Cx43 / Cx45 GJ channels were indicated in a grey dashed line. Error bars on the plots represent SD, and the number of cell pairs is indicated.

Unitary channel conductance of Cx43 R76S GJs

To investigate how the mutant Cx43 R76S affects the rate of ion permeation for individual GJ channels, we found a cell pair with two apparent functional GJ channels at different V_js (Fig. 2-8A). All point histograms of a stretch of the current recordings were used to measure the current amplitudes of different main opening levels (O_1 and O_2, Fig. 2-8A). Half of the current amplitude of two main openings (O_2) was used as amplitude of a single GJ current, i_j, which was plotted against different levels of V_js. Linear regression of $i_j - V_j$ plot was used to obtain slope single channel conductance (γ_j) for R76S (78 pS) GJs (Fig. 2-8B). Various levels of subconductance states (white arrows on Fig. 2-8A left panels and 's' on the right panels) were also observed, likely due to the combinations of the following factors: 1) different levels of subconductance for each of these GJ channels; 2) 1 or 2 GJ channels in the subconductance state.
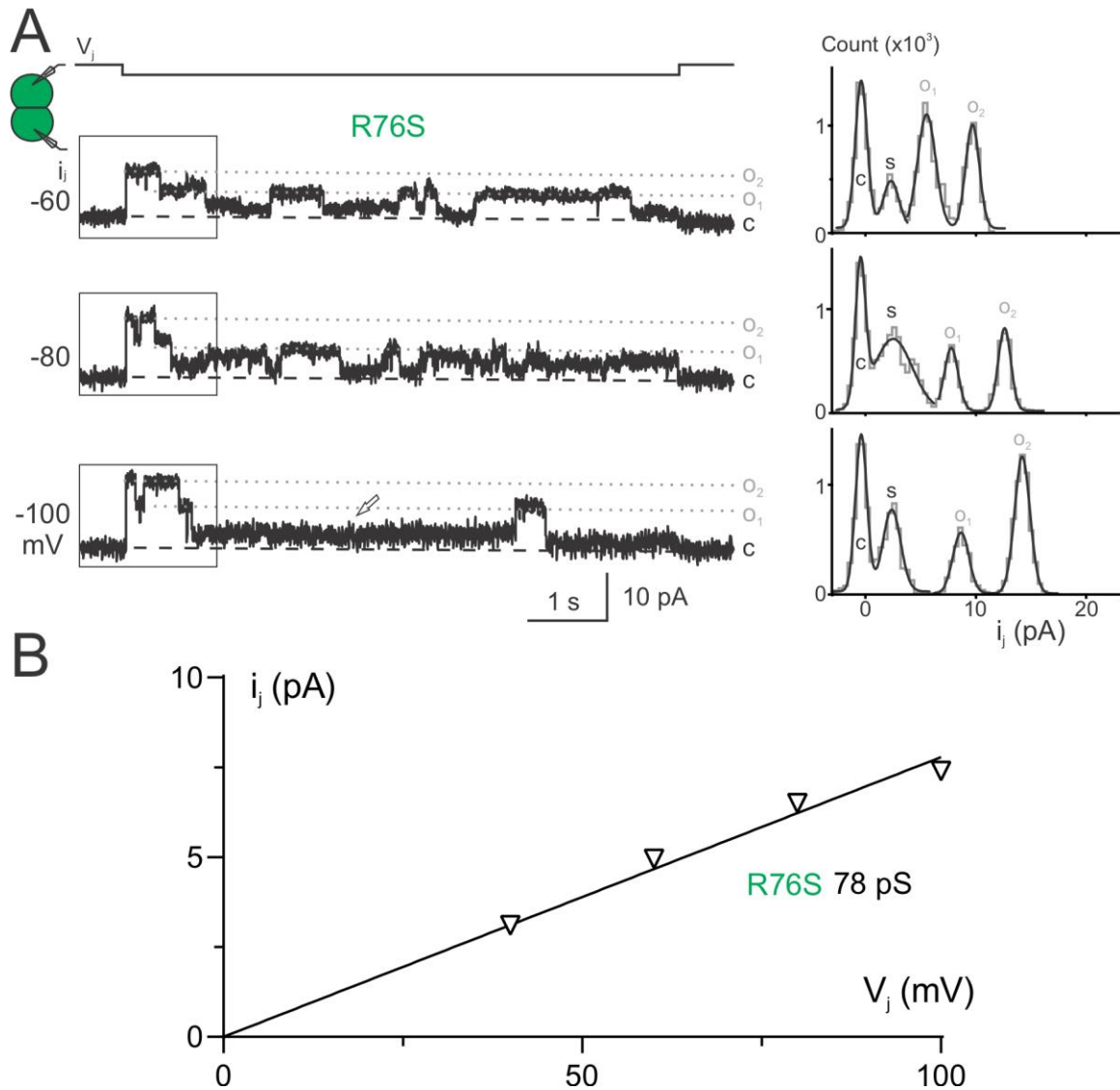
Fig. 2-8. Unitary channel properties for Cx43 R76S GJs.

(A) Unitary channel currents (i_js) of R76S GJs were recorded as a response to the administration of negative V_j pulses ($-V_j$) as indicated. Two channels were identified, and the fully open states are indicated as O_1 and O_2 for one or two channels opening, respectively. After the channels are fully open (O_1 or O_2), they go to either a subconductance state (open arrows) or to a fully closed state (indicated as c). Rectangle areas outlined represent the region used to create the corresponding all-point histograms shown on the right for each V_j. All-point histogram (grey lines) and Gaussian fits (smooth black lines) for i_js of R76S at -60, -80 and -100 mV V_j pulses. They show the i_j amplitude at the main open state of two channels (O2), the open state of a single channel (O1), the subconductance states (s), and the fully closed state (c). (B) The amplitude of i_js (O$_2$ level devided by 2) for the main open state at each tested V_j was plotted against V_j. Linear regression of data on the $i_j - V_j$ plot for R76S GJs was used to obtain slope unitary channel conductance (γ_j).

Cx45 mutant, R76H showed a decreased percentage of cell pairs coupled and coupling conductance (G_j) than those of the wildtype Cx45

To investigate the functional states of the progressive atrial conduction defect-associated Cx45 mutant, R75H, isolated N2A cell pairs expressing Cx45-IRES-GFP or Cx45-R75H-IRES-GFP were selected for dual whole cell patch clamp. The I_js of cell pairs expressing R75H or wildtype Cx45 was recorded in response to a 5 mV V_j pulse. Representative I_js are shown in Fig. 2-9A (left panel). None of the R75H GJs exhibited I_js in response to V_js (N = 7), which was significantly different from the wildtype Cx45 GJs (50 (33.3-66.7)%, N = 7, ***P < 0.001). Moreover, G_j was measured for each cell pair expressing R75H (Fig. 2-9B left panel). The average G_j was 0 (n = 30) for R75H GJs, which was significantly different from the wildtype Cx45 (0 (0-3.6) nS, n = 34, ***P < 0.001).

Cx45 mutant, R75H pairing with wildtype Cx45 or Cx43

Similar experiments were conducted on cell pairs expressing mutant R75H in one cell and the wildtype Cx45 or Cx43 in the other cell. Representative I_js are shown in Fig. 2-9A middle and right panels. The percentage of cell pairs coupled were measured as shown in Fig. 2-9B middle and right panels. Cell pairs with one expressing R75H and the other expressing wildtype Cx45 showed no coupling at all from six independent transfections (Fig. 2-9B middle panel, % cell pairs coupled = 0, N = 6), which was significantly lower than the wildtype Cx45 GJs (66.7 (50-75)%, N = 7, ***P < 0.001). Cell pairs expressing R75H in one cell and wildtype Cx43 in the other cell showed a percentage of cell pairs coupled at 0 (0-27.5)% (N = 6), and it was decreased compared to the wildtype Cx45 / Cx43 (Fig. 2-9B right panel, 75 (68.8-100)%, N = 6, **P = 0.004). The G_js were measured of cell pairs expressing one R75H and the other expressing either wildtype Cx45 or Cx43 (0 (0) nS, n = 25, ***P < 0.001 for R75H / Cx45; 0 (0) nS, n = 24, ***P < 0.001 for Cx75H / Cx43) were also significantly lower than that of their respective controls (2.3 (0-6.4) nS, n = 32 for Cx45 GJs; 11.3 (0.2-22.6) nS, n = 26 for Cx45 / Cx43 GJs; Fig. 2-9C middle and right panels).
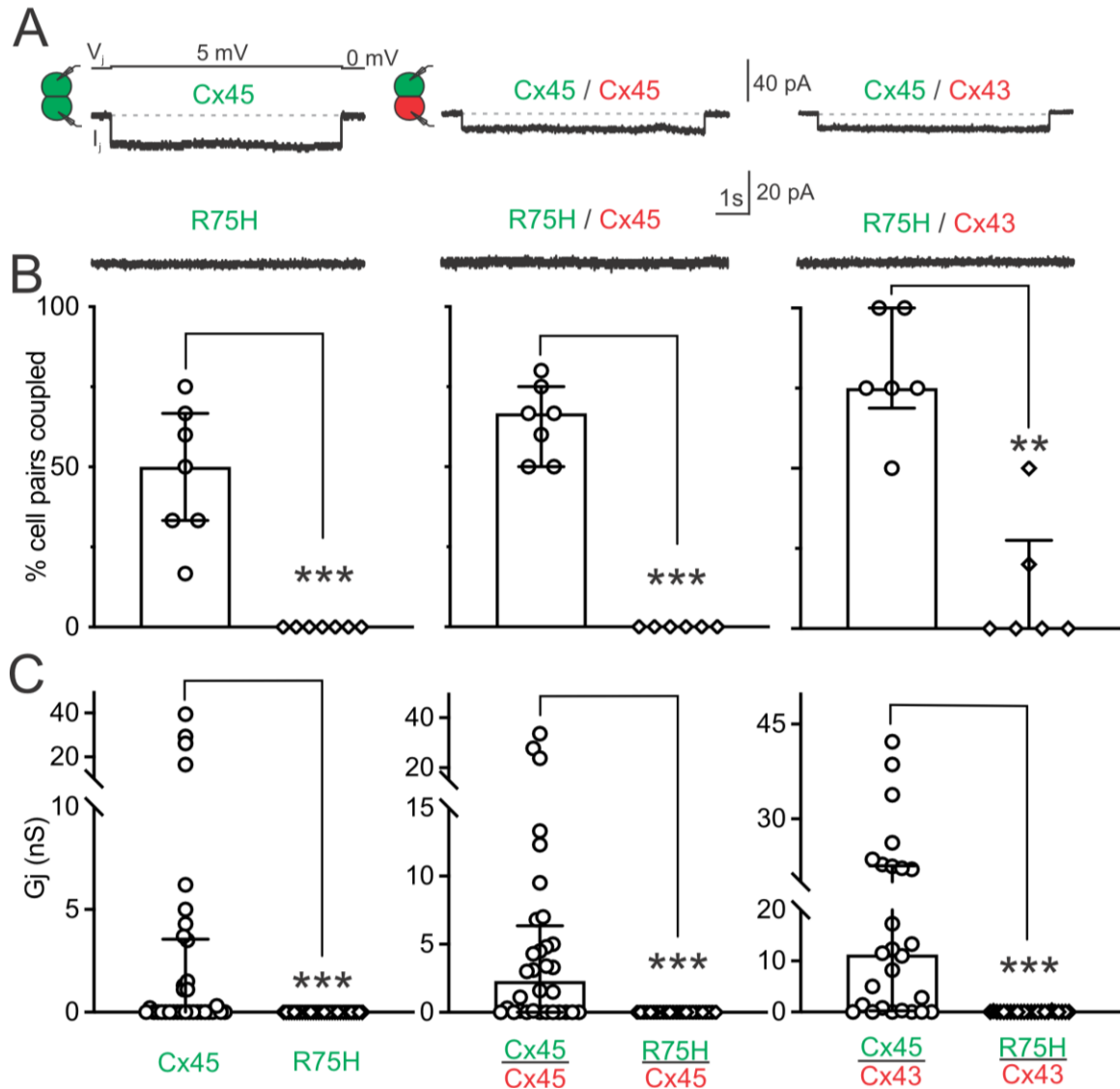
Fig. 2-9. Representative junctional current (I_js) and bar graphs to show percentages (%) of cell pairs coupled and coupling conductance (G_j) of homotypic Cx45 R75H GJs, R75H expressing cell paired with cell expressing wildtype Cx45 or Cx43.

(A) Dual whole cell patch clamp technique was used to measure junctional current (I_j) in response to indicated V_j in N2A cell pairs expressing homotypic wildtype and mutant GJs (left panel), mutant expressing cell paired with wildtype Cx45 (middle panel) or Cx43 (right panel) expressing cell. Representative I_js are shown, and the text colour indicates the untagged fluorescent proteins, green (GFP) and red (DsRed). (B) Bar graphs summarize the average % cell pairs coupled expressing homotypic wildtype and mutant GJs (left panel), mutant expressing cell paired with wildtype Cx45 (middle panel) or Cx43 (right panel) expressing cell. Data points represent the number of transfections, and the error bars are ± standard deviation (SD). (C) Bar graphs illustrate the average coupling conductance (G_j ± SD) of cell pairs examined expressing homotypic wildtype or mutant GJs, mutant expressing cell paired with wildtype Cx45 or Cx43 expressing cell as indicated. A

nonparametric Mann-Whitney test was used to compare R75H with their respective controls for all bar graphs. The statistical significance was indicated (* P < 0.05, ** P < 0.01, and *** P < 0.001).

V_j-gating properties of homotypic Cx45 GJ channels

Cell pairs expressing wildtype Cx45 were selected to study homotypic Cx45 GJs. The I_js were measured in response to a series of V_j pluses from ±5 to ±100 mV, displaying symmetrical V_j-dependent deactivation (Fig. 2-10A). I_js showed strong deactivation to V_j values in the range ±20 to ±100 mV and no apparent deactivation when V_j absolute values were at 5mV (Fig. 2-10A). The normalized steady state conductance ($G_{j,ss}$) was plotted as a function of V_j, which could be fitted by a Boltzmann equation for each V_j polarity (Fig. 2-10B). Boltzmann fitting parameters of Cx45 GJs are listed (Table 2-1.). V_j-gating analysis for cell pairs expressing R75H or expressing R75H in one cell and wildtype Cx45 or Cx43 in the other was not shown as the majority of the cell pairs could not form functional GJs (Fig. 2-9).
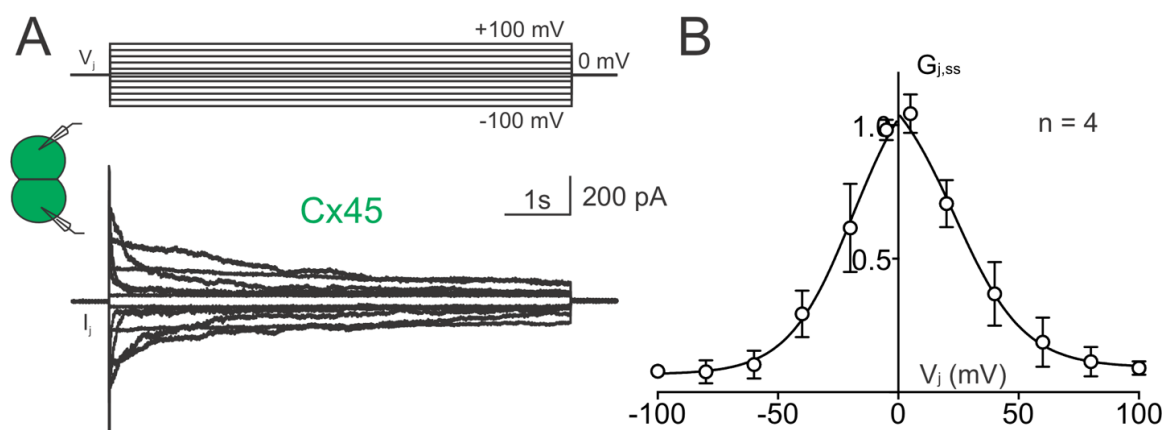
Fig. 2-10. V_j-gating of homotypic wildtype Cx45 GJs.

(A) Superimposed junctional currents (I_js) were recorded from cell pairs expressing Cx45 GJs in response to a series of V_j pulses (shown on the top of Fig 2-9A, ±5 to ±100 mV). (B) Normalized steady state junctional conductance, $G_{j,ss}$ of Cx45 were plotted as a function of V_js. A Boltzmann equation was used to fit $G_{j,ss} - V_j$ plots. Error bars represent SD and the number of cell pairs is indicated.

Table 2-1. Boltzmann fitting parameters for homotypic Cx50, homotypic Cx45, and heterotypic Cx50 / Cx46 GJs.

	V_j Polarity	G_{min}	G_{max}	V_0	A
Cx50	+	0.18 ± 0.05	1.05 ± 0.05	38.6 ± 2.5	0.09 ± 0.02
(n = 4)	-	0.15 ± 0.03	1.02 ± 0.06	40.5 ± 2.7	0.13 ± 0.05
Cx50 / Cx46	+	0.23 ± 0.04	1.04 ± 0.06	37.8 ± 2.4	0.18 ± 0.12
(n = 4)	-	0.17 ± 0.02	1.01 ± 0.04	36.3 ± 1.6	0.18 ± 0.06
Cx45	+	0.09 ± 0.03	1.23 ± 0.16	23.4 ± 4.9	0.07 ± 0.02
(n = 4)	-	0.07 ± 0.03	1.26 ± 0.19	18.8 ± 5.3	0.07 ± 0.02

Data is presented as mean $\pm$ SEM, and V_0 and A are absolute values.

Table 2-2. Boltzmann fitting parameters for homotypic Cx43 and mutants GJs, heterotypic Cx43 / Cx45 GJs, and mutants expressing cell paired with wildtype Cx43 or Cx45 expressing cell.

	V_j Polarity	G_{min}	G_{max}	V_0	A
Cx43 / Cx43	+	0.26 ± 0.05	1.03 ± 0.03	65.6 ± 2.2	0.16 ± 0.05
(n = 3)	-	0.37 ± 0.05	1.02 ± 0.02	71.2 ± 2.7	0.14 ± 0.03
R76H	+	N/A	N/A	N/A	N/A
(n = 5)	-	0.48 ± 0.07	1.02 ± 0.03	75.9 ± 4.1	0.12 ± 0.06
R76S	+	0.23 ± 0.04	1.04 ± 0.02	59.2 ± 1.9	0.12 ± 0.03
(n = 6)	-	0.19 ± 0.03 *	0.99 ± 0.02	56.9 ± 1.7**	0.13 ± 0.03
R76H / Cx43	+	0.31 ± 0.03	1.01 ± 0.03	58.6 ± 3.1	0.28 ± 0.60
(n = 3)	-	N/A	N/A	N/A	N/A
R76S / Cx43	+	0.29 ± 0.04	1.03 ± 0.04	53.8 ± 3.2*	0.19 ± 0.08
(n = 4)	-	N/A	N/A	N/A	N/A
Cx43 / Cx45	+	0.02 ±0.02	2.91 ± 2.95	8.5 ± 21.5	0.08 ± 0.02
(n = 5)	-	N/A	N/A	N/A	N/A
R76H / Cx45	+	0.02 ± 0.03	1.22 ± 0.16	17.8 ± 3.9	0.09 ± 0.02
(n = 5)	-	N/A	N/A	N/A	N/A
R76S / Cx45	+	0.02 ± 0.02	1.22 ± 0.02	12.8 ± 4.3	0.12 ± 0.03
(n = 4)	-	N/A	N/A	N/A	N/A
R76C / Cx45	+	0.03 ± 0.02	1.1 ± 0.1	14.2 ± 2.1	0.17 ± 0.04
(n = 4)	-	N/A	N/A	N/A	N/A

Data are presented as mean $\pm$ SEM. V_0 and *A* are absolute values. Unpaired t-test was used to compare the Boltzmann fitting parameters of each mutant against those of wildtype at the corresponding V_j polarity. N/A, not applicable. * $P < 0.05$ and ** $P < 0.01$.

The effect of net charge at the R76 residue for Cx50 R76H and Cx45 R75H GJ channel function

Under physiological conditions the intracellular and extracellular pH are around 7.2 and 7.4, respectively, the arginine (R or Arg) residue carries a +charge at these pH values. However, when the arginine residue mutated to histidine (H or His), such as R76H in Cx50 (or R75H in Cx45), the probability of H76 (or H75 in Cx45) carrying a +charge is very low (only about 10% of His will be protonated; Betts & Russell, 2003). The loss or substantial reduction of +charge on this residue could play a role in our observed impairment of GJ function. To test this idea further, we manipulated our experimental conditions by decreasing the pH values for either the intracellular solution or the extracellular solution to 6.8 to increase the probability of histidine carrying a +charge and hopefully that one of these manipulations could functionally rescue the mutant GJs.

The GJ functional status of cell pairs expressing Cx45 R75H (or Cx50 R76H) was tested with lower intracellular pipette solution pH of 6.8 and the extracellular pH was kept at 7.4. The I_js of cell pairs expressing Cx45 R75H (or Cx50 R76H) and wildtype Cx45 (or Cx50) were recorded as shown in Fig. 2-11A. No GJ coupling was observed for Cx45 R75H expressing cell pairs in 5 independent transfections (Fig. 2-11B, N = 5), while cell pairs expressing wildtype Cx45 were frequently coupled with an average % cell pair coupled (50 (45-75)%, N = 5, **P = 0.008, Fig. 2-11B). Similarly, cell pairs expressing Cx50 R76H also showed no GJ coupling in 5 independent transfections (Fig. 2-11B, N = 5), which is significantly different from cell pairs expressing wildtype Cx50 (50 (40-87.5)%, N = 5, **P = 0.008). The G_j of cell pairs expressing Cx45 R75H was significantly different from the G_j of cell pairs expressing wildtype Cx45 (1.4 (0-8.8) nS, n = 19, ***P < 0.001). Similarly, the G_j of cell pairs expressing Cx50 R76H was also significantly lower than that of wildtype Cx50 cell pairs (0 (0-2) nS, n = 19, **P = 0.001).

Similar results were obtained for Cx45 R75H and Cx50 R76H with extracellular pH reduced to 6.8 while maintaining the intracellular pH at 7.2. As shown in Fig. 2-12, both the % cell pairs coupled and G_j of either Cx45 R75H or Cx50 R76H were significantly reduced from those of Cx45 (For Cx45 % cell pair coupled: 57.5 (22.5-93.8)%, N = 4 and for Cx45 Gj: 0.2 (0-11.5) nS, n = 19) or Cx50 (For Cx50 % cell pair coupled: 80 (62.5-100)%, N = 5 and for Cx50 Gj: 1.6 (0.3-19.5) nS, n = 17), respectively (For Cx45 R75H % cell pair coupled: N = 5, **P = 0.008 and for G_j: n = 19, ***P < 0.001; For Cx50 R76H % cell pairs coupled: N = 5, **P = 0.008 and for G_j: n = 19, ***P < 0.001, see Fig. 2-12B, C). In summary, reducing either intracellular or extracellular pH to 6.8 failed to rescue the % cell pair coupled or G_j of Cx45 R75H and Cx50 R76H function.

Fig. 2-11. Representative junctional current (I_js) and bar graphs to show percentages (%) of cell pairs coupled and coupling conductance (G_j) of homotypic Cx45 and its mutant R75H GJs, and Cx50 and its mutant R76H GJs. The intracellular pH (pH_i) and the extracellular pH (pH_e) were 6.8 and 7.4, respectively.

(A) Dual whole cell patch clamp technique was used to measure junctional current (I_j) in response to indicated V_j in N2A cell pairs expressing homotypic Cx45 wildtype and R75H GJs (left panel), and Cx50 wildtype and R76H GJs (right panel). Representative I_js are shown, and the text colour indicates the untagged fluorescent proteins in green (GFP). (B) Bar graphs summarize the % cell pairs coupled expressing homotypic Cx45 wildtype or

R75H GJs (left panel), and Cx50 wildtype or R76H GJs (right panel). Data points represent the number of transfections, and the error bars are ± SD. (C) Bar graphs illustrate the average coupling conductance (G_j ± SD) of cell pairs examined expressing homotypic Cx45 wildtype and R75H GJs (left panel) and Cx50 wildtype and R76H GJs (right panel) as indicated. A nonparametric test Mann-Whitney test was used to compare each mutant with their respective controls for all bar graphs. The statistical significance was indicated (* $P < 0.05$, ** $P < 0.01$, and *** $P < 0.001$).
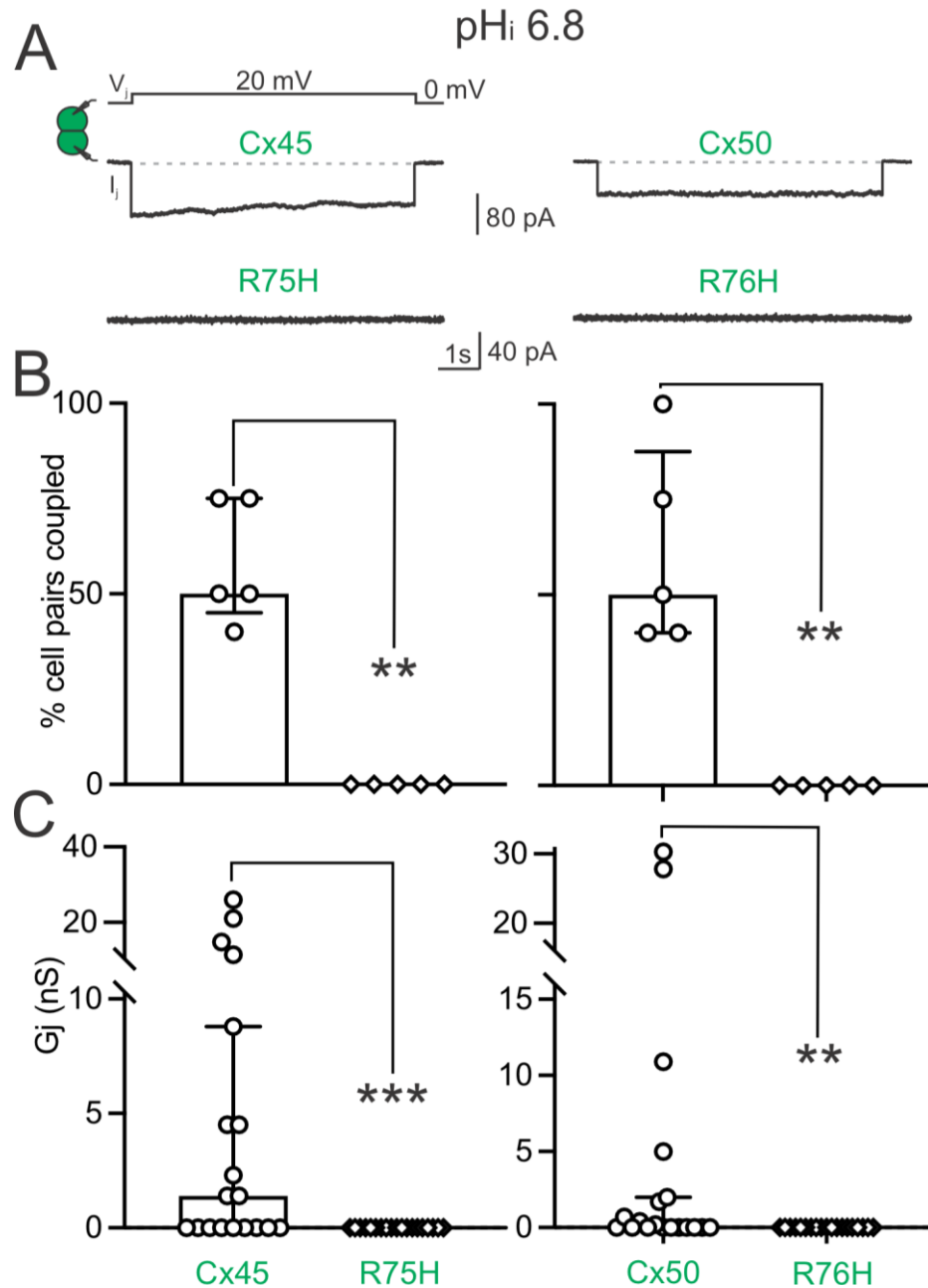
Fig. 2-12. Representative junctional current (I_js) and bar graphs to show percentages (%) of cell pairs coupled and coupling conductance (G_j) of homotypic Cx45 and its mutant R75H GJs, and Cx50 and its mutant R76H GJs. The intracellular pH (pH_i) and the extracellular pH (pH_e) were 7.2 and 6.8, respectively.

(A) Dual whole cell patch clamp technique was used to measure junctional current (I_j) in response to indicated V_j in N2A cell pairs expressing homotypic Cx45 wildtype and R75H GJs (left panel), and Cx50 wildtype and R76H GJs (right panel). Representative I_js are shown, and the text colour indicates the untagged fluorescent proteins in green (GFP). (B) Bar graphs summarize the % cell pairs coupled expressing homotypic Cx45 wildtype or R75H GJs (left panel), and Cx50 wildtype or R76H GJs (right panel). Data points represent the number of transfections, and the error bars are ± SD. (C) Bar graphs illustrate the average coupling conductance (G_j ± SD) of cell pairs examined expressing homotypic Cx45 wildtype and R75H GJs (left panel) and Cx50 wildtype and R76H GJs (right panel) as indicated. A nonparametric test Mann-Whitney test was used to compare each mutant with their respective controls for all bar graphs. The statistical significance was indicated (* $P < 0.05$, ** $P < 0.01$, and *** $P < 0.001$).

Structure modes of wildtype Cx50, Cx43 and Cx45 and their mutants at the R76 (or R75) residue

In order to gain further insights into the structural mechanisms of the R76 mutants, we developed homology models for Cx43 and Cx45 GJs, using the newly resolved high-resolution Cx50 GJ structure as a template (Flores *et al.*, 2020), then performed mutagenesis analysis using PyMOL (Fig. 2-13). A side view of Cx50, Cx43 and Cx45 GJ structures are shown on the left panels of Fig. 2-13. Zoom-in views of R76 residues in each of these wildtype GJs are shown as indicated. In all cases, the R76 (or R75 in Cx45) side chain showed similar non-covalent interactions, specifically salt bridges with E48 (or E47 in Cx45) of the same subunit (intra-subunit interaction) and salt-bridge interactions with E208 in Cx50, E205 in Cx43, or E227 in Cx45 in the next subunit (inter-subunit interaction) as shown with yellow dashed lines in Fig. 2-13. Substitution of arginine with histidine (R76H) in Cx50, Cx43, and Cx45 (in this case R75H) could maintain similar salt-bridge interaction (between the side chains of H76 and E208 in Cx50, H76 and E205 in Cx43, or H75 and E227 in Cx45). However, the intra-subunit salt-bridge interactions are lost as the H76 is too far away from E48 (or E47 in Cx45) in Cx50 and Cx43. Lastly, the R76C in Cx50 as well as both R76S and R76C substitutions in Cx43 showed a completely

loss of both intra- and inter-subunit salt-bridge interactions at the respective C76 or S76 sidechains (Fig. 2-13).
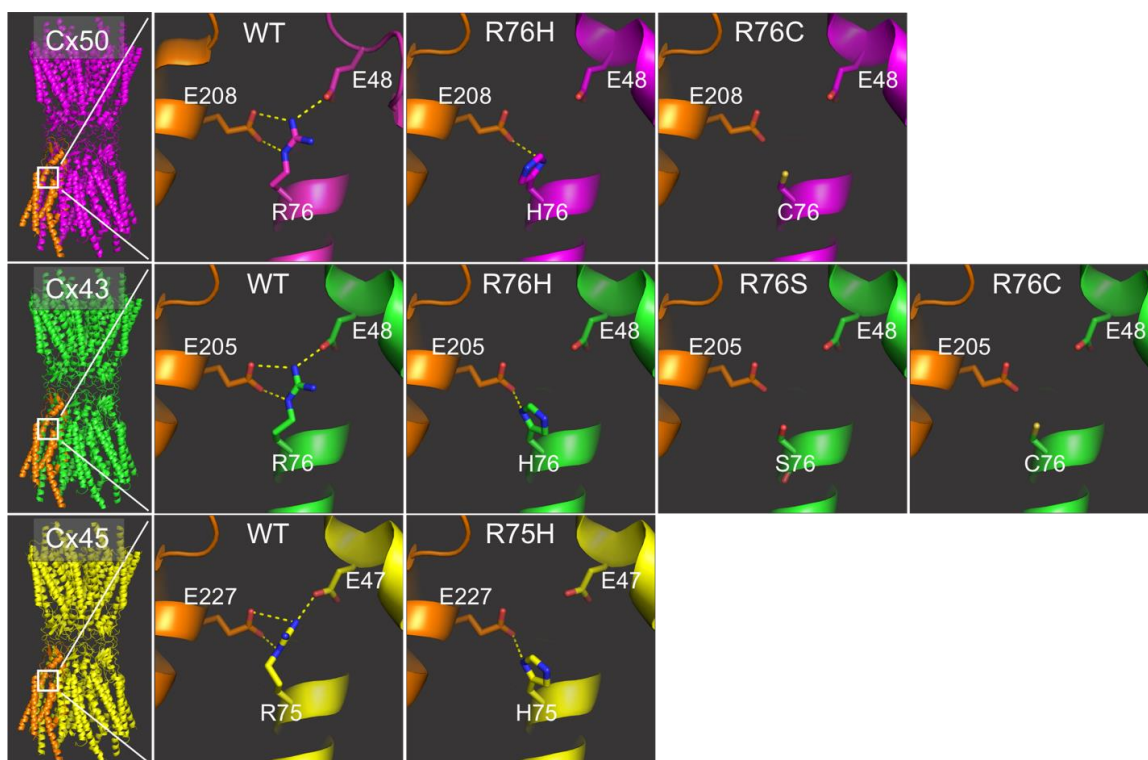
Fig. 2-13. Structural models of Cx50, Cx43, and Cx45 and their mutants.

The wildtype (WT) Cx50 GJ model was based on Cryo-EM determined structure (PDB: 7JJP) (Flores *et al.*, 2020) and is presented on the left with a side view. The homology models of wildtype (WT) Cx43 GJ and Cx45 GJ were created based on the Cx50 GJ structure (7JJP) and are both presented in a similar side view as that of Cx50 GJ. The mutagenesis modelling of mutations at the 76th residue in these GJs was performed using PyMOL. The zoom-in views of all the mutants at R76 residue in Cx50, Cx43 and Cx45 are shown as indicated. The yellow dashed lines on each panel represent possible salt-bridge interactions with an estimated distance under 4 Å.

Discussion

This present study is to investigate the functional status and properties of GJs formed by the disease-linked R76 mutants in Cx50 (R76H, R76C), Cx43 (R76H, R76S, and R76C) and Cx45 (R75H) with a particular focus on the formation of functional heterotypic GJs. Our results showed that most of the studied mutants at this residue were unable to form functional GJs except Cx43 R76H and R76S, which formed functional GJs with some altered V_j-gating properties. Interestingly, all three Cx43 mutants, R76H, R76S and R76C were able to form functional GJs when paired with the docking compatible Cx45, but only R76H and R76S formed functional GJs with wildtype Cx43. Our preliminary data suggested a decreased unitary channel conductance (γ_j) for R76S GJ. The homology structure models on these mutants predicted a partial or complete loss of intra- and/or inter-subunit non-covalent interactions (salt bridges) at the arginine residue sidechain in each mutant model, presumably these intra- and inter-subunit interactions are critical for connexin subunit folding and/or oligomerization into proper hemichannel structure that is required for the formation of functional GJs in these and possibly other connexins.

Arg76 is highly conserved and its interactions within and between connexin subunits likely play an important role in GJ function

Several independent lines of evidence argue that arginine76 (Arg76 or R76) or its equivalent residue in connexins are critical for biological function. First, R76 in Cx50 and its equivalent residue in other connexins are fully conserved in the same connexin of different species and also across different connexin families (Fig. 2-14) indicating that this connexin residue is likely to play an important role in biology during the evolution process and cannot tolerate for changes to other residues, which exist in many connexin residue positions (Fig. 2-14). Second, several high-resolution crystal and Cryo-EM structure models have been developed for Cx26, Cx46, and Cx50 GJs and all of them showed that R76 is located at the junction of E1 and M2 domains displaying multiple non-covalent interactions with residues of the same subunit and/or from the neighbouring subunit (Maeda *et al.*, 2009; Bennett *et al.*, 2016; Myers *et al.*, 2018; Flores *et al.*, 2020), suggesting that this residue may be important for connexin subunit folding as well as assembling into a hexameric hemichannel. Interestingly, two Cx26 R75 (equivalent to R76 in Cx50)

interacting residues, E42 and E47, have also been proposed to be the key residues for Ca^{2+}-binding in Cx26 GJs. Ca^{2+} is a well-known GJ modulator, and elevation of intracellular Ca^{2+} concentrations could promote gating (closing) of the channel in several GJs (Rose & Loewenstein, 1975; Peracchia, 1978, 2004; Lurtz & Louis, 2007). Third, R76 in Cx50, Cx43, Cx46 or equivalent residue in other connexins is an inherited disease-linked mutation hot-spot. Five inherited human diseases are linked to mutations in six connexin genes, including genes encoding Cx26, Cx32, Cx43, Cx45, Cx46, and Cx50 (Richard *et al.*, 1998; Uyguner *et al.*, 2002; Yum *et al.*, 2002; Paznekas *et al.*, 2003; Pizzuti *et al.*, 2004; Burdon *et al.*, 2004; Devi *et al.*, 2005; Reis *et al.*, 2013; Izumi *et al.*, 2013; Yu *et al.*, 2016). Most of these R76 connexin mutation-linked diseases are inherited in an autosomal dominant fashion in patients and their families and in one case in Cx43 autosomal recessive inheritance was also observed (Pizzuti *et al.*, 2004). Co-segregation of the connexin R76 mutants with relevant diseases argues strongly that the mutants at this position are most likely pathogenic and unlikely to be coincidental. Finally, previous functional studies on disease-linked connexin R76 mutants in some connexins, including Cx26 (R75Q and R75W), Cx32 (R75P, R75Q and R75W), and Cx46 (R76H and R76G) in recombinant expression studies showed that all these mutants impaired GJ function in cell pairs expressing the mutants (Chen *et al.*, 2005*a*; Piazza *et al.*, 2005; Abrams *et al.*, 2013, 2018). Our present study characterized several recently identified mutants on this residue in Cx50 (R76H, R76C) and Cx43 (R76S, R76C). Homotypic combinations of these mutants, including Cx50 R76H and R76C as well as Cx43 R76C, showed impaired GJ function, consistent with those previous findings in Cx26, Cx32, and Cx46. Homotypic Cx43 R76S and R76H displayed functional GJs in our model cells but with some altered V_j-gating properties and/or unitary channel conductance. The impairment of GJ is not restricted to homotypic mutant GJs, when mutant expressing cells paired with either corresponding wildtype or a docking compatible connexin, Cx50 R76H (or R76C) and Cx45 R75H also show impaired GJ function. Interestingly, Cx43 R76S showed altered V_j-gating properties when paired with wildtype Cx43. Cx43 R76C showed GJ functional impairments when paired with wildtype Cx43 but not with Cx45, suggesting that Cx43 R76C could form hemichannels with an altered structure which is unable to form functional GJs with Cx43, but capable forming heterotypic GJs with Cx45. In summary, the total impairments of GJs

function or alteration of GJ channel properties observed in the R76 or equivalent residue mutants could play a role in their pathogenesis in patients carrying these mutants.
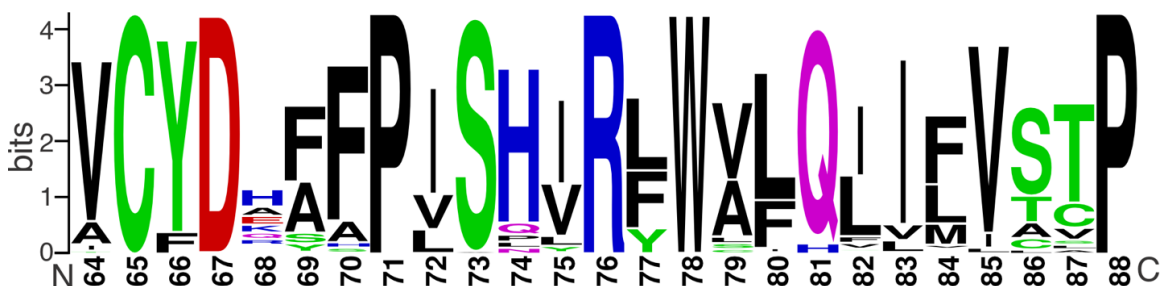
Fig. 2-14. Sequence logo of 19 connexins in all available species including 1656 sequences.

Connexin sequences were downloaded from the OMA Orthologous Matrix browser for 19 connexins of different species to have a total of 1656 connexin sequences and imported into Jalview. Sequence alignment was performed using ClustalOmega with default settings. The Arg 76 (R76) is fully conserved in this collection of connexins as a single large letter R. Several other residue positions are also fully conserved (the 65th, 67th, 71st, 78th, 88th), but other residue positions have two or more residues with different probabilities reflected by the height of the letters.

The functional status and properties of GJs formed by six R76 mutants

In line with the previous functional studies of disease-linked mutations at the R76 residue in Cx26, Cx32, Cx43, Cx45 and Cx46, the majority of the mutants in Cx43, Cx45 and Cx50 we have examined were unable to form functional GJs, indicating the prevalence of loss-of-function mutations at the R76 residue (Chen *et al.*, 2005*a*; Huang *et al.*, 2013; Abrams *et al.*, 2013; Seki *et al.*, 2017; Abrams *et al.*, 2018). Among the mutants, Cx50 R76H and R76C, Cx43 R76C and Cx45 R75H were all unable to form functional homotypic GJs, only Cx43 R76H and R76S could form functional homotypic GJs. Interestingly, we found that a substitution of arginine with serine at the 76th position (R76S) resulted in a functional GJ that had reduced γ_j (78 pS) from our preliminary data. At the macroscopic level, the R76S had lower G_{min} (increased extent of V_j-gating) and lower level of half deactivation voltage (V_0) for one V_j polarity as compared with the V_j-gating properties of wildtype Cx43 GJs. The V_j-gating properties in R76H GJ were likely changed as well as for one V_j polarity as we were unable to fit the Boltzmann equation with

meaningful parameters (e.g., at $+V_j$ the G_{min} showed negative values out of the expected range between $0 - 1$). We believe that this is likely due to an increased V_0, which cannot be estimated properly with our tested V_j range. Our previous study on a tagged Cx43 R76H showed a decreased γ_j (41 pS) (Huang *et al.*, 2013). The differences in the functional properties of these two mutations could be explained by structural changes caused by different amino acid substitutions at the R76 residue. Based on our homology model of Cx43, R76 side chain interacts (forming salt bridges) with two residues, E48 of the same subunit and E205 of the neighbouring subunit in Cx43 GJ and these intra- and inter-subunit interactions are likely facilitating subunit folding and oligomerization to form the hemichannel structure and may also affect proper docking between the two hemichannels. The substitution to histidine (R76H) resulted in a loss of the intra-subunit salt bridge and may also alter the inter-subunit salt bridge at this site, whereas both intra- and inter-salt bridges were likely disrupted in the case of R76S. It is possible that these inter- and intra-subunit interactions are critical to maintain the channel structure for proper V_j-gating, partial or complete modification of these interactions could modify the V_j-gating parameters, such as V_0. Our current study and previous study also showed a reduction of unitary channel conductance (γ_j) in both R76S and R76H, which could also change the V_j-distribution along the GJ channel and indirectly modify the V_j-gating properties, giving rise to asymmetrical $G_{j,ss} - V_j$ curves. Even though both salt bridges were lost in R76S and R76C mutants, R76C was incapable of forming functional GJs in contrast to R76S. This indicates the requirement of specific amino acids appearing at the 76th position of Cx43 or the R76C could form an abnormal disulfide bridge within E1 or between E1 – E2 domains altering those normally formed triple disulfide bridges between E1 – E2. High resolution Cx43 and Cx45 GJ structures are currently not available, that is the reason we used the homology models for these two connexins. With sequence identity at 60% to Cx43 and 55% to Cx45 for the structural resolved domains, we believe that the Cx50 GJ structure is a great template for these homology models, but we cannot rule out the possibility that these connexins could have different GJ structures from that of Cx50. A recent unpublished study (in bioRxiv) showed a Cryo-EM resolved Cx43 GJ structure (Qi *et al.*, 2022), but the detailed structure coordinates are not currently available, and we could not use that to develop structure models for our studied mutants on R76 in Cx43. Perhaps this and future

Cx43 GJ structure models will help to explain why R76 in this connexin could tolerate some mutations and still show GJ function but with altered properties.

The functional status and properties of GJs formed by pairing R76 mutants and wildtype connexins

As a highlight of this study, we characterized the GJs function formed by the mutants paired with the wildtype docking compatible connexins, providing new mechanistic insights into the mutations at this well-conserved residue in different connexins. Most of the R76 (or R75 in Cx45) mutants impaired GJ function in a dominant-negative manner on homomeric homotypic or heterotypic wildtype connexins, such as Cx50 R76H (or R76C) / wildtype Cx50 (or Cx46), Cx45 R75H / wildtype Cx45 (or Cx43), or Cx43 R76C / wildtype Cx43. Cx43 R76H and R76S formed functional GJs when paired with Cx43, but R76C / Cx43 did not. R76S / Cx43 showed altered V_j-gating properties with a lower level of half deactivation voltage (V_0) as compared to Cx43. Interestingly, all three Cx43 mutants formed functional GJs when paired with Cx45, indicating that the R76C mutant could be biosynthesized and trafficked to the plasma membrane when making contact with cells expressing Cx45, allowing for the formation of functional heterotypic GJs at the cell junctions. We believe that the Cx43 R76C hemichannel structure is likely altered substantially so that they lose the ability to dock and form functional channels with cells expressing either the same mutant or wildtype Cx43, but Cx45 hemichannels could be adapted to the structural change on Cx43 R76C. We have obtained some morphological data (H. Chen and D. Bai unpublished observations) that showed a higher probability of observing GJ plaque-like structures between cell pairs expressing Cx43 R76C-GFP and Cx45-RFP than those expressing wildtype Cx43-GFP and Cx45-RFP, indicating that Cx43 R76C is easier to form morphological GJs with wildtype Cx45 than Cx43.

Possible pathophysiological mechanisms of R76 mutant-linked diseases in different connexins

The pathophysiological significance of the R76 residue is supported by numerous inherited disease-linked mutations at this residue (or the corresponding one) in at least six connexins: hearing loss and palmoplantar keratoderma (PPK)-linked mutations in Cx26 (Yum *et al.*, 2010), Charcot-Marie-Tooth disease-linked mutations in Cx32 (Yum *et al.*, 2002), ODDD-linked mutations in Cx43 (Paznekas *et al.*, 2003; Pizzuti *et al.*, 2004; Izumi *et al.*, 2013), progressive atrial conduction defect-linked mutation in Cx45 (Seki *et al.*, 2017), and congenital cataract-linked mutations in Cx46 and Cx50 (Burdon *et al.*, 2004; Reis *et al.*, 2013; Yu *et al.*, 2016; Wang *et al.*, 2020). A summary of disease-linked mutations at the 76/75 residue in these connexins and a summary of studies of their functional status is shown in Table 2-3. The majority of the mutants failed to form functional GJs in recombinant expression studies. For example, Cx26 R76W, Cx46 R76H and R76G were all unable to form functional GJs (Chen *et al.*, 2005*b*; Abrams *et al.*, 2018); Cx32 R75P, R75Q and R75W formed GJ channels with low or no coupling (Abrams *et al.*, 2013). It has not been well studied whether heterotypic GJs formed by R76 mutants when paired with docking-compatible connexins may play a role in pathogenesis. Lens connexins form GJs which are important in the lens circulation of ions, nutrients and metabolic (Beyer *et al.*, 2013). Impairment of GJ function is a common molecular mechanism for cataract formation. One study has shown that a point mutation (D47A) in mouse Cx50 led to a reduction in lens circulation that reduced water and ion outflow, resulting in cataracts (Berthoud *et al.*, 2013). This mutation was also predicted to have a dominant-negative effect on co-expressed Cx50 and Cx46 as the GJ coupling was more severely decreased in D47A than that in Cx50 knockout mouse lenses, in which only the Cx50 abundance was affected (Berthoud *et al.*, 2013). Here, we showed that Cx50 R76H (or R76C) expressing cells paired with wildtype Cx50 or Cx46 expressing cells failed to form functional GJs, suggesting a potential etiology of congenital cataracts by the dominant-negative behaviour of R76 mutations in homomeric homotypic and heterotypic GJs leading to impaired intercellular communication. Connexins in the heart are essential for rapid action potential propagation. Because of the cardiac connexin expression pattern, where Cx43 and Cx40 are expressed in the atria and Cx45 is expressed only in the sino-atrial (SA) and atrio-

ventricular (AV) nodes and the ventricular conduction system, heterotypic Cx45 / Cx43 GJs could be formed between SA node and Cx43-expressing cardiomyocytes as well as between the Cx43-abundant atrial cardiomyocytes and the Cx45-abundant SA or AV nodal cells to mediate electrical coupling (Ye *et al.*, 2017). We have demonstrated that Cx45 R75H / Cx45 (or Cx43) GJs were not functional. This could eliminate the action potential propagation within the SA and AV nodes as well as from the SA node to atrial cardiomyocytes and/or from atrial cardiomyocytes to the AV node. It is possible that this impairment plays a role in the development of AV block observed in patients carrying R75H mutation as reported by Seki et al. (Seki *et al.*, 2017). It has been reported that the affected family members with R75H mutation also had an atrial standstill (a total elimination of the atrial electrical activity) (Seki *et al.*, 2017). We speculated that this could be due to the impaired Cx45 R75H / Cx43 GJs formed at the boundary between the SA node and atrium and prevented electrical signal transmission from the SA node to the atrium. In conclusion, the impairments of heterotypic GJs formed by R76 (or R75) mutants when paired with docking-compatible connexins, could participate in the pathophysiology of congenital cataracts and progressive atrial conduction defects.

Table 2-3. Summary of disease-linked mutations at the 76/75 residue in Cx26, Cx32, Cx46, Cx43, Cx45 and Cx50 and summary of in vitro functional studies.

Conn-exins	Linked diseases	Mutations	References (identification)	Functional data	References
Cx26	Sensori-neural hearing loss (with PPK)	R75W (AD)	(Richard *et al.*, 1998)	-Normal expression in the PM using Western blot -Non-functional GJs -Dominant-negative effect on co-expressed wt Cx26 GJ function.	(Richard *et al.*, 1998) (Chen *et al.*, 2005*b*); (Deng *et al.*, 2006)
		R75Q (AD)	(Uyguner *et al.*, 2002); (Feldmann *et al.*, 2005)	-Able to form morphological GJ plaques (HeLa) -Non-functional GJs	(Piazza *et al.*, 2005)
Cx32	CMT1X	R75P (X-linked)	(Bone *et al.*, 1997)	-Localized at Golgi (HeLa) -Able to form morphological GJ plaques (N2A) -GJ function reduced -Altered V_j-gating when paired with wt Cx32	(Yum *et al.*, 2002); (Abrams *et al.*, 2013)
		R75Q (X-linked)	(Silander *et al.*, 1997); (Tan *et al.*, 1996)	Same defects as Cx32 R75P	(Yum *et al.*, 2002); (Wang *et al.*, 2004); (Abrams *et al.*, 2013)
		R75W (X-linked)	(Bone *et al.*, 1997) (Latour *et al.*, 1997) (Silander *et al.*, 1997)	Same defects as Cx32 R75P	(Abrams *et al.*, 2013)
Cx46	Congenital cataracts	R76H (AD)	(Burdon *et al.*, 2004)	-Morphological GJ plaque reduced/eliminated (N2A) -GJ function reduced	(Abrams *et al.*, 2018)
		R76G (AD)	(Devi *et al.*, 2005)	Same defects as Cx46 R76H	(Abrams *et al.*, 2018)
Cx43	ODDD	R76H (AR)	(Pizzuti *et al.*, 2004)	-Able to form morphological GJ plaques (HeLa and NRK) -GJ function reduced or normal when paired with wt Cx43 and Cx45, but V_j-gating property altered in R76H -γ_j reduced	(Huang *et al.*, 2013); Current study
		R76S (AD)	(Paznekas *et al.*, 2003)	-Able to form morphological GJ plaques -GJ function normal when paired with wt Cx43 and Cx45, but with V_j-gating property altered in R76S/Cx43 -γ_j reduced	Current study
		R76C (AD)	(Izumi *et al.*, 2013)	-Morphological GJ plaques reduced (HeLa) -Non-functional GJs -Non-functional GJs paired with wildtype Cx43 -GJ function normal when paired with wtCx45	Current study
Cx45	Progressive atrial conduction defect	R75H (AD)	(Seki *et al.*, 2017)	-Able to form morphological GJ plaques (N2A) -Unable to form morphological GJ plaques (HeLa) -Non-functional GJs -Non-functional GJs paired with wtCx45 and wtCx43 -Dominant-negative effect on heteromeric wtCx45	(Seki *et al.*, 2017); Current study
Cx50	Congenital cataracts	R76H (AD)	(Wang *et al.*, 2020); (Yu *et al.*, 2016)	-No GJ plaque (HeLa) (Wang *et al.*, 2020) - Able to form morphological GJ plaques (Hek293) (Yu *et al.*, 2016) -Non-functional GJs -Non-functional GJs paired with wildtype Cx50 or Cx46	(Wang *et al.*, 2020); (Yu *et al.*, 2016); Current study
		R76C (AD)	(Reis *et al.*, 2013)	-Non-functional GJs. -Non-functional GJs paired with wt Cx50 or wt Cx46	Current study

AD autosomal dominant; AR autosomal recessive. CMT1X: Type 1 X-linked Charcot-Marie-Tooth disease; PPK: palmoplantar keratoderma; ODDD: Oculodentodigital dysplasia; GJ/GJs: gap junctions; wt: wildtype; V_j-gating: transjunctional voltage dependent gating; γ_j: unitary channel conductance.

Molecular and structural insights on mechanisms of R76 mutants

Our homology structure models based on the recently resolved high resolution structure model of Cx50 (Flores *et al.*, 2020) showed salt bridges could be formed between Cx50 R76 (or equivalent residue in Cx43 and Cx45) and E48 (or equivalent residue) of the same subunit and E208 (or equivalent residue) of a neighbouring subunit. In the case of Cx45 homology model, an additional salt bridge could be formed between the S42 of the

neighbouring subunit and of R75 as the distance is around 3.5 Å (Fig. 2-15). Previous studies developed their homology models of Cx32 and Cx46 using the Cx26 (PDB: 2ZW3) structure as a template, which showed an additional inter-subunit salt bridge between R75 (or R76) and E42 in Cx26 (or S42 in Cx32, D43 in Cx46) in close proximity (Fig. 2-15A) (Abrams *et al.*, 2013, 2018). In contrast, this inter-subunit salt bridge does not exist according to our homology Cx50 and Cx43 structure models but a similar interaction could be identified in the Cx45 structure. As shown in Fig. 2-15A, the corresponding residues of E42 in Cx26 are F43 in Cx50, S43 in Cx43, and S42 in Cx45 (grey arrow). The amino acid serine in Cx43 and Cx45 contains a hydroxyl group, which is possible to form a salt bridge with R76/75; However, the structure model of Cx43 illustrated that the corresponding residue of S43 is less likely to establish a salt bridge as the distance between the side chains was at least 4.6 Å away from R76 sidechain (Fig. 2-15B, white line) while Cx45 S42 is 3.5 Å from R75 sidechain and has the potential to form a salt bridge with R75 to stabilize the protein structure. Nonetheless, it was not included in the structure models in the Results as this interaction is likely to be much weaker. The intra-subunit salt bridge may be important in folding the connexins structures at the E1 domain, while the inter-subunit interaction is likely to contribute to the oligomerization of six connexin subunits into a hemichannel and maintain a proper structure of the docking interface. The mutagenesis analyses demonstrated that different R76 mutations lead to a partial or complete loss of these interactions. Note that the disruption of these salt bridges in different mutants does not necessarily correspond to the functional status of the mutant GJs. For example, although some (or all) salt bridges were disrupted in Cx43 R76H, R76S and R76C, R76H and R76S could still form functional GJs, but not Cx43 R76C.

In conclusion, R76 in Cx50 or its equivalent residue in other family connexins is highly conserved and mutations on this residue are frequently linked to inherited connexin diseases. Our functional characterizations in mutants on this or equivalent residue in Cx50, Cx43, and Cx45 revealed most of the mutants showed impaired GJ function and/or with apparently normal GJ function but with altered V_j-gating or γj. Our homology models indicate mutations on R76 or R75 could impair intra- and inter-subunit interactions, which could lead to misfolding and/or improper oligomerization of the connexin to impair or alter

GJ function in these and possibly other connexins to promote the as sociated connexin diseases.
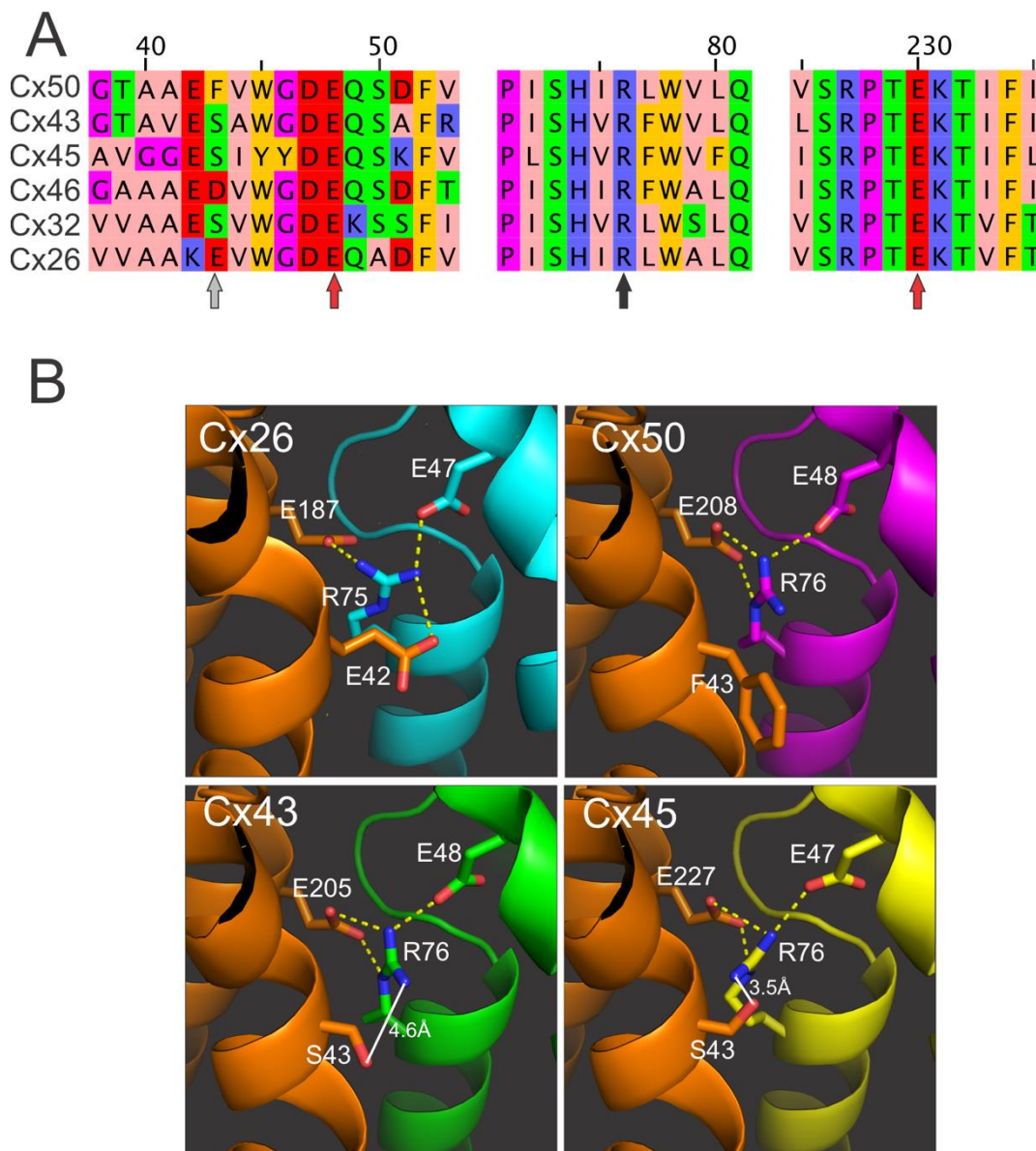
Fig. 2-15. Sequence alignments of six human connexins at R76 and nearby domains and homology structure models of Cx26, Cx50, Cx43 and Cx45 GJs at R76 or equivalent R75.

(A) The sequence alignments of human Cx50, Cx43, Cx45, Cx46, Cx32 and Cx26 are shown in three short stretches, near R76 at the junction of E1 - M2 domain, M1 - E1 domain, and the E2 - M4 domain. Each sequence was downloaded from UniProt individually and imported into Jalview (2.11.2.4) for alignment using ClustalOmega with default setting. The position number was labelled according to Cx50. R76 is indicated by a black arrow, and the E48 and E208 that form salt bridges with R76 are indicated by red

arrows. In addition, the grey arrow indicates the 43rd position or the equivalent that was predicted by previous studies to form a salt bridge with R76/75 in Cx46, Cx32 and Cx26 (Abrams *et al.*, 2013, 2018). (B) The structure models of Cx26 and Cx50 as well as the homology structure models of Cx43 and Cx45 are presented in a zoom-in view of R76 (or R75). These four connexin GJ structures all share similar R76 interactions with E48 and E208 in Cx50, E48 and E205 in Cx43, and E47 and E227 in Cx45. R75 in Cx26 and Cx45 are likely to form an additional salt bridge with E42 of a neighbouring subunit in Cx26 and S42 of a neighbouring subunit in Cx45, respectively (the distance between S42 to R75 in Cx45 is 3.5 Å). The distance between S43 and R76 side chains in Cx43 is over 4 Å.

References

Abrams CK, Islam M, Mahmoud R, Kwon T, Bargiello TA & Freidin MM (2013). Functional Requirement for a Highly Conserved Charged Residue at Position 75 in the Gap Junction Protein Connexin 32*. *J Biol Chem* **288,** 3609–3619.

Abrams CK, Peinado A, Mahmoud R, Bocarsly M, Zhang H, Chang P, Botello-Smith WM, Freidin MM & Luo Y (2018). Alterations at Arg76 of human connexin 46, a residue associated with cataract formation, cause loss of gap junction formation but preserve hemichannel function. *Am J Physiol Cell Physiol* **315,** C623–C635.

Bai D & Wang AH (2014). Extracellular domains play different roles in gap junction formation and docking compatibility. *Biochem J* **458,** 1–10.

Bai D, Wang J, Li T, Chan R, Atalla M, Chen RC, Khazaneh MT, An RJ & Stathopulos PB (2021). Differential Domain Distribution of gnomAD- and Disease-Linked Connexin Missense Variants. *Int J Mol Sci*; DOI: 10.3390/ijms22157832.

Bai D, Yue B & Aoyama H (2018). Crucial motifs and residues in the extracellular loops influence the formation and specificity of connexin docking. *Biochim Biophys Acta BBA - Biomembr* **1860,** 9–21.

Bao M, Kanter EM, Huang RY, Maxeiner S, Frank M, Zhang Y, Schuessler RB, Smith TW, Townsend RR, Rohrs HW, Berthoud VM, Willecke K, Laing JG & Yamada KA (2011). Residual Cx45 and its relationship to Cx43 in Murine ventricular myocardium. *Channels* **5,** 489–499.

Bao X, Chen Y, Reuss L & Altenberg GA (2004). Functional expression in Xenopus oocytes of gap-junctional hemichannels formed by a cysteine-less connexin 43. *J Biol Chem* **279,** 9689–9692.

Bargiello TA, Oh S, Tang Q, Bargiello NK, Dowd TL & Kwon T (2018). Gating of Connexin Channels by transjunctional-voltage: Conformations and models of open and closed states. *Biochim Biophys Acta Biomembr* **1860,** 22–39.

Bennett BC, Purdy MD, Baker KA, Acharya C, McIntire WE, Stevens RC, Zhang Q, Harris AL, Abagyan R & Yeager M (2016). An electrostatic mechanism for Ca2+-mediated regulation of gap junction channels. *Nat Commun*; DOI: 10.1038/ncomms9770.

Berthoud VM, Minogue PJ, Yu H, Schroeder R, Snabb JI & Beyer EC (2013). Connexin50D47A decreases levels of fiber cell connexins and impairs lens fiber cell differentiation. *Invest Ophthalmol Vis Sci* **54,** 7614–7622.

Betts MJ & Russell RB (2003). Amino Acid Properties and Consequences of Substitutions. In *Bioinformatics for Geneticists*, pp. 289–316. John Wiley & Sons, Ltd. Available at: http://onlinelibrary.wiley.com/doi/abs/10.1002/0470867302.ch14 [Accessed August 4, 2022].

Beyer EC, Ebihara L & Berthoud VM (2013). Connexin mutants and cataracts. *Front Pharmacol* **4,** 43.

Beyer EC, Kistler J, Paul DL & Goodenough DA (1989). Antisera directed against connexin43 peptides react with a 43-kD protein localized to gap junctions in myocardium and other tissues. *J Cell Biol* **108,** 595–605.

Bone LJ, Deschenes SM, Balice-Gordon RJ, Fischbeck KH & Scherer SS (1997). Connexin32 and X-linked Charcot–Marie–Tooth Disease. 10.

Burdon K, Wirth M, Mackey D, Russell-Eggitt I, Craig J, Elder J, Dickinson J & Sale M (2004). A novel mutation in the Connexin 46 gene causes autosomal dominant congenital cataract with incomplete penetrance. *J Med Genet* **41,** e106.

Chen Y, Deng Y, Bao X, Reuss L & Altenberg GA (2005*a*). Mechanism of the defect in gap-junctional communication by expression of a connexin 26 mutant associated with dominant deafness. *FASEB J* **19,** 1516–1518.

Chen Y, Deng Y, Bao X, Reuss L & Altenberg GA (2005*b*). Mechanism of the defect in gap-junctional communication by expression of a connexin 26 mutant associated with dominant deafness. *FASEB J* **19,** 1516–1518.

Dahl G, Levine E, Rabadan-Diehl C & Werner R (1991). Cell/cell channel formation involves disulfide exchange. *Eur J Biochem* **197,** 141–144.

Deng Y, Chen Y, Reuss L & Altenberg GA (2006). Mutations of connexin 26 at position 75 and dominant deafness: essential role of arginine for the generation of functional gap-junctional channels. *Hear Res* **220,** 87–94.

Desplantez T (2017). Cardiac Cx43, Cx40 and Cx45 co-assembling: involvement of connexins epitopes in formation of hemichannels and Gap junction channels. *BMC Cell Biol* **18,** 3.

Devi RR, Reena C & Vijayalakshmi P (2005). Novel mutations in GJA3 associated with autosomal dominant congenital cataract in the Indian population. *Mol Vis* **11,** 846–852.

Feldmann D, Denoyelle F, Blons H, Lyonnet S, Loundon N, Rouillon I, Hadj-Rabia S, Petit C, Couderc R, Garabédian E-N & Marlin S (2005). TheGJB2 mutation R75Q can cause nonsyndromic hearing loss DFNA3 or hereditary palmoplantar keratoderma with deafness. *Am J Med Genet A* **137A,** 225–227.

Flores JA, Haddad BG, Dolan KA, Myers JB, Yoshioka CC, Copperman J, Zuckerman DM & Reichow SL (2020). Connexin-46/50 in a dynamic lipid environment resolved by CryoEM at 1.9 Å. *Nat Commun* **11,** 4331.

Foote CI, Zhou L, Zhu X & Nicholson BJ (1998). The Pattern of Disulfide Linkages in the Extracellular Loop Regions of Connexin 32 Suggests a Model for the Docking Interface of Gap Junctions. *J Cell Biol* **140,** 1187–1197.

Goldberg GS, Lampe PD & Nicholson BJ (1999). Selective transfer of endogenous metabolites through gap junctions composed of different connexins. *Nat Cell Biol* **1,** 457–459.

Gong X-Q, Nakagawa S, Tsukihara T & Bai D (2013). A mechanism of gap junction docking revealed by functional rescue of a human-disease-linked connexin mutant. *J Cell Sci* **126,** 3113–3120.

Goodenough DA (1992). The crystalline lens. A system networked by gap junctional intercellular communication. *Semin Cell Biol* **3,** 49–58.

Goodenough DA & Paul DL (2009). Gap Junctions. *Cold Spring Harb Perspect Biol* **1,** a002576.

Guo Y-H & Yang Y-Q (2022). Atrial Fibrillation: Focus on Myocardial Connexins and Gap Junctions. *Biology* **11,** 489.

Huang T, Shao Q, MacDonald A, Xin L, Lorentz R, Bai D & Laird DW (2013). Autosomal recessive GJA1 (Cx43) gene mutations cause oculodentodigital dysplasia by distinct mechanisms. *J Cell Sci* **126,** 2857–2866.

Izumi K, Lippa AM, Wilkens A, Feret HA, McDonald-McGinn DM & Zackai EH (2013). Congenital heart defects in oculodentodigital dysplasia: Report of two cases. *Am J Med Genet A* **161,** 3150–3154.

Jassim A, Aoyama H, Ye WG, Chen H & Bai D (2016). Engineered Cx40 variants increased docking and function of heterotypic Cx40/Cx43 gap junction channels. *J Mol Cell Cardiol* **90,** 11–20.

Karademir LB, Aoyama H, Yue B, Chen H & Bai D (2016). Engineered Cx26 variants established functional heterotypic Cx26/Cx43 and Cx26/Cx40 gap junction channels. *Biochem J* **473,** 1391–1403.

Kim NK, Santos-Miranda A, Chen H, Aoyama H & Bai D (2019). Heterotypic docking compatibility of human connexin37 with other vascular connexins. *J Mol Cell Cardiol* **127,** 194–203.

Kumar NM & Gilula NB (1996). The Gap Junction Communication Channel. *Cell* **84,** 381–388.

Latour P, Lévy N, Paret M, Chapon F, Chazot G, Clavelou P, Couratier P, Dumas R, Ollagnon E, Pouget J, Setiey A, Vallat JM, Boucherat M, Fontes M & Vandenberghe A (1997). Mutations in the X-linked form of Charcot-Marie-Tooth disease in the French population. *neurogenetics* **1,** 117–123.

Lurtz MM & Louis CF (2007). Intracellular calcium regulation of connexin43. *Am J Physiol-Cell Physiol* **293,** C1806–C1813.

Maeda S, Nakagawa S, Suga M, Yamashita E, Oshima A, Fujiyoshi Y & Tsukihara T (2009). Structure of the connexin 26 gap junction channel at 3.5 Å resolution. *Nature* **458,** 597–602.

Myers JB, Haddad BG, O'Neill SE, Chorev DS, Yoshioka CC, Robinson CV, Zuckerman DM & Reichow SL (2018). Structure of native lens connexin-46/50 intercellular channels by CryoEM. *Nature* **564,** 372–377.

Nakagawa S, Gong X-Q, Maeda S, Dong Y, Misumi Y, Tsukihara T & Bai D (2011). Asparagine 175 of Connexin32 Is a Critical Residue for Docking and Forming Functional Heterotypic Gap Junction Channels with Connexin26. *J Biol Chem* **286,** 19672–19681.

Paul DL, Ebihara L, Takemoto LJ, Swenson KI & Goodenough DA (1991). Connexin46, a novel lens gap junction protein, induces voltage-gated currents in nonjunctional plasma membrane of Xenopus oocytes. *J Cell Biol* **115,** 1077–1089.

Paznekas WA, Boyadjiev SA, Shapiro RE, Daniels O, Wollnik B, Keegan CE, Innis JW, Dinulos MB, Christian C, Hannibal MC & Jabs EW (2003). Connexin 43 (GJA1) Mutations Cause the Pleiotropic Phenotype of Oculodentodigital Dysplasia. *Am J Hum Genet* **72,** 408–418.

Peracchia C (1978). Calcium effects on gap junction structure and cell coupling. *Nature* **271,** 669–671.

Peracchia C (2004). Chemical gating of gap junction channels: Roles of calcium, pH and calmodulin. *Biochim Biophys Acta BBA - Biomembr* **1662,** 61–80.

Piazza V, Beltramello M, Menniti M, Colao E, Malatesta P, Argento R, Chiarella G, Gallo L, Catalano M, Perrotti N, Mammano F & Cassandro E (2005). Functional analysis of R75Q mutation in the gene coding for Connexin 26 identified in a family with nonsyndromic hearing loss. *Clin Genet* **68,** 161–166.

Pizzuti A, Flex E, Mingarelli R, Salpietro C, Zelante L & Dallapiccola B (2004). A homozygousGJA1 gene mutation causes a Hallermann-Streiff/ODDD spectrum phenotype. *Hum Mutat* **23,** 286–286.

Qi C, Acosta-Gutierrez S, Lavriha P, Othman A, Lopez-Pigozzi D, Bayraktar E, Schuster D, Picotti P, Zamboni N, Bortolozzi M, Gervasio FL & Korkhov VM (2022). Structure of the connexin-43 gap junction channel reveals a closed sieve-like molecular gate. 2022.03.26.485947. Available at: https://www.biorxiv.org/content/10.1101/2022.03.26.485947v1 [Accessed September 13, 2022].

Reis LM, Tyler RC, Muheisen S, Raggio V, Salviati L, Han DP, Costakos D, Yonath H, Hall S, Power P & Semina EV (2013). Whole exome sequencing in dominant cataract identifies a new causative factor, CRYBA2, and a variety of novel alleles in known genes. *Hum Genet* **132,** 761–771.

Richard G, White TW, Smith LE, Bailey RA, Compton JG, Paul DL & Bale SJ (1998). Functional defects of Cx26 resulting from a heterozygous missense mutation in a family with dominant deaf-mutism and palmoplantar keratoderma. *Hum Genet* **103,** 393–399.

Rose B & Loewenstein WR (1975). Permeability of cell junction depends on local cytoplasmic calcium activity. *Nature* **254,** 250–252.

Saez JC, Berthoud VM, Branes MC, Martinez AD & Beyer EC (2003). Plasma membrane channels formed by connexins: their regulation and functions. *Physiol Rev* **83,** 1359–1401.

Schadzek P, Schlingmann B, Schaarschmidt F, Lindner J, Koval M, Heisterkamp A, Ngezahayo A & Preller M (2016*a*). Data of the molecular dynamics simulations of mutations in the human connexin46 docking interface. *Data Brief* **7,** 93–99.

Schadzek P, Schlingmann B, Schaarschmidt F, Lindner J, Koval M, Heisterkamp A, Preller M & Ngezahayo A (2016*b*). The cataract related mutation N188T in human connexin46 (hCx46) revealed a critical role for residue N188 in the docking process of gap junction channels. *Biochim Biophys Acta* **1858,** 57–66.

Seki A et al. (2017). Progressive Atrial Conduction Defects Associated With Bone Malformation Caused by a Connexin-45 Mutation. *J Am Coll Cardiol* **70,** 358–370.

Silander K, Meretoja P, Pihko H, Juvonen V, Issakainen J, Aula P & Savontaus M-L (1997). Screening for connexin 32 mutations in Charcot-Marie-Tooth disease families with possible X-linked inheritance. *Hum Genet* **100,** 391–397.

Spray DC, Harris AL & Bennett MV (1981). Equilibrium properties of a voltage-dependent junctional conductance. *J Gen Physiol* **77,** 77–93.

Sun Y, Yang Y-Q, Gong X-Q, Wang X-H, Li R-G, Tan H-W, Liu X, Fang W-Y & Bai D (2013). Novel Germline GJA5/Connexin40 Mutations Associated with Lone Atrial Fibrillation Impair Gap Junctional Intercellular Communication. *Hum Mutat* **34,** 603–609.

Tan CC, Ainsworth PJ, Hahn AF & MacLeod PM (1996). Novel mutations in the connexin 32 gene associated with X-linked Charcot-Marie tooth disease. *Hum Mutat* **7,** 167–171.

Tong D, Li TY, Naus KE, Bai D & Kidder GM (2007). In vivo analysis of undocked connexin43 gap junction hemichannels in ovarian granulosa cells. *J Cell Sci* **120,** 4016–4024.

Uyguner O, Tukel T, Baykal C, Eris H, Emiroglu M, Hafiz G, Ghanbari A, Baserer N, Yuksel-Apak M & Wollnik B (2002). The novel R75Q mutation in the GJB2 gene causes autosomal dominant hearing loss and palmoplantar keratoderma in a Turkish family. *Clin Genet* **62,** 306–309.

van der Velden HMW & Jongsma HJ (2002). Cardiac gap junctions and connexins: their role in atrial fibrillation and potential as therapeutic targets. *Cardiovasc Res* **54,** 270–279.

Wang H-L, Chang W-T, Yeh T-H, Wu T, Chen M-S & Wu C-Y (2004). Functional analysis of connexin-32 mutants associated with X-linked dominant Charcot-Marie-Tooth disease. *Neurobiol Dis* **15,** 361–370.

Wang KJ, Da Wang J, Chen DD, Wang MY, Yun B & Zhu SQ (2020*a*). Characterization of a p.R76H mutation in Cx50 identified in a Chinese family with congenital nuclear cataract. *J Formos Med Assoc* **119,** 144–149.

Wang KJ, Da Wang J, Chen DD, Wang MY, Yun B & Zhu SQ (2020*b*). Characterization of a p.R76H mutation in Cx50 identified in a Chinese family with congenital nuclear cataract. *J Formos Med Assoc* **119,** 144–149.

White TW, Bruzzone R, Goodenough DA & Paul DL (1992). Mouse Cx50, a functional member of the connexin family of gap junction proteins, is the lens fiber protein MP70. *Mol Biol Cell* **3,** 711–720.

Ye WG, Yue B, Aoyama H, Kim NK, Cameron JA, Chen H & Bai D (2017*a*). Junctional delay, frequency, and direction-dependent uncoupling of human heterotypic Cx45/Cx43 gap junction channels. *J Mol Cell Cardiol* **111,** 17–26.

Ye WG, Yue B, Aoyama H, Kim NK, Cameron JA, Chen H & Bai D (2017*b*). Junctional delay, frequency, and direction-dependent uncoupling of human heterotypic Cx45/Cx43 gap junction channels. *J Mol Cell Cardiol* **111,** 17–26.

Yu Y, Wu M, Chen X, Zhu Y, Gong X & Yao K (2016). Identification and functional analysis of two novel connexin 50 mutations associated with autosome dominant congenital cataracts. *Sci Rep* **6,** 26551.

Yum SW, Kleopa KA, Shumas S & Scherer SS (2002). Diverse trafficking abnormalities of connexin32 mutants causing CMTX. *Neurobiol Dis* **11,** 43–52.

Yum SW, Zhang J & Scherer SS (2010). Dominant connexin26 mutants associated with human hearing loss have trans-dominant effects on connexin30. *Neurobiol Dis* **38,** 226–236.

Chapter 3

General Discussion

Overall study

This study aimed to address the knowledge gap on the functional status and properties of GJs formed by connexins with disease-associated mutations, especially on the ability of these mutants to form heterotypic GJs. We showed that most of the mutations in Cx50, Cx43, and Cx45 were unable to form functional homotypic GJs, with the exception of Cx43 R76H and R76S where functional GJs were formed and both of them can also form functional GJs when paired with wildtype Cx43. Surprisingly, all three Cx43 mutants, R76H, R76S and R76C were able to form functional heterotypic GJs with Cx45. The transjunctional voltage-dependent gating (V_j-gating) properties of the functional GJs were compared with their respective controls, and R76H, R76S and R76S / Cx43 GJs exhibited altered V_j-gating properties. Our preliminary data of the unitary conductance (γ_j) of the Cx43 R76S GJ was lower than the wildtype Cx43 GJs. The homology structure models and mutagenesis analysis illustrated that these mutants had different levels of disruption of salt bridges of the R76 sidechain with neighbouring residues and were not necessarily correlated to the functional data. Especially in the functional Cx43 R76H and R76S GJs, the partial or complete loss of salt bridges on the sidechain of the 76th residue did not affect the formation of functional GJs. The R76 residue is highly likely to be critical in connexin subunit folding and the oligomerization into proper hemichannel structure. Finally, our results showed that restoring the partial positive charge at the 76th position was not sufficient to restore the function of Cx50 R76H and Cx45 R75H mutant GJs. Overall, this study contributed to the understanding of the cellular and molecular mechanisms of disease-linked mutations at R76 (or R75) residues in three common connexins. Our study also highlighted the importance of R76 residue in forming functional GJs, which could imply the pathophysiological mechanisms of the relevant connexin diseases.

Potential role of the R76/75 residue in hemichannel docking

R76 is located on the border of E1 and M2 domains and is more than ten amino acid residues away from the nearest triple cysteine residue in E1, which form disulfide bridges with three cysteine residues on the E2. These intra-subunit disulfide bonds between E1 and E2 domains are known to be important in folding a single connexin subunit (Bai *et al.*, 2018). From co-variation analysis, we have shown that R76/75 residue co-evolves with those hydrogen bonds (HB) forming residues at the hemichannel docking interface, which implies that despite R76/75 is not directly on the docking interface, it is a part of a network with other docking residues on the E1 and E2 domains to mediate hemichannel docking (Bai *et al.*, 2021). In addition, Abram et al. (2018) demonstrated that R76 residue is important in forming functional Cx46 GJs. Their homology structure model of Cx46 based on the crystal structure of Cx26 revealed that the R76th residue forms one intra- and two inter-subunit salt bridges, which might be critical to stabilize the conformation of the extracellular loop domains that are required in the proper docking between two hemichannels. Our current study on Cx50 and Cx45 also supports this idea, in which R76 or equivalent residue plays an important role in the formation of functional GJs and the intra- and inter-subunit salt bridges at the R76 sidechain which might be important for the connexin subunit folding to form a proper structured hemichannels to from functional GJs. It is very interesting, but currently not clear how mutations in R76 in Cx43 GJ are still able to form functional GJs, perhaps that Cx43 GJ structure is very different from those of Cx50 and Cx26, which could accommodate some structural changes around R76 and still able to form homotypic functional GJs with the mutants (R76S and R76H) or only form heterotypic GJs with Cx45 (R76C). More mutagenesis studies will be needed to explore this further, but Cx43 and Cx45 GJs or their hemichannels displayed some structural flexibility to adapt the structural changes associated with some mutations on R76 in Cx43.

The restoration of a positive net charge at the 76th residue did not restore the Cx50 R76H and Cx45 R75H GJ function

We investigated whether the positive charge at the R76 residue is critical to establish the intra- and/or inter-subunit salt bridges and whether it is possible to rescue GJ function of Cx50 R76H and Cx45 R75H GJs under experimental conditions favouring protonation of

the histidine. By lowering the pH of the intracellular or extracellular solution to 6.8, we expected to have the histidine side chain partially protonated in R76H mutant GJs, restoring the positive charge at the 76th residue at least in some of the GJs might be sufficient to rescue their GJ function. Our electrophysiology results showed that lowering the pH of intracellular (pH_i) or extracellular (pH_e) solution to 6.8 did not rescue mutant GJ function, which suggested that the partially restored +charge at the 76th position was insufficient to restore the local interactions with neighbouring residues, thereby the mutant connexins were unable to form functional GJs. Many factors could also play a role in the structural interactions between residues in the 3-dimensional protein structure. Perhaps the size or the conformation of the amino acid side chain is also important to stabilize the interactions between R76 and others neighbouring residues.

Lens Cx46 and Cx50 orthologs in sheep, human and mouse

Our functional studies of pathogenic mutations at R76 (or 75 in some connexins) have revealed the functional importance of R76 in connexin function and most importantly, the importance of this residue in formation of functional GJs of Cx50. Sheep Cx50 and Cx46 were selected for our recombinant expression study because 1) we can directly align our functional data with the high-resolution GJ structures (Myers *et al.*, 2018; Flores *et al.*, 2020) and 2) human Cx46 cDNA construct is not expressed well in N2A cells and too difficult to obtain experimental data routinely. The sheep Cx50 and Cx46 have 96% and 95% sequence identity to human Cx50 and Cx46 for the structural-resolved domains, respectively (Fig. 3-1A, B). The sheep Cx50 and Cx46 have 97.4% and 95% sequence identity to mouse Cx50 and Cx46 for the structure-resolved domains, respectively (Fig. 3-1A, B). With the high level of sequence identities, we believe that sheep Cx50 and Cx46 GJ structures are good models for the homolog connexins from human to study disease-linked mutations while providing structural insights. Furthermore, our functional study has revealed similar V_j-gating properties to those previously reported on the mouse and human Cx50 and Cx46 (White *et al.*, 1994; Pal *et al.*, 1999; Hopperstad *et al.*, 2000; Xin *et al.*, 2010). The V_j-gating properties and the Boltzmann fitting curves of wildtype sheep Cx50 are also similar to previous functional studies using sheep Cx50, in which the wildtype

Cx50 GJ has a lower G_{min}, high sensitivity (big A value), and a half-deactivation voltage of ~ 40 mV (Yue *et al.*, 2021).
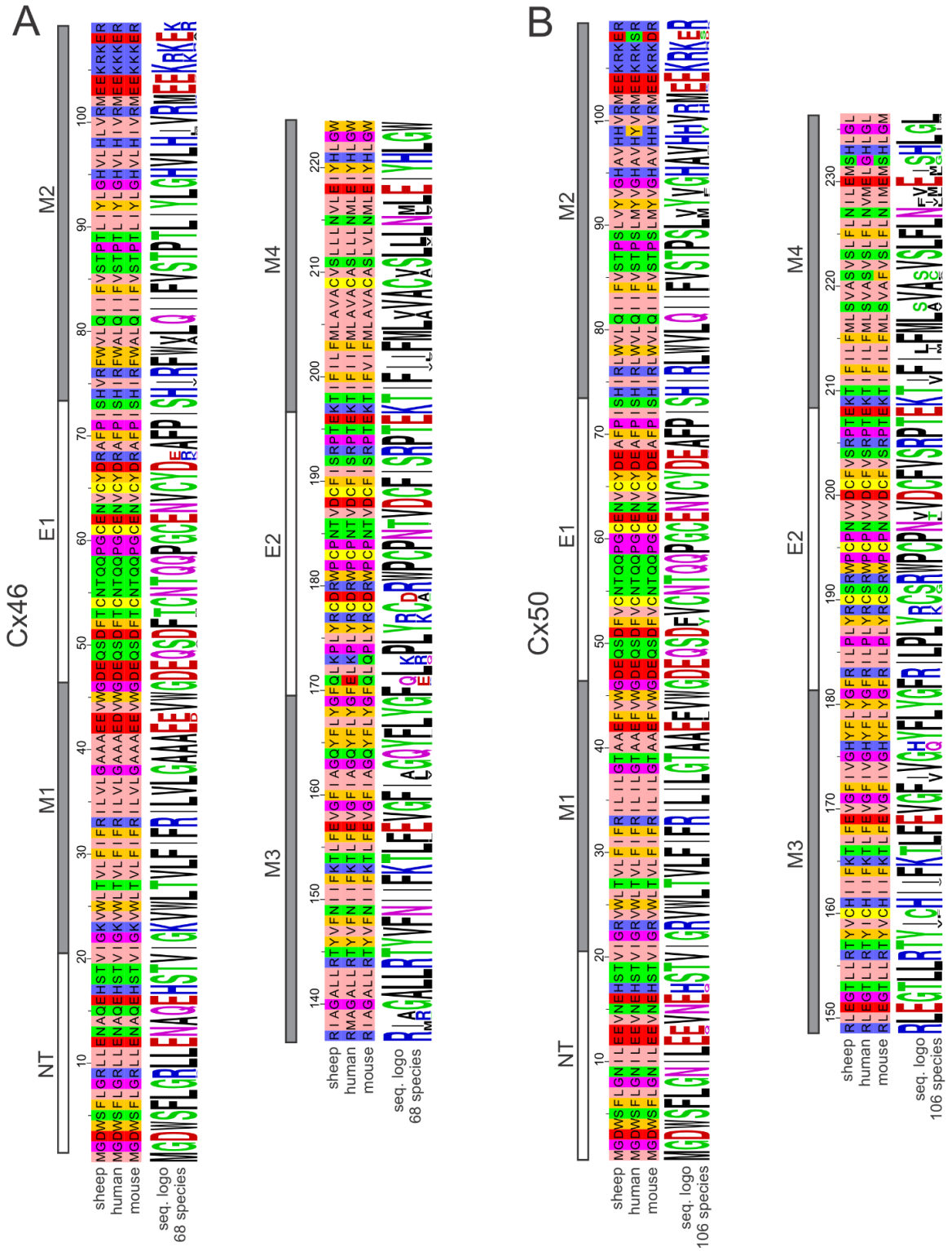
Fig. 3-1. Sequence alignments and sequence logo of the structural-resolved domains of Cx46 and Cx50.

(A) Sheep, human and mouse Cx46 sequences were downloaded from the Uniport website and imported into Jalview (2.11.2.4) for sequence alignment. ClustalOmega with default setting was used for the sequence alignment of the structural-resolved domains, including NT, M1, E1, M2, M3, E2 and M4 domains. The sequence logo of Cx46 contains 68 species for the corresponding domains are shown under the alignment. (B) Sheep, human and mouse Cx50 sequences were downloaded from the Uniport website and imported into Jalview (2.11.2.4) for sequence alignment. ClustalOmega with default setting was used for the sequence alignment of structural-resolved domains, including NT, M1, E1, M2, M3, E2 and M4 domains. The sequence logo of Cx50 contains 106 species for the corresponding domains are shown under the alignment. The percentages of sequence identity between sheep and human (or sheep and mouse) were calculated by dividing the number of identical residues by the total number of residues within the entire structural-resolved domains.

Limitations and future studies

Our study together with previous studies provided compelling evidence for the importance of R76/75 residue in the formation of functional GJs (Chen *et al.*, 2005; Huang *et al.*, 2013; Abrams *et al.*, 2013, 2018). The results are mostly consistent with previous findings that R76 mutations led to a loss-of-function of GJs as well as have dominant-negative effects in GJs function formed by pairing the mutant connexin with its corresponding wildtype or docking compatible connexins. Nevertheless, there are a few limitations in the experimental condition of this study. First, our electrophysiological recordings on cell pairs expressing Cx43 were technically difficult. Cx43 forms too many functional GJ channels with a fast pace when expressed GFP-untagged Cx43 in N2A cells. Dual whole cell voltage clamp recordings could have voltage clamp errors, especially those cell pairs with a high level of GJ coupling conductance (Van Rijen *et al.*, 1998). To ensure the quality of our patch clamp recording (lower voltage clamp errors) for voltage-dependent gating (V_j-gating) analysis, we shortened the replating time to as low as ~30 mins, a minimum time for cells to be stably attached to the coverslip to allow us to perform patch clamp recording. This allowed us to record cell pairs that were just adhered to the coverslip and not having too high of a GJ coupling conductance, ideally with a $G_j \leq 9$ nS for optimal voltage clamp. However, the chance of obtaining analyzable results without having a too high level of G_j

in selected cell pairs (we set a cut-off to eliminate cell pairs that had $G_j > 50$ nS to avoid cytoplasmic bridge) was relatively low, and it was even more difficult to acquire unitary channel conductance (γ_j) from cell pairs that had one or two GJ channels. We have already tried to look for cell pairs with a very low level of GFP expression. We still could not obtain enough cell pairs with only 1-2 Cx43 or its mutants GJ channels to do proper analyses. It would be ideal to obtain more unitary channel recordings for γ_j analysis of Cx43 R76H and R76S GJ to consolidate our current preliminary findings.

We decided to investigate the effects of +charge on arginine or histidine at the 76th position in establishing local salt bridges on their sidechain and whether it is necessary for the function of Cx50 R76H and Cx45 R75H GJs by lowering the intracellular (pH_i) or extracellular pH (pH_e) solutions to 6.8 in dual whole cell patch clamp experiments. Previous studies showed that wildtype Cx50 and Cx45 GJs tend to close in low pH_i. Cx50 GJs had a decreased G_j by 78% with a drop in pH_i from 7.73 (the physiological pH_i of oocytes on average) to 6.83 (Peracchia & Peracchia, 2005), and the G_j was reduced by 80% in SKHep1 cells when the pH_i was dropped from 7 to 6.7 (Hermans *et al.*, 1995). The side chain of histidine has a pKa value of 6, so we decided to adjust the pH_i or pH_e to 6.8 to slightly protonate the histidine side chain while making sure the channel remains open or not gated by too low of a pH level. The high-resolution Cx50 GJ structure (PDB: 7JJP) showed that the R76 side chain faces toward the channel pore; however, we could not rule out the possibility that the R76H or R75H in Cx50 or Cx45 faces away from the intracellular space in the undocked Cx50 R76H or Cx45 R75H hemichannel structures (Cx50 R76H and Cx45 R75H were unable to form functional GJs). Thus, we changed the pH_i or pH_e independently from 7.2 or 7.4 to 6.8 to study the charge effect at the 76th residue. As indicated in our results, lowering the pH_i or pH_e to 6.8 did not restore the R76H mutant channel function. It is possible that changing the pH to 6.8 is not acidic enough to protonate the histidine side chain in the mutants and perhaps performing experiments with pH at 6.5~6.8 is needed to further investigate the +charge effect at R76. Aside from this, lowering the pH did not necessarily protonate the histidine at the 76th position specifically. Many histidine side chains could be protonated and collectively affect the channel structure and function.

Lastly, the co-localization experiments using GFP-tagged connexin mutants were not included in this thesis because of the restricted time frame (the co-localization study is currently in progress and is performed by H. Chen and D. Bai). It has been described that the docking of two hemichannels is an independent process from the formation of functional GJs, because undocked hemichannels could open under certain experimental conditions in most connexins, implying that the docking process is not a prerequisite for the GJ function (L. Harris, 2001; Bai *et al.*, 2018). Thus, it is possible that two docked hemichannels could not open to form functional GJs. Morphological studies using fluorescent protein-tagged connexins identify the GJ plaque-like structure at cell interfaces, indicating the formation of functional GJs in most cases, but not always (Bai *et al.*, 2018). In addition, it also provides information on connexin biosynthesis and trafficking to the cell plasma membrane, helping to rule out the possibility that a connexin mutant has not been properly expressed in the plasma membrane. Hence, we are performing co-localization experiments using fluorescent protein-tagged connexins (or mutants) to provide additional evidence on the localization changes of the mutant connexins.

Summary

The extracellular loop domains of connexin play an important role in the docking and formation of functional GJs. Several residues on both extracellular loop domains are found to be docking relevant that form non-covalent interactions to stabilize connexin structures for proper docking and forming functional GJs. Arg 76 (or 75 in some connexins) is located at the boundary of the E1 and M2 domains and has been characterized to be important in the docking and formation of function GJs in Cx26, Cx32 and Cx46 (Chen *et al.*, 2005; Piazza *et al.*, 2005; Abrams *et al.*, 2013, 2018). Here, we investigated the functional status and properties of six additional R76 (or R75) mutants in Cx50, Cx43 and Cx45 that have been associated with inherited diseases. We found that Cx50 R76H, R76C and Cx45 R75H were unable to form functional GJs, nor to form functional GJs when paired with corresponding wildtype or docking compatible connexins. Cx43 R76H and R76S formed function GJs and formed functional heterotypic GJs when paired with Cx45. Nonetheless, the channel properties (i.e., V_j-gating or γ_j) of Cx43 R76H, R76S, or R76S / Cx43 GJs were

altered. The homology structure models of different connexins imply a possible role of R76 residue in connexin folding (intra-subunit interaction) and oligomerization (inter-subunit interactions) to establish a proper structure to have GJ channel function. Overall, our study and previous studies formed a strong line of evidence that the R76 residue is critical in the formation of functional GJs, and impairment of GJ function or altered GJ properties could play a role in their respective connexin-linked human diseases.

References

Abrams CK, Islam M, Mahmoud R, Kwon T, Bargiello TA & Freidin MM (2013). Functional Requirement for a Highly Conserved Charged Residue at Position 75 in the Gap Junction Protein Connexin 32*. *J Biol Chem* **288,** 3609–3619.

Abrams CK, Peinado A, Mahmoud R, Bocarsly M, Zhang H, Chang P, Botello-Smith WM, Freidin MM & Luo Y (2018). Alterations at Arg76 of human connexin 46, a residue associated with cataract formation, cause loss of gap junction formation but preserve hemichannel function. *Am J Physiol Cell Physiol* **315,** C623–C635.

Bai D, Wang J, Li T, Chan R, Atalla M, Chen RC, Khazaneh MT, An RJ & Stathopulos PB (2021). Differential Domain Distribution of gnomAD- and Disease-Linked Connexin Missense Variants. *Int J Mol Sci*; DOI: 10.3390/ijms22157832.

Bai D, Yue B & Aoyama H (2018). Crucial motifs and residues in the extracellular loops influence the formation and specificity of connexin docking. *Biochim Biophys Acta BBA - Biomembr* **1860,** 9–21.

Chen Y, Deng Y, Bao X, Reuss L & Altenberg GA (2005). Mechanism of the defect in gap-junctional communication by expression of a connexin 26 mutant associated with dominant deafness. *FASEB J* **19,** 1516–1518.

Flores JA, Haddad BG, Dolan KA, Myers JB, Yoshioka CC, Copperman J, Zuckerman DM & Reichow SL (2020). Connexin-46/50 in a dynamic lipid environment resolved by CryoEM at 1.9 Å. *Nat Commun* **11,** 4331.

Hansen AL & Kay LE (2014). Measurement of histidine pKa values and tautomer populations in invisible protein states. *Proc Natl Acad Sci* **111,** E1705–E1712.

Hermans M, Kortekaas P, Jongsma H & Rook M (1995). pH sensitivity of the cardiac gap junction proteins, connexin 45 and 43. *Pflüg Arch* **431,** 138–140.

Hopperstad MG, Srinivas M & Spray DC (2000). Properties of gap junction channels formed by Cx46 alone and in combination with Cx50. *Biophys J* **79,** 1954–1966.

Huang T, Shao Q, MacDonald A, Xin L, Lorentz R, Bai D & Laird DW (2013). Autosomal recessive GJA1 (Cx43) gene mutations cause oculodentodigital dysplasia by distinct mechanisms. *J Cell Sci* **126,** 2857–2866.

L. Harris A (2001). Emerging issues of connexin channels: biophysics fills the gap. *Q Rev Biophys* **34,** 325–472.

Myers JB, Haddad BG, O'Neill SE, Chorev DS, Yoshioka CC, Robinson CV, Zuckerman DM & Reichow SL (2018). Structure of native lens connexin-46/50 intercellular channels by CryoEM. *Nature* **564,** 372–377.

Pal JD, Berthoud VM, Beyer EC, Mackay D, Shiels A & Ebihara L (1999). Molecular mechanism underlying a Cx50-linked congenital cataract. *Am J Physiol-Cell Physiol* **276,** C1443–C1446.

Peracchia C & Peracchia LL (2005). Inversion of both gating polarity and CO_2 sensitivity of voltage gating with D3N mutation of Cx50. *Am J Physiol-Cell Physiol* **288,** C1381–C1389.

Piazza V, Beltramello M, Menniti M, Colao E, Malatesta P, Argento R, Chiarella G, Gallo L, Catalano M, Perrotti N, Mammano F & Cassandro E (2005). Functional analysis of R75Q mutation in the gene coding for Connexin 26 identified in a family with nonsyndromic hearing loss. *Clin Genet* **68,** 161–166.

White TW, Bruzzone R, Wolfram S, Paul DL & Goodenough DA (1994). Selective interactions among the multiple connexin proteins expressed in the vertebrate lens: the second extracellular domain is a determinant of compatibility between connexins. *J Cell Biol* **125,** 879–892.

Xin L, Gong X-Q & Bai D (2010). The Role of Amino Terminus of Mouse Cx50 in Determining Transjunctional Voltage-Dependent Gating and Unitary Conductance. *Biophys J* **99,** 2077–2086.

Yue B, Haddad BG, Khan U, Chen H, Atalla M, Zhang Z, Zuckerman DM, Reichow SL & Bai D (2021). Connexin 46 and connexin 50 gap junction channel properties are shaped by structural and dynamic features of their N-terminal domains. *J Physiol* **599,** 3313–3335.

Van Rijen HVM, Wilders R, Van Ginneken ACG & Jongsma HJ (1998). Quantitative analysis of dual whole-cell voltage-clamp determination of gap junctional conductance. *Pflügers Arch* **436,** 141–151.

Curriculum Vitae

Name: Tianhe Li

Post-secondary   McMaster University
Education and   Hamilton, Ontario, Canada
Degrees: 2016-2020 Honours B.Sc. (Neuroscience)

                      The University of Western Ontario
                      London, Ontario, Canada
                      2020-2022 M.Sc.

Honours and   Dean's Honour List
Awards: 2016-2020

                      Entrance Scholarship
                      2016

Related Work   Teaching Assistant
Experience   The University of Western Ontario
                      2020-2022

Publication:

Bai D, Wang J, Li T, Chan R, Atalla M, Chen RC, Khazaneh MT, An RJ & Stathopulos
    PB (2021). Differential Domain Distribution of gnomAD- and Disease-Linked
    Connexin Missense Variants. *Int J Mol Sci*; DOI: 10.3390/ijms22157832.